Influence of Ageing Heating Rates on the Microstructure and Mechanical Properties of Ti-5553 Alloy

A thesis

submitted in fulfilment

of the requirements for the degree

of

Master of Engineering in Materials and Processing

at

The University of Waikato

by

Mengqi Jia

THE UNIVERSITY OF
WAIKATO
Te Whare Wānanga o Waikato

2024

Abstract

The Ti-5553 alloy, a high-strength β-titanium alloy, is increasingly recognised for its exceptional mechanical properties, making it a preferred material for critical aerospace applications. This thesis examines the effects of varying ageing heating rates on the microstructure and mechanical properties of the forged Ti-5553 alloy, focusing on hardness, tensile properties, and fatigue performance. Following solution treatment at 810°C, the alloy was aged at 610°C with heating rates of 1°C/min, 5°C/min, 10°C/min, and 15°C/min. Detailed microstructural analysis was conducted using Scanning Electron Microscopy (SEM) and Energy Dispersive X-ray Spectroscopy (EDX). The microstructural examination revealed that different ageing heating rates caused only minor variations in the alloy's bimodal microstructure. Slower ageing heating rates produced a relatively fine, homogeneously distributed primary α phase within the β grains, while faster rates resulted in a slightly coarser bimodal microstructure. Chemical homogeneity analysis confirmed a consistent distribution of critical elements, with α stabilisers concentrated in the primary α phase and β stabilisers in the β phase, ensuring stable phase compositions across all samples. The observed slight microstructural changes were reflected in the alloy's mechanical properties. Hardness across different ageing heating rates varied between 357.4 HV and 372.6 HV. The ultimate tensile strength (UTS) declined from 1307.2 MPa at 1°C/min to 1264.5 MPa at 15°C/min, while ductility improved from 15.6% to 17.1% over the same range. The alloy demonstrated good fatigue resistance at lower stress amplitudes and ageing heating rates, enduring over 10 million cycles at 337.5 MPa under the 1°C/min condition. However, fatigue life decreased with higher stress amplitudes and ageing heating rates, highlighting the alloy's sensitivity to more extreme conditions. In summary, while the varying ageing heating rates resulted in only minor changes to the microstructure, these alterations had some impact on the mechanical properties of the Ti-5553 alloy. These findings highlight the importance of precise microstructural control in optimising the alloy's performance, especially in applications where achieving a balance between strength, ductility, and fatigue resistance is crucial.

Acknowledgement

First and foremost, I would like to express my deepest gratitude to my supervisor, Dr Ajit Pal Singh, for allowing me to pursue my master's degree at the University of Waikato. His patient and unwavering support and guidance have been instrumental in completing my studies. It has been an honour to learn under his mentorship. Additionally, I would like to thank Dr Giribaskar Sivaswamy for his valuable guidance and support.

I also wish to sincerely thank the University of Waikato's technical staff—Stella Raynova, Sophia Rodrigues, and Jonathan van Harselaar—for their invaluable technical assistance during my experiments and for resolving the unexpected instrument issues that arose. Furthermore, I am grateful to my friends and fellow students in the Waikato Centre for Advanced Materials and Manufacturing (WaiCAMM) group for their advice and support, which have been vital to my academic progress and mental well-being. Special thanks to Yaqi Chang, Yutao Zhai, Balakrishnan Manogan, Rajkumar Das, Jingnan Ma, Abdullah Hussein, Qinghe Zheng, Junqi Liu, Runqi Zhang, Pan Gao, Shan Zhou, and Ziyao Fan.

Finally, I am deeply thankful to my parents for their unwavering understanding and emotional support. Their encouragement and belief in me have been a constant source of inspiration.

Disclaimer

As I am not a native English speaker, I utilised an AI (Artificial Intelligence) language model as an editing tool during the writing of this thesis to:

- Review and correct grammatical and spelling errors,
- Ensure linguistic consistency and coherence, and
- Refine the wording of the research study

I ensured that the AI language model did not introduce any plagiarised content while making corrections or enhancing the language.

Contents

List of Tables

List of Figures

List of Abbreviations

Acronym	Abbreviations
AC	Air Cooling
AI	Artificial Intelligence
ASTM	American Society for Testing and Materials
BASCA	Beta Annealing with Slow Cooling and Ageing
BCC	Body-Centred Cubic
CBC	Ceramic Blanket Cooling
CCT	Continuous Cooling Transformation curves
CNC	Computer Numerical Control machine
CP	Commercial Purity Titanium
EDM	Electronic Discharge Machine
EDX	Energy Dispersive X-ray Spectroscopy
FC	Furnace Cooling
HCP	Hexagonal Close-Packed
HIP	Hot Isostatic Pressing
HV	Hardness Values
MPa	Unit for Stress
SEM	Scanning Electron Microscopy
STA	Solution Treatment followed by Ageing
TEM	Transmission Electron Microscopy
Ti-5553	Titanium alloy containing 5% aluminium, 5% molybdenum, 5% vanadium, and 3% chromium
TTT	Time-Temperature-Transformation curves
UTS	Ultimate Tensile Strength
WQ	Water Quenching
XRF	X-ray Fluorescence analytical technique
YS	0.2% Yield Strength

Chapter 1

1 Introduction

1.1 Background

Titanium and its alloys are renowned for their exceptional properties, which make them critical materials across various industries. These properties include high specific strength, outstanding corrosion resistance, low modulus, excellent fatigue resistance, biological compatibility, and thermal stability. Due to these attributes, titanium alloys find extensive applications in aerospace, power generation, marine, chemical processing, heat exchangers, medical devices, sports equipment, and automotive engineering. The unique combination of durability, lightweight, and high performance under extreme conditions makes titanium alloys a preferred choice for critical applications.

One such alloy, Ti-5553, contains 5% aluminium, 5% molybdenum, 5% vanadium, and 3% chromium and is a metastable β titanium alloy. It is an improvement over traditional alloys like Ti-10-2-3, offering easier processing and improved mechanical properties. Ti-5553 is primarily used in constructing airframe structures and landing gears for modern aircraft such as the Boeing 787 and 777. It benefits from a higher β transus temperature, facilitating forging at elevated temperatures. This property is essential for producing large and complex components and gives the alloy better hardenability and a wider processing window than other titanium alloys. Various heat treatments and ageing procedures can tailor the mechanical properties of this alloy.

The purpose of this study is to investigate the mechanical performance of Ti-5553 alloy by examining the effects of different microstructural states induced through ageing treatments. The samples from cogged Ti-5553 billets will undergo a solution treatment followed by ageing at various heating rates to standardise the ageing temperature. The microstructure of these samples will be evaluated using different microscopy techniques. The study will also focus on testing mechanical properties such as strength, ductility, hardness, and fatigue resistance at room temperature. Some attention will be given to the fatigue fracture behaviour of the alloy.

1.2 Research Focus and Objectives

This research examines the mechanical performance of Ti-5553, focusing on how microstructural transformations induced by various ageing treatments impact its mechanical properties. The primary goal is to understand how different heating rates during the ageing process influence the microstructure and, consequently, the alloy's mechanical attributes, particularly fatigue resistance. This is especially important for components like aircraft landing gears, which undergo repeated stress cycles throughout their service life. Enhancing the fatigue resistance of Ti-5553 through microstructural control can significantly improve the performance and safety of these critical components.

The ageing treatments can significantly affect the morphology and distribution of the primary and secondary α phase within the β matrix, a critical factor in determining the alloy's final mechanical properties. While previous studies have extensively examined the impacts of ageing temperatures and cooling rates, the role of heating rates during ageing has often been overlooked. This research seeks to fill this gap by systematically exploring how variations in heating rates can modify the microstructure and thus influence the mechanical properties, including the fatigue behaviour of Ti-5553.

Given its widespread application in airframe structures and aircraft landing gears, a comprehensive understanding of Ti-5553's fatigue behaviour is essential. This understanding not only helps predict the lifespan of these components but also ensures their operational safety and reliability. The insights gained from this study will enable aircraft designers to refine processing techniques, selecting optimal heating rates that yield superior mechanical properties. Ultimately, this research aims to optimise the mechanical performance of Ti-5553, contributing to the development of more robust and reliable aerospace components.

1.3 Methodology Overview

The thesis explores the effects of ageing treatments at different heating rates on the fatigue behaviour of Ti-5553. The investigation begins with samples from cogged Ti-5553 alloy billets undergoing a solution treatment, followed by ageing at various

heating rates (1°C/min, 5°C/min, 10°C/min, and 15°C/min). This process evaluates the impact of these conditions on the globular primary α phase, the secondary α lamellar structure within the β matrix, the morphology of the grain boundary α phase, and the overall mechanical properties of the alloy. The microstructural changes of these samples will be analysed using optical microscopy and scanning electron microscopy (SEM). These analyses offer detailed insights into the microstructural changes across various orientations and large cross-sectional areas of individual samples exposed to different thermal conditions. In addition to microstructural analysis, the study evaluates the alloy's mechanical properties, including tensile strength, ductility, hardness, and fatigue resistance. The mechanical tests are conducted at room temperature to ascertain the influence of the varied microstructural states induced by the different heating rates during ageing. Furthermore, the research extends to examining the fatigue fracture behaviour of Ti-5553. This comprehensive approach documents the microstructural characteristics and correlates these findings with the mechanical behaviours observed, providing a holistic understanding of the alloy's performance under specified ageing conditions.

1.4 Thesis Structure

The thesis is divided into five main chapters. The details of what is included in each chapter are provided below:

Chapter 1: Introduction — provides background, research aim, methodology, and general thesis structure.

Chapter 2: Literature Review — introduces titanium alloys, discusses their role in various industries, and provides a detailed review of the Ti-5553 alloy.

Chapter 3: Experimental Procedures — describes the experimental methodology for ageing treatments, microstructural analysis and mechanical testing.

Chapter 4: Results and Discussion — presents experimental results, analysing the microstructural characteristics and mechanical properties.

Chapter 5: Conclusion — summarises the findings and discusses the implications of using Ti-5553 in the industry, offering recommendations for future research.

Chapter 2

2 Literature Review

2.1 Introduction

Titanium is Earth's fourth most abundant structural metal, after aluminium, iron, and magnesium. It was first identified in the mineral rutile by W. Gregor and M.H. Klaproth in 1790. Extracting titanium from minerals such as ilmenite or rutile was initially costly and energy-intensive. It was not until around 1950 that the first commercial mill products were developed, allowing for broader commercial use of titanium [1]. As shown in Figure 1, titanium has a lower density than iron, steel, and copper, but it possesses greater tensile strength and exceptional mechanical properties at high temperatures than aluminium. Additionally, titanium alloys exhibit superior corrosion resistance over steel, making them highly valuable in various industrial sectors [2].

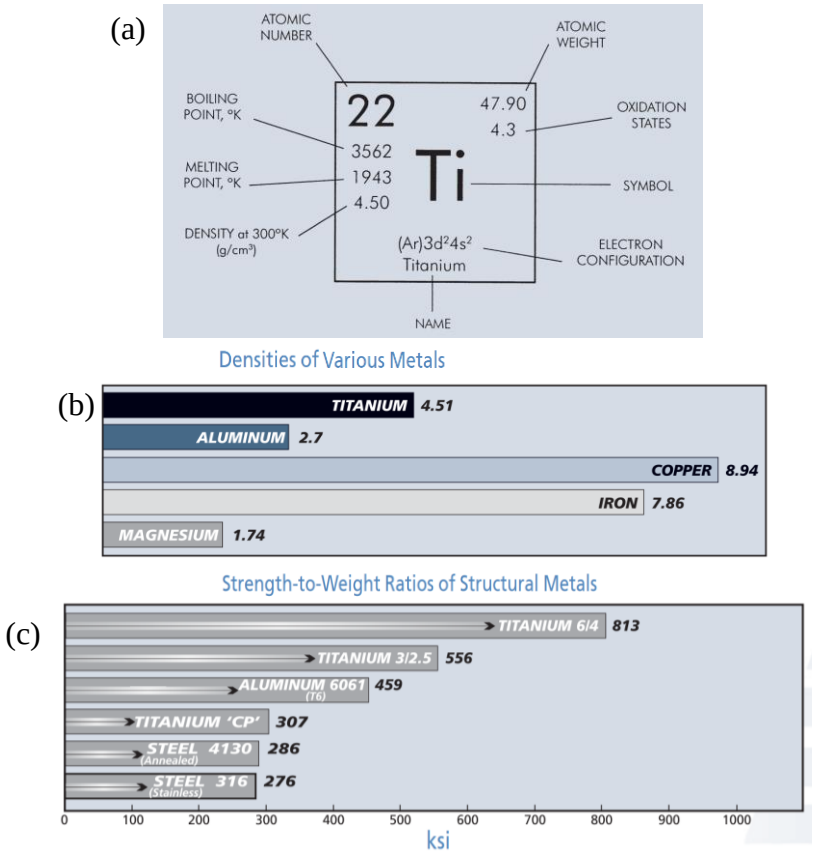

Figure 1: (a) General information about titanium (b) Comparison of titanium's density with other metals (c) Highlighting the superior strength-to-weight ratio of titanium and its alloys [3]

Despite its benefits, the high production cost of titanium remains a significant challenge even today. However, investment in titanium alloys is often justified by their long-term benefits of reduced maintenance costs and extended equipment life, particularly in industries where reliability and performance under extreme conditions are essential [4]. Researchers are constantly developing new and innovative manufacturing techniques to reduce the cost of producing titanium. As a result, the applications of titanium are expected to expand, further integrating this metal into new and innovative industrial solutions.

2.1.1 Titanium Properties and Industrial Applications

Titanium alloys are crucial in fields that require materials to withstand rigorous conditions while maintaining performance and integrity (Figure 2). Titanium is distinguished by its excellent strength-to-weight ratio, superior corrosion resistance, and high fatigue resistance, making it ideal for many applications [5, 6]. These properties reduce maintenance costs and extend the service life of the applications in which they are used. The following information explains why Titanium is utilised in different industrial applications such as aerospace, medical, automotive, and marine industries, among others.

Aerospace: Titanium alloys are primarily used in the aerospace industry to manufacture structural components and engine parts. The metal's strength significantly reduces aircraft weight, enhancing fuel efficiency and speed. Its ability to withstand high temperatures and resist corrosion also minimises maintenance requirements [7, 8].

Medical Industry: Titanium's biocompatibility makes it a preferred material for surgical implants. These implants are resistant to body fluid corrosion and well-tolerated by human tissue, making them durable and safe for long-term use [4, 9].

Automotive Industry: Titanium's low density is highly valued in the automotive industry, where it is used to reduce the mass of components such as piston connecting rods and valve trains, thereby reducing overall vehicle weight and improving fuel efficiency [7].

Marine and Architectural Applications: Titanium's resistance to corrosion by seawater makes it suitable for marine applications, including drilling risers, which benefit from both the material's strength and its lightweight nature. Similarly, in architecture, titanium is used for features like exterior walls and roofing, where its longevity and resistance to atmospheric corrosion are critical [4, 10].

Petrochemical and Chemical Industries: Titanium alloys are preferred over stainless steel for manufacturing containers, mixers, and heat exchangers in environments exposed to highly corrosive substances due to their superior durability and corrosion resistance [4].

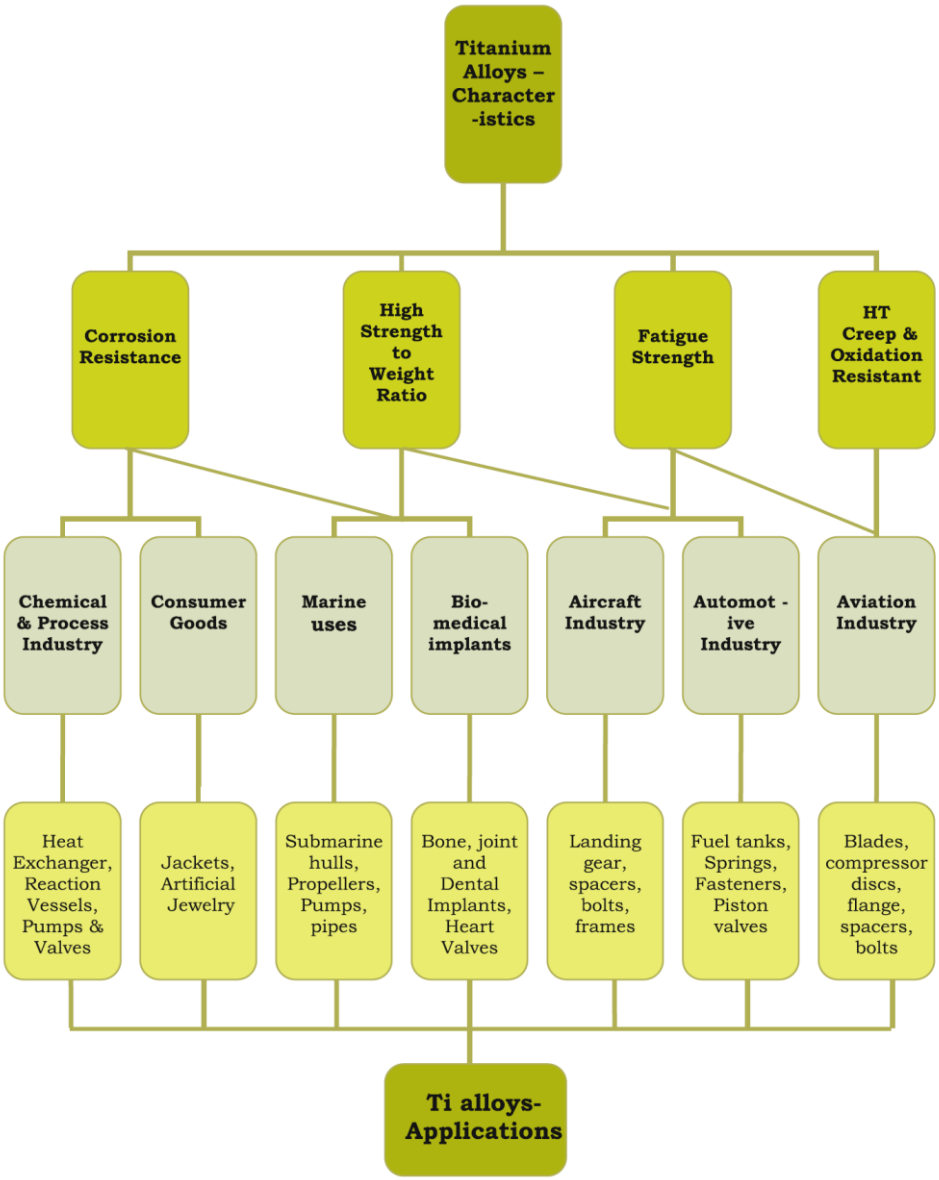

Figure 2: Attributes and typical use of titanium alloys [11]

2.2 Classification of Titanium Alloys

Unalloyed titanium is commonly known as commercial purity (CP) titanium [5]. This metal demonstrates a pure hexagonal close-packed (HCP) α-crystal structure at room temperature [1]. At 882.5 °C, pure titanium undergoes an allotropic transformation, transitioning from a hexagonal close-packed (HCP) α structure to a body-centred cubic (BCC) β structure [1, 12]. This BCC structure persists until the metal's melting point, which is approximately 1668°C [13]. CP titanium possesses the lowest strength but the highest corrosion resistance. Nevertheless, introducing certain interstitial elements, such as nitrogen and oxygen, can considerably enhance its strength. Due to the differences in mechanical properties, CP titanium is categorised into various Grades.

Various alloying elements are incorporated into pure titanium to achieve preferred properties for different commercial applications. These alloying elements are classified based on their capacity to affect the phase transition temperature. Elements that elevate the transformation temperature are called "α-stabilisers", such as oxygen, nitrogen, carbon, and aluminium. Conversely, those that lower the transformation temperature are designated as "β-stabilisers," including chromium, iron, and hydrogen [13-15]. The effect of these supplementary elements is more noticeable in Figure 3. The influence of α-stabilisers is displayed in Figure 3(A), where the transus temperature is increased with the alloying element. Figure 3(B) and (C) represent two distinct categories of β-stabilisers; both can lower the transus temperature. In Figure 3(B), this decrease is achieved by forming a "β-isomorpher" [13], as elements like V, Mo, and Ta are preferentially dissolved in the β phase [5]. Conversely, Figure 3(C) achieves a decrease by causing a eutectoid reaction (β—α+γ), as seen with elements such as Cu, Mn, and Cr.

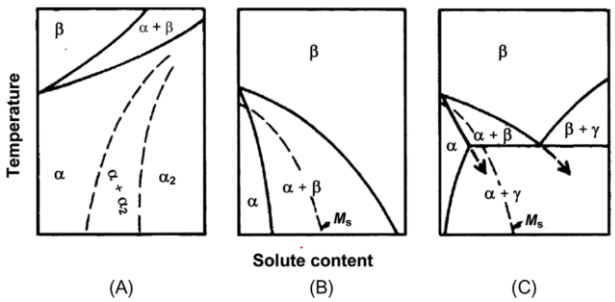

Figure 3: Basic types of phase diagrams for titanium alloys [13]

2.2.1 Categories of Titanium Alloys

Titanium alloys are usually classified into five main categories based on their chemical composition and microstructure (Figure 4). These categories are α alloys, near-α alloys, α+β alloys, near- β alloys, and β alloys. The α alloys are composed mainly of α-phase titanium, characterised by a hexagonal close-packed crystal structure. The near-α Alloys contain both α and small amounts of β-phase titanium. The α+β alloys are made up of a mixture of α and β-phase titanium, while the near-β Alloys contain mostly β-phase titanium with small amounts of α. The β Alloys, on the other hand, consist mainly of β-phase titanium. For the sake of simplicity, in this particular review, the near-α Alloys and α Alloys categories, as well as the near-β Alloys and β Alloys categories, have been combined. This combination allows a more comprehensive analysis of the properties and applications of these alloys [1, 5, 7, 15].

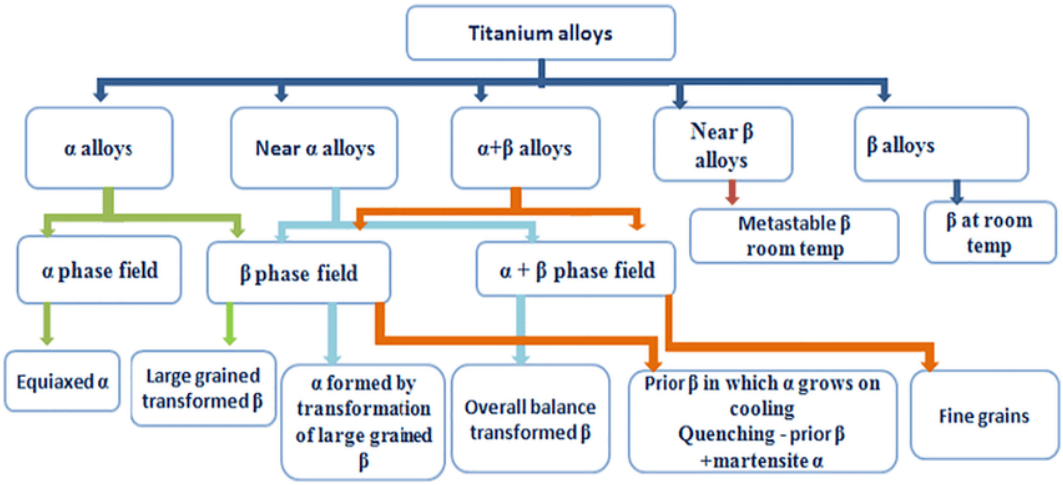

Figure 4: Classification of titanium alloys [16]

2.2.1.1 α Alloys and near-α Alloys

The α alloys are primarily composed of a significant quantity of α-stabilisers and a relatively limited amount of β-stabilisers, making their microstructure and performance similar to that of typical CP titanium. These alloys are known for their reasonable strength, notch toughness, and creep resistance and exhibit excellent corrosion resistance. Their composition predominantly includes the α phase, although near-α alloys may contain slightly higher amounts of β-stabilisers. Typically, these materials are mainly known for their ability to operate in cryogenic

environments because they do not undergo a ductile-brittle transformation. This characteristic makes them suitable for extreme temperature applications, although it is essential to note that their ductility and toughness may decrease at low temperatures, as indicated in the literature [5, 15]. Furthermore, at room temperature, α alloys consist mainly of a single α phase or nearly all α phase due to the influence of α-stabilisers, which elevate the transus temperature. As a result, it becomes more difficult to form the β phase during the heat treatment process. Consequently, these alloys exhibit a limited response to thermal processing, leading to notable weldability. However, in the case of near-α alloys, incorporating specific β stabilisers allows for retaining small amounts of β phase after cooling from the two-phase region. This enables the improvement of properties through subsequent heat treatments, such as the ageing process [5].

2.2.1.2 α+β alloy

The α+β titanium alloys contain a higher proportion of β-stabilisers compared to near-α alloys. This composition promotes the transformation from a mixed α and β phase structure to a predominantly β phase during heating processes. After cooling, these alloys are capable of retaining a significant portion of the β phase at room temperature, allowing for enhanced mechanical properties through various heat treatments [5, 7, 17]. A substantial β phase in these alloys supports improvements in strength and ductility, making them suitable for diverse applications. A notable example of an α+β alloy is Ti-6Al-4V, known for its optimal balance of strength and ductility, essential for high-performance engineering applications. Typically, α+β alloys exhibit commendable strength at both room and elevated temperatures, making them highly versatile in industrial use. However, it is essential to manage the β phase content carefully; exceeding 20% can render the alloy non-weldable, thus limiting its applicability in scenarios requiring welding [1].

2.2.1.3 near- β Alloys and β Alloys

Metastable β alloys, compared to α-β alloys, contain a higher proportion of β-stabilisers, enabling them to maintain a 100% β phase after cooling from the high-temperature β field to room temperature [5]. The quantity of β-stabilisers must be

sufficient to inhibit martensite formation [13], as highlighted in Figure 5. Stable β alloys, as shown in Figure 5, are characterised by an exclusive composition of the β phase and do not respond to ageing processes. Notable examples of stable β alloys include Ti-35V-15Cr and Ti-25V-15Cr-0.3Si [13].

The term "β alloys" generally refers to metastable β alloys that exist between the between β_C (the minimum addition of β-stabilisers to achieve a 100% β phase after quenching) and β_S (the β-transus temperature). These alloys, when cooled rapidly, are prone to instability; minor environmental changes like a slight increase in temperature can trigger a phase transformation [13]. After solution treatment, β alloys display a fully β phase, which exhibits high ductility and toughness, although their strength may be slightly reduced. These alloys are also noted for their excellent cold formability, forgeability, and hardenability.

To further enhance their mechanical properties, ageing processes often employ post-solution treatment to induce α precipitation within the metastable β region. This transition not only boosts the alloys' strength at room temperature but also improves their YS and fracture toughness while slightly decreasing their tensile ductility and creep strength due to increased alloy density. Consequently, β alloys are particularly well-suited for use in moderate-temperature environments due to their enhanced mechanical properties and adaptability to various manufacturing processes [5, 13].

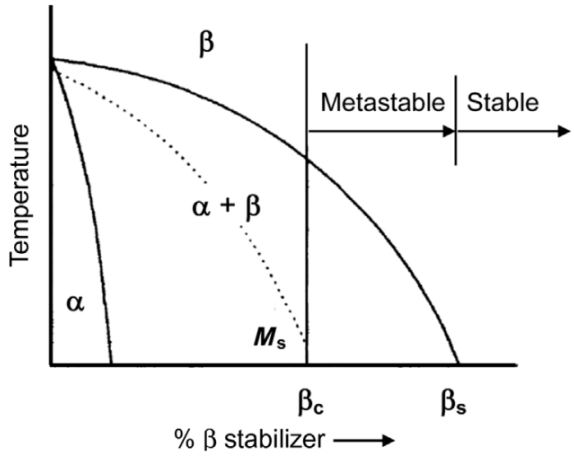

Figure 5: Pseudo-binary β-isomorphous phase diagram showing locations of metastable and stable β-titanium alloys [13]

2.2.2 Evolution and Impact of β Titanium Alloys in Aerospace Applications

The β titanium alloys, recognised as a distinct category in the late 1950s, are notable for their excellent formability due to their Body-Centred Cubic (BCC) crystal structure. These alloys can retain a 100% β phase at room temperature, allowing them to be cold-formed in their softer state and strengthened through ageing treatments. However, their high concentration of β-stabilisers can lead to challenges such as complex melting processes and segregation during ingot solidification.

The aerospace industry began incorporating β titanium alloys in the early to mid-1960s, with the Lockheed SR-71 Blackbird being the first aircraft predominantly constructed from these materials. Comprising nearly 90% titanium alloys, with a significant portion being the β alloy Ti-13V-11Cr-3Mo (B120VCA), this aircraft showcased the alloy's capability to achieve a tensile strength of approximately 1300MPa through specialised heat treatments. Despite its processing challenges, including susceptibility to segregation and limited weldability due to its high chromium content, Ti-13V-11Cr-3Mo was selected for the SR-71 Blackbird due to its performance under extreme aerodynamic heating, reaching speeds up to 3200 km/h.

Throughout the 1970s and 1980s, the use of β-titanium alloys expanded. McDonnell Douglas first used Ti-13V-11Cr-3Mo for titanium springs in the commercial aircraft DC-10, a practice later adopted by other aircraft due to its effectiveness. The 1980s saw the introduction of the North American Rockwell B-1B bomber, which utilised over 250 components made from Ti-15V-3Cr-3Al-3Sn, another β alloy known for its more excellent formability and potential cost-effectiveness in manufacturing thin-gauge components.

By the 1990s, Boeing significantly advanced its materials technology by incorporating stronger β titanium alloys, such as Ti-10V-2Fe-3Al, into the Boeing 777. This move, aimed at replacing high-strength, low-alloy steel in landing gear applications, notably reduced the aircraft's overall weight [18]. Landing gear plays an essential role in aviation safety, bearing the total weight of an aeroplane during take-off and absorbing considerable impact during landing. Research by Yonggang, W. and L. Honglang highlights that landing gear system failures constitute 8.69%

of all aircraft failures [19]. Further studies indicate that nearly 60% of aircraft failures are associated with landing gears, predominantly due to fatigue [20]. Consequently, the materials selected for landing gear manufacturing must exhibit exceptional strength, fracture toughness, and fatigue resistance—qualities vital for the longevity and reliability of landing gears. The adoption of β titanium alloys in this era was due to their superior mechanical properties. It reduced life cycle costs, necessitating less frequent maintenance than traditional materials, enhancing operational efficiency and safety in aerospace applications.

In addition to its widespread use in the U.S., the β alloy VT22 was extensively employed in Russia, known for its weldability and application in landing gears, among other components. In 1997, Boeing and Russian titanium alloy manufacturers VSMPO introduced a new β alloy, Ti-5Al-5Mo-5V-3Cr, to replace Ti-1023 for the Boeing 7E7, showcasing the ongoing evolution and significance of β titanium alloys in modern aerospace engineering. This continuous innovation in alloy development highlights the critical role of β-titanium alloys in enhancing the performance and durability of contemporary aircraft [21].

2.3 Ti-5553 Alloy

Ti-5553, a metastable β titanium alloy composed of 5% aluminium, 5% molybdenum, 5% vanadium, and 3% chromium, is gaining prominence as a formidable alternative to traditional aerospace alloys like Ti-10-2-3 [13, 22, 23]. Representing 5-7% of Russia's total titanium alloy production, Ti-5553 is extensively utilised in the airframes and landing gears of high-profile aircraft such as the Boeing 787 and 777. This alloy offers a superior balance of mechanical properties and more straightforward processing methods than its predecessor, VT22, and outperforms Ti-1023 due to its wider processing window and higher β transus temperature [24]. These features facilitate high-temperature forging essential for manufacturing large and intricate components [25].

Moreover, the exceptional hardenability of Ti-5553 permits air cooling following solution treatments, preserving excellent mechanical properties in sections up to 150 mm thick [22, 24]. This attribute enables Ti-5553 to achieve greater strength

through heat treatment than Ti-1023 and VT22, positioning it as a material of choice for demanding aerospace applications like landing gears [21, 25]. These applications necessitate materials with outstanding strength, fracture toughness, and fatigue resistance to endure the substantial weight and impact loads experienced during aircraft take-off and landing.

Additionally, Ti-5553, refined from the Russian alloy VT22 but with increased chromium content and reduced iron content, exhibits reduced susceptibility to segregation. This advancement significantly improves the alloy's manufacturability, enabling higher amperage and melt rates during production, which in turn enhances output efficiency [13, 22]. The minimal risk of segregation and improved manufacturing capabilities establish Ti-5553 as a critical material in the production of vital aircraft components, including fuselages and landing gear systems, where high strength and reliability are paramount [6, 22].

In summary, Ti-5553 not only offers mechanical and processing benefits but also significantly contributes to the advancement of aerospace technology. By ensuring aircraft components are lighter, stronger, and more durable, Ti-5553 is pivotal in the evolution of aerospace materials. This evolution aims to enhance performance and operational efficiency while simultaneously reducing maintenance frequencies and costs, thereby fundamentally changing the dynamics of material usage in high-performance environments.

2.3.1 Typical Microstructures and Mechanical Properties of Ti-5553 Alloy

The typical microstructure and mechanical properties of the Ti-5553 alloy vary depending on the specific thermal processing and heat treatment it undergoes (Figure 6) [26]. This variability is essential as the alloy's strengthening essentially results from forming α precipitates within the β matrix [23]. Generally, when the alloy is processed above its β transus temperature, a lamellar or bi-lamellar secondary α microstructure can be obtained. Conversely, processing the alloy below the β transus temperature provides a bimodal microstructure [27, 28].

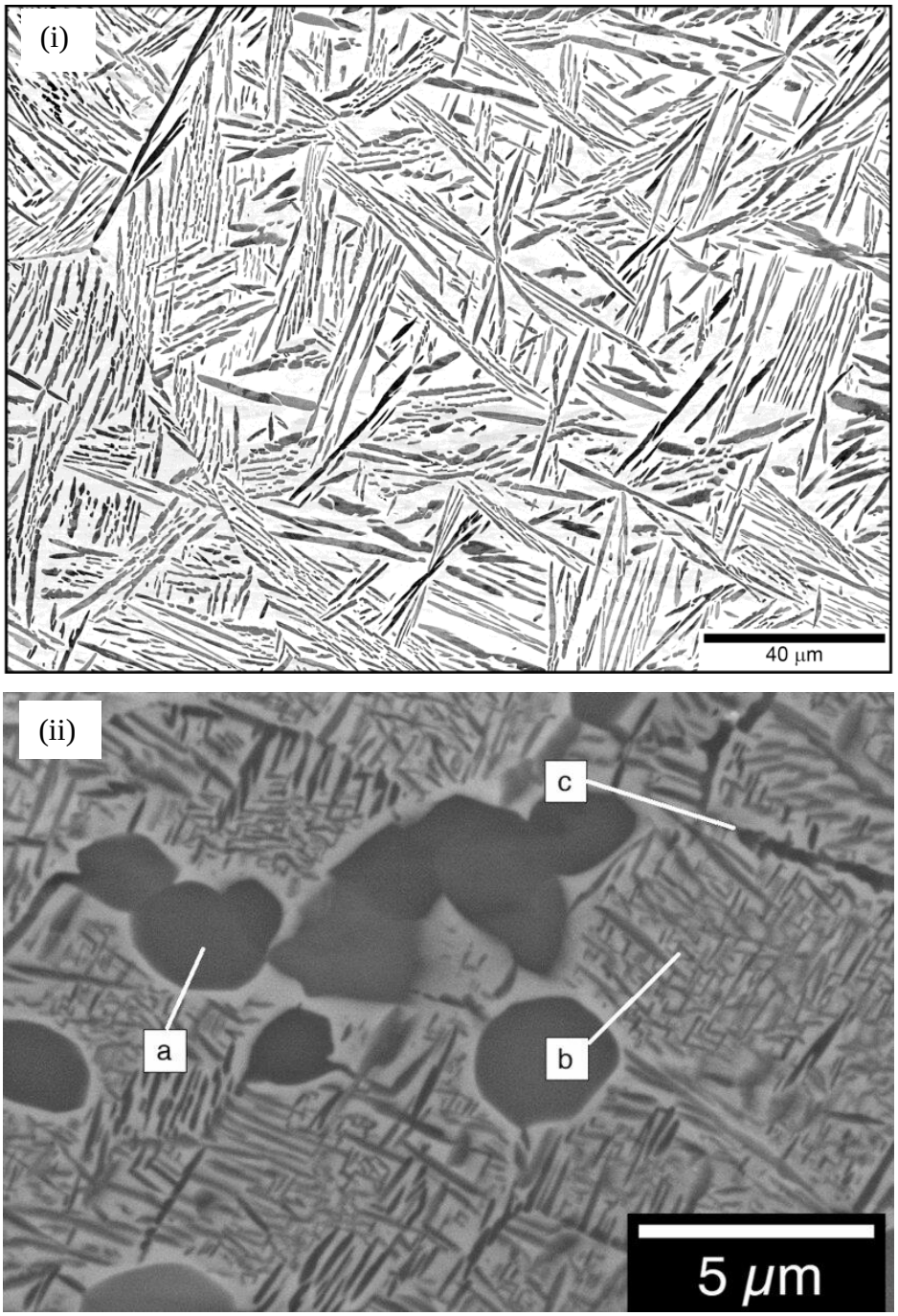

Figure 6: illustrates the different microstructures of Ti-5553: (i) Lamellar microstructure [29], (ii) Bimodal microstructure with (a) globular α phase, (b) fine lamellar α phase, and (c) coarse α phase at the grain boundaries [30]

As previously stated, Ti-5553 offers exceptional mechanical features such as strength, durability, hardening ability, ability to resist fractures, and resistance to fatigue [6, 22, 23]. This is evident from Table 1 and Figure 7 where comparison of the static properties and fatigue behaviour of Ti-5553 with those of commonly used α+β Ti-6Al-4V alloy are included [21].

Table 1: Ti-5553 room temperature static tensile properties compared to Ti-6Al-4V alloy [21]

Property	Cast and HIP'ed Ti-5553	Cast and HIP'ed Ti-64
UTS, MPa	1159	910
YS, MPa	1055	828
El, %	9	8.9
Compressive YS, MPa	1138	897
Max shear, MPa	690	655

The maximum stress that Ti-5553 can handle before succumbing to fatigue is approximately 790MPa, which is nearly twice that of Ti-6Al-4V (Figure 7). Ti-5553's composition, which includes vanadium, molybdenum, and chromium, stabilises the β phase and supports a fine dispersion of the α phase, enhancing its strength and toughness. These characteristics contribute to its higher resistance to crack initiation and propagation, making it more durable under cyclic loading conditions and preferable for high-stress applications [31].

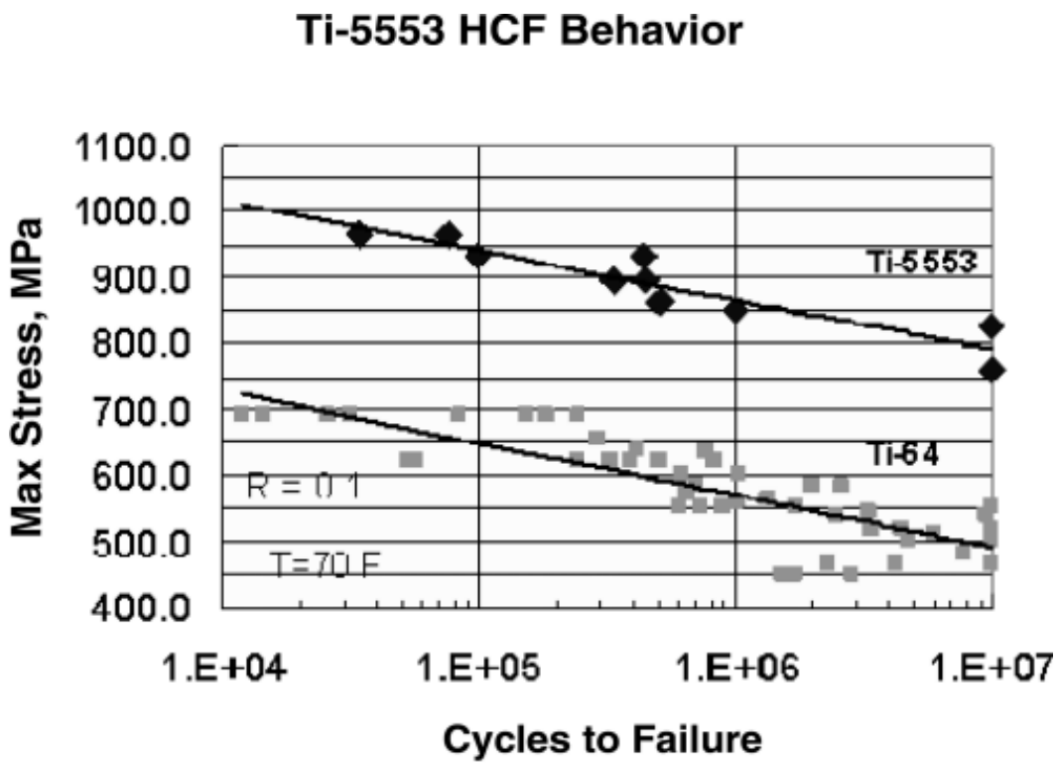

Figure 7: High-cycle fatigue characteristics of Ti-5553 Alloy (hot isostatic pressing (HIP) + heat treated) compared with cast Ti-64 (HIP + mill anneal) [21]

2.3.2 Heat Treatment Influence on Ti-5553 Alloy Microstructures and Mechanical Properties

Three heat treatments are typically used to enhance the mechanical properties of Ti-5553 alloy: Solution Treatment, Solution Treatment followed by Ageing (STA), and β Annealing with Slow Cooling and Ageing (BASCA).

Solution Treatment: This process mainly results in a β matrix with minimal primary α particles, enhancing ductility and providing a baseline of strength.

Solution Treatment and Ageing (STA): After solution treatment, ageing promotes the precipitation of α particles within the β matrix, resulting in a microstructure with evenly distributed globular primary α precipitates. This significantly boosts the alloy's strength and fatigue resistance, though it may slightly reduce ductility compared to the ST condition.

Beta Annealing with Slow Cooling and Ageing (BASCA): This treatment involves annealing above the β transus temperature, followed by controlled cooling and further ageing. The slow cooling allows for a more thorough decomposition of the β phase, producing a microstructure with coarsened lamellar α phases and retained β phases, enhancing the balance between strength and toughness.

Cotton, J.D.'s study details the mechanical properties of each treatment (Table 2), indicating that ST offers greater ductility while STA and BASCA enhance strength and fatigue resistance through different ageing and cooling protocols [22].

Table 2: Mechanical properties of heat-treated Ti-5553 for section sizes up to 150 mm [22]

Heat-treatment conditions	Tensile yield strength (MPa)	Ultimate tensile strength (MPa)	Elongation (%)	Reduction of area (%)	KIc (MPa$\sqrt{m}$)
ST	800	880	15	50	
STA	1170	1240	4	10	33
BASCA	965	1080	6	–	65

In STA (Figure 8(a)), the microstructure features globular primary α precipitation evenly distributed throughout the aged β matrix, resulting in enhanced strength and

fatigue resistance but reduced ductility. In BASCA (Figure 8(b) and Figure 8(c)), the slow cooling and ageing allow the β phase to decompose, leaving behind a limited β phase and a high proportion of coarsened lamellar α phase. This condition leads to an optimal strength-toughness balance [32].

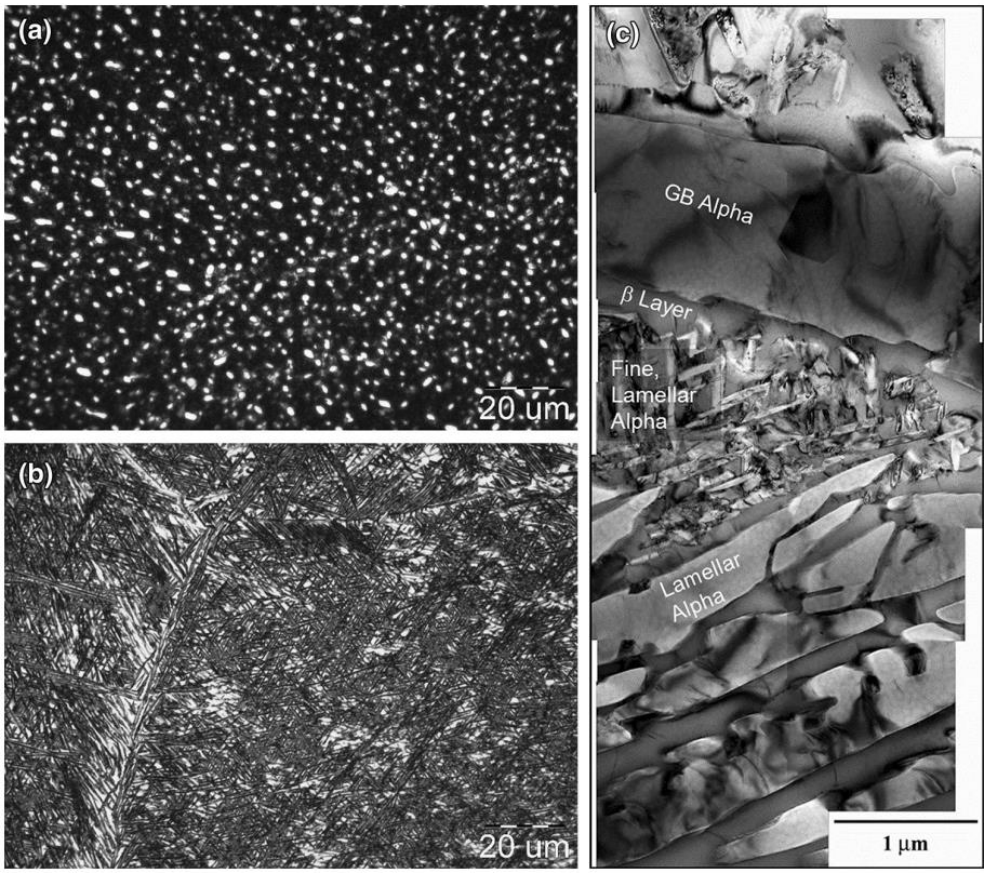

Figure 8: Depictions of the typical microstructures in Ti-5553 after STA and BASCA treatments: (a) Light optical image in the STA condition (b) Light optical image in the BASCA condition (c) Transmission Electron Microscopy (TEM) bright field image of the BASCA condition [22]

The results, as shown in Figure 9, indicate a general trend where UTS decreases and elongation increases with rising ageing temperatures. Specimens treated at higher temperatures demonstrate enhanced UTS at the same ageing conditions, though with a compromise in ductility. Notably, ageing below 500°C can initiate the formation of a metastable omega phase, acting as nucleation sites for the α phase, significantly influencing the precipitation of secondary α phases and, consequently, the alloy's final mechanical properties. When fully aged, the alloy displays an approximately equal α/β balance in its microstructure [22].

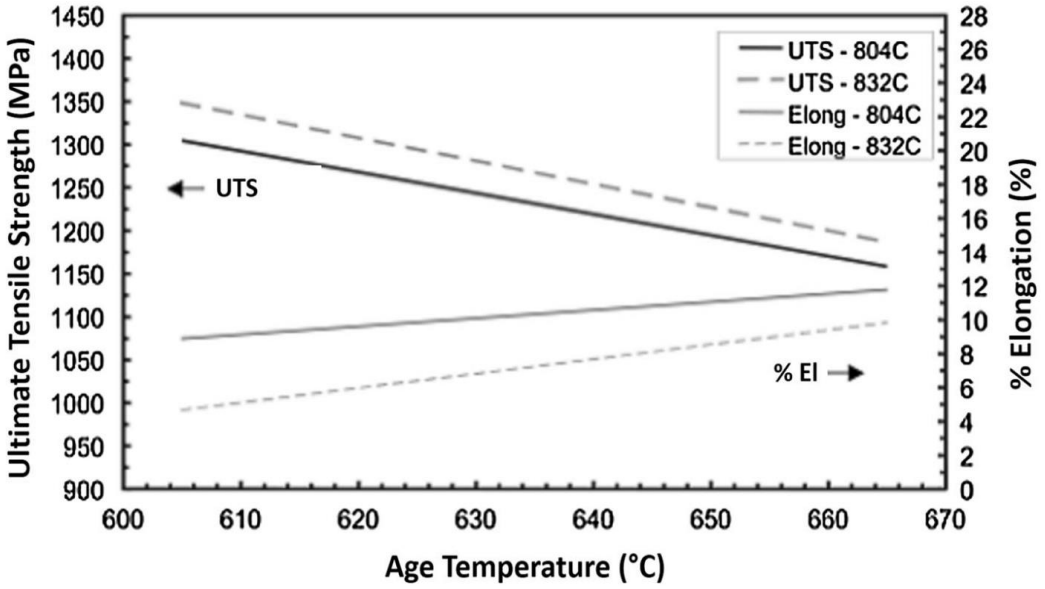

Figure 9: Ultimate tensile strength (UTS) and elongation versus ageing temperature for a Ti-5553 billet (178 mm diameter and 89 m long), treated at either 804℃ or 832℃ [9]

2.3.3 Time-Temperature-Transformation (TTT) and continuous cooling transformation (CCT) curves for Ti-5553 Alloy

Cotton, J. investigated the effects of ageing temperature on α-phase precipitation in Ti-5553 by presenting TTT curves. These curves illustrate the times required for the initiation and completion of α-phase transformations at various temperatures. For the study, α-β-forged samples were heated to either 25°C above or below the β transus temperature of 863°C and held there for three hours. They were then rapidly cooled to different temperatures (800°C, 700°C, 600°C, 500°C, 400°C, and 350°C) and aged until the phase transformation was no longer observable, up to a maximum of three hours [23, 33].

The TTT diagrams (Figure 10) do not show curves for grain boundary α and α_2 phases but indicate that treatments at 838°C slightly hasten the start of transformation while extending its duration. Notably, the curves reveal a pronounced protrusion within the 600 to 700°C range, attributed to α phase precipitation starting 1 to 2 minutes sooner at 600°C compared to other temperatures. This suggests that ageing temperature has a limited impact on the transformation timings.

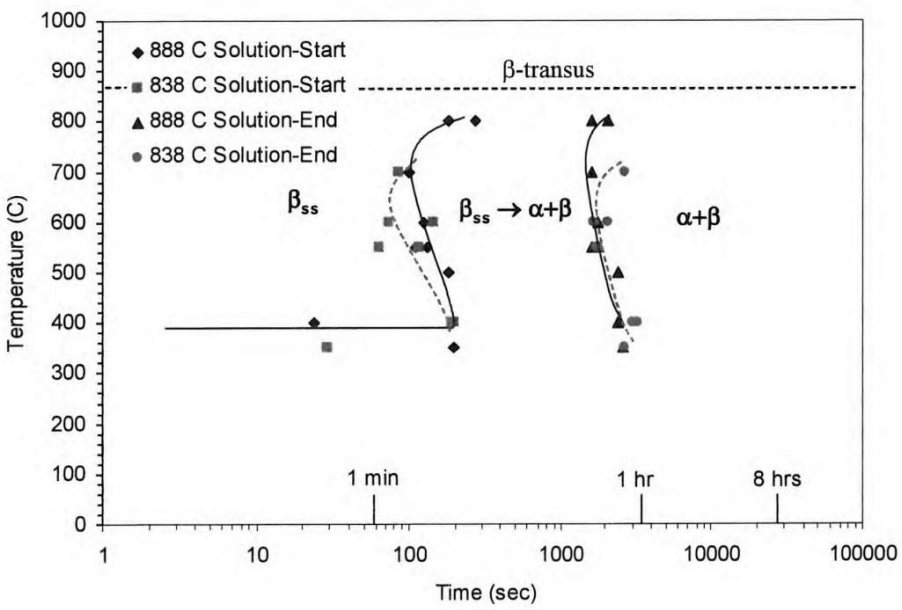

Figure 10: Time-Temperature-Transformation diagram for Ti-5553 [23]

Moreover, as a metastable β alloy, Ti-5553 can retain a full β phase when rapidly cooled from the β region, depending on the cooling rate. To further explore this, Cotton, J. presented Continuous Cooling Transformation (CCT) diagrams created after β-annealing the alloy at 888°C for an hour and then cooling it to 300°C at varying rates (Figure 11). These diagrams reveal that α phase transformation is completely inhibited at cooling rates faster than 0.25°C/s, with rapid cooling potentially leading to the formation of a thermal omega phase.

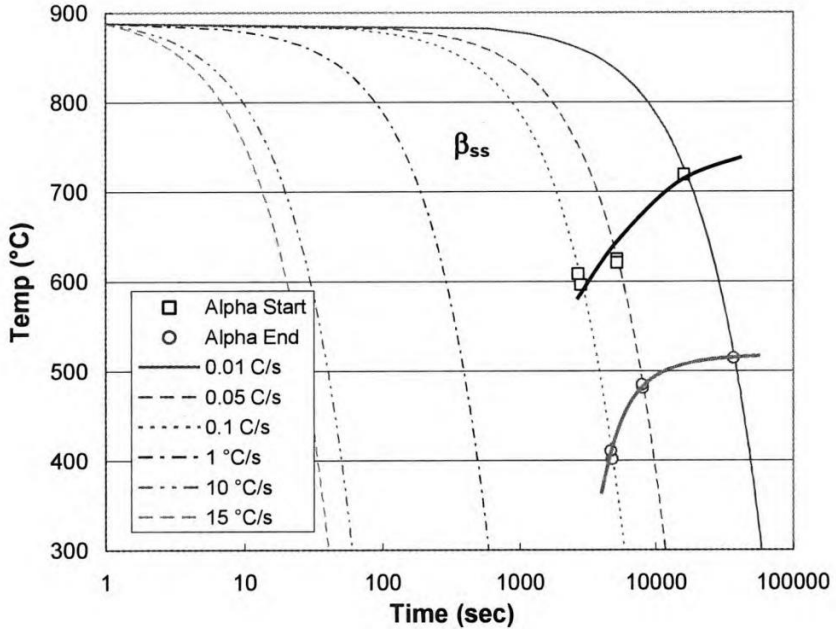

Figure 11: Continuous-Cooling-Transformation diagram for Ti-5553 [23]

2.3.4 Effect of Secondary α phase on Fatigue behaviour of Ti5553

Bettaieb et al. studied the impact of the secondary α phase's morphology and volume on the mechanical and fatigue properties of Ti5553 alloy, creating two distinct microstructures (Ti5553-1 and Ti5553-3 refer to Figure 12) differentiated primarily by the size of the secondary α phase [34]. This was achieved by adjusting the second ageing temperature: 610°C for Ti5553-1 and 670°C for Ti5553-3. This led to finer, needle-like secondary α phases in Ti5553-1.

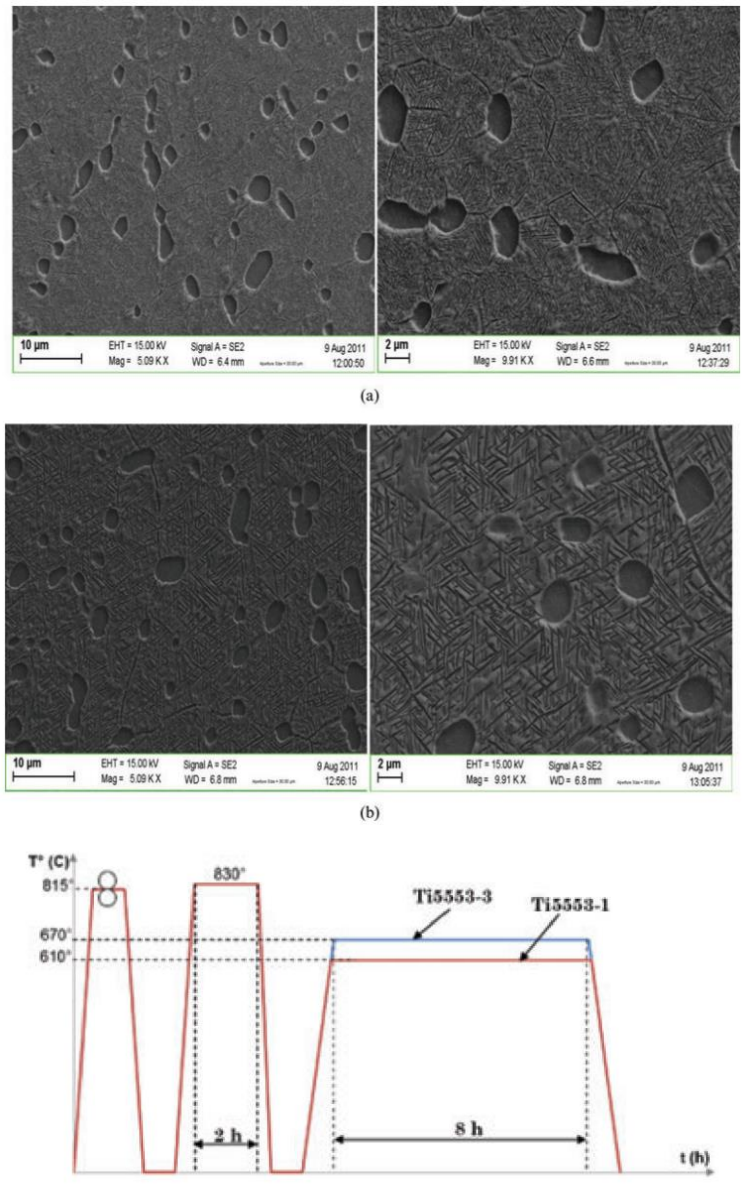

Figure 12: illustrates the microstructures and ageing cycles applied to Ti-5553 alloy forged pancakes, (a) Ti-5553-1 microstructure after ageing at a lower temperature of 610°C. (b) Ti-5553-3 microstructure after ageing at a higher ageing temperature of 670°C (c) heat treatment cycle applied [34]

Both microstructures started with an identical first ageing temperature at 830°C, resulting in nodule-shaped primary α phases (Figure 12 (c)). Tensile tests showed that Ti5553-1, with its finer secondary α phases, consistently demonstrated higher strength across various strain rates Figure 13. This was attributed to the increased hindrance to dislocation movement caused by the dense grain boundaries. However, this increase in strength resulted in decreased ductility, with stress concentrations at grain boundaries more likely to induce microcracks.

	Ti5553-1		Ti5553-3	
$\dot{\varepsilon}(s^{-1})$	$\sigma_{p0.2}$	σ_u	$\sigma_{p0.2}$	σ_u
5×10^{-5}	1285	1398	1142	1282
2×10^{-4}	1313	1419	1150	1297
4×10^{-3}	1332	1423	1185	1300
10^{-2}	1370	1452	1199	1318

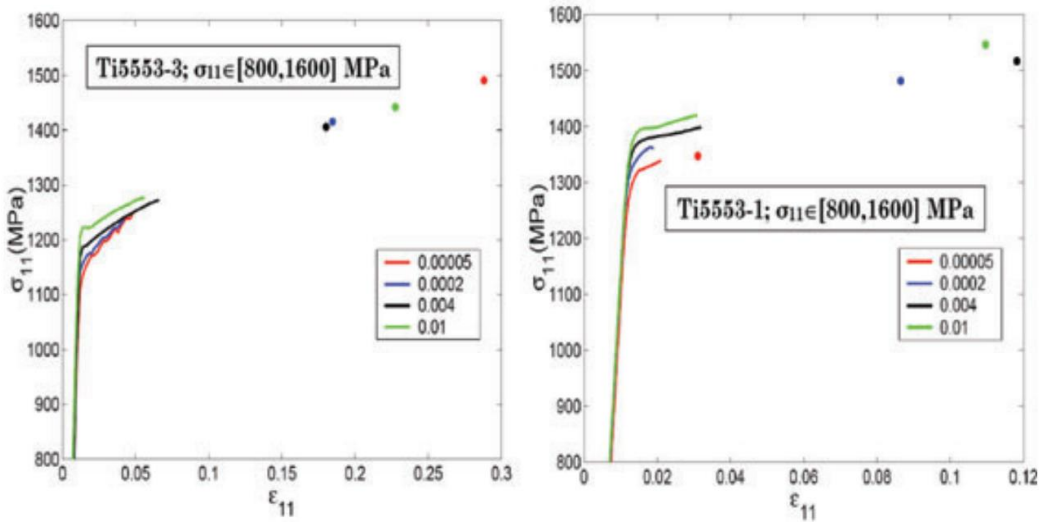

Figure 13: demonstrates the tensile properties of the Ti5553 alloy, showcasing stress-strain curves for both Ti5553-1 and Ti5553-3 microstructures after undergoing specific ageing cycles [34]

High-cycle fatigue tests further confirmed that Ti5553-1 exhibited superior fatigue resistance (Figure 14), likely due to the same obstructive effect of its finer grains on dislocation movement. Despite the variations in microstructure, the fracture

surfaces of both microstructures in fatigue tests showed similar features, with cracks often initiating in the primary α phase.

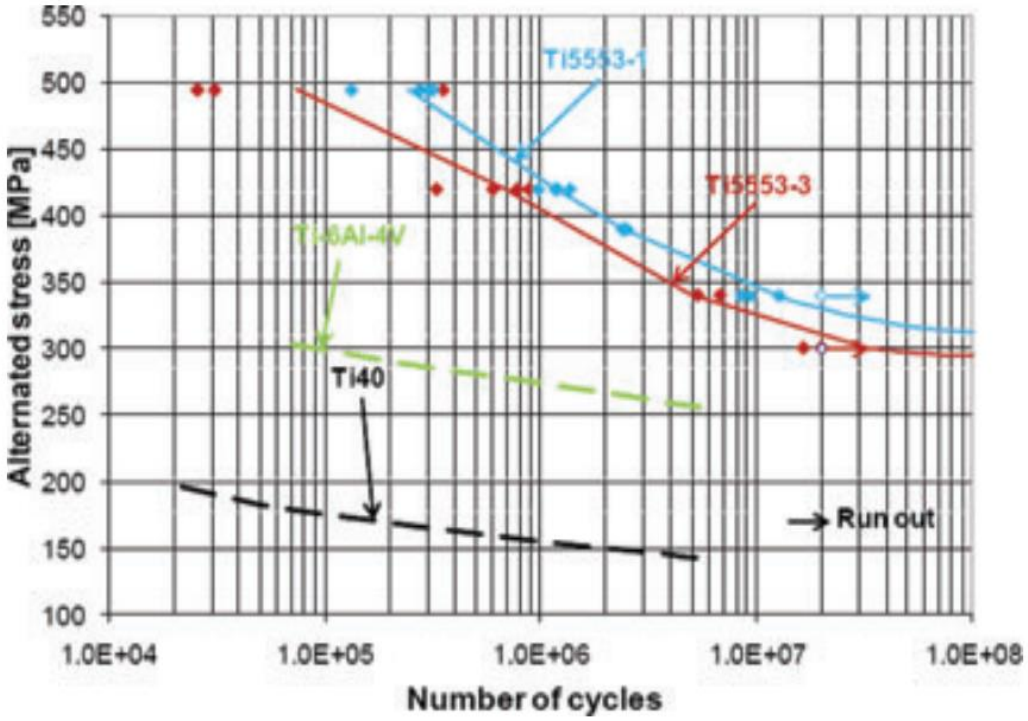

Figure 14: S-N curves of Ti5553, TA6V and Ti40 alloys (R = 0.1) [34]

In conclusion, the study by Bettaieb et al. illustrates that finer secondary α phases in Ti5553 can significantly enhance fatigue resistance, suggesting a beneficial correlation between microstructural refinement and mechanical performance [34].

In a comprehensive study, Campanelli et al. explored the impact of α-phase morphologies on the high-cycle fatigue behaviour of Ti5553, distinguishing their research by examining variations in the primary α-phase [35]. The study involved different heat-treating schedules, notably BASCA and double ageing, as shown in Figure 15. The BASCA process starts with creating primary α laths during a slow cooling phase from approximately 900°C to 607°C, taking about 2.5 hours. This stage allows ample time for the nucleation and growth of the primary α phase, as depicted in the water-quenched micrograph (Figure 15). Secondary α needles form during a subsequent ageing phase, producing a microstructure with thick α layers around grain boundaries, as shown in the SEM micrographs (Figure 16).

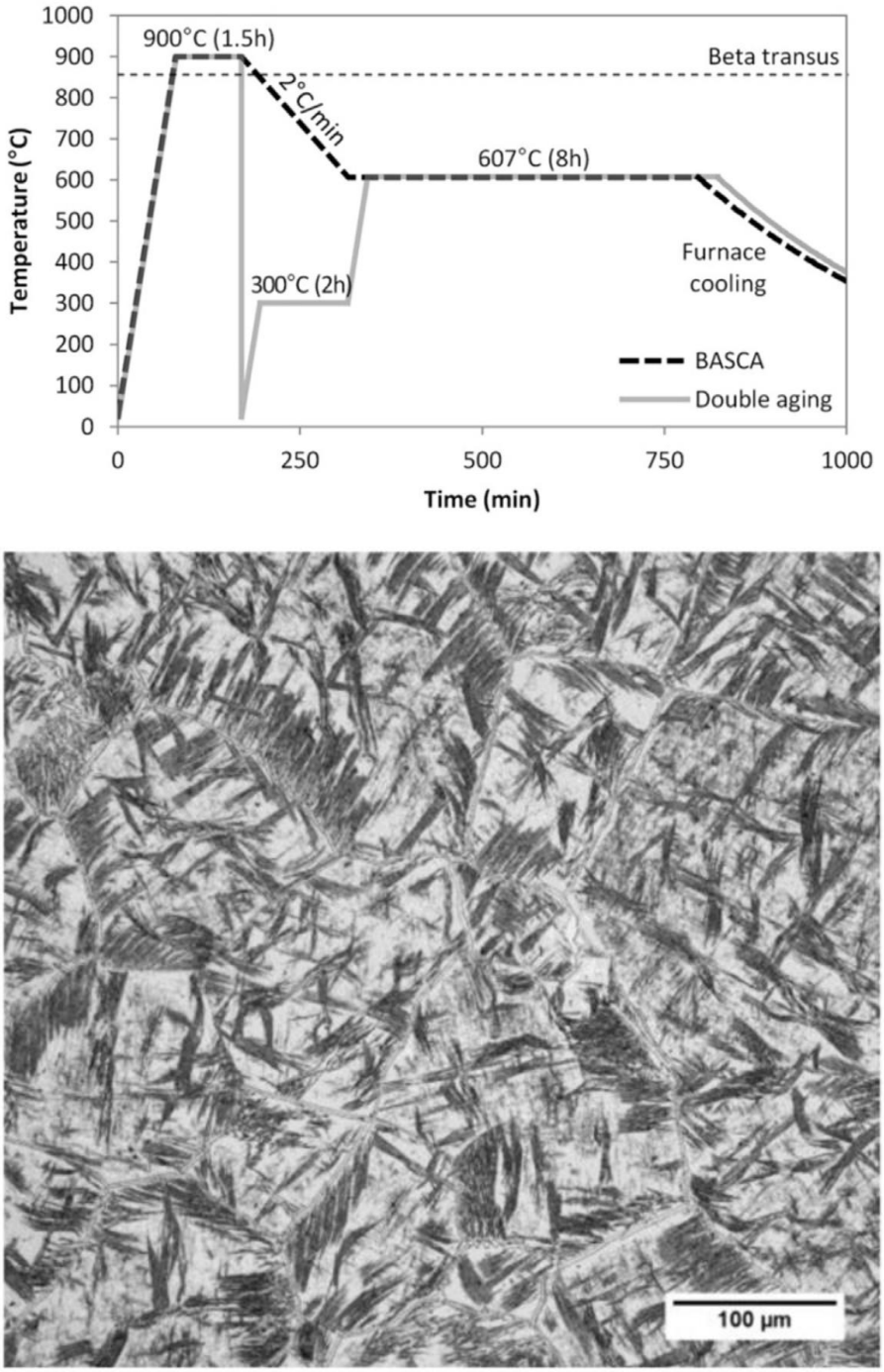

Figure 15: (a) Heat treatment schedules for Ti-5553 alloy involving two distinct processes: BASCA and double ageing (b) optical micrograph shows the BASCA-treated Ti-5553 alloy immediately after water quenching and before ageing [35]

Conversely, the double ageing process employs rapid cooling and a lower initial ageing temperature, leading to the formation of metastable omega phases that act as nucleation sites for secondary α phases. This results in a finer and more uniformly distributed globular α phase within the β grains, as seen in Figure 16. This refined

microstructure correlates with a higher hardness value observed in double-aged samples compared to BASCA-treated ones.

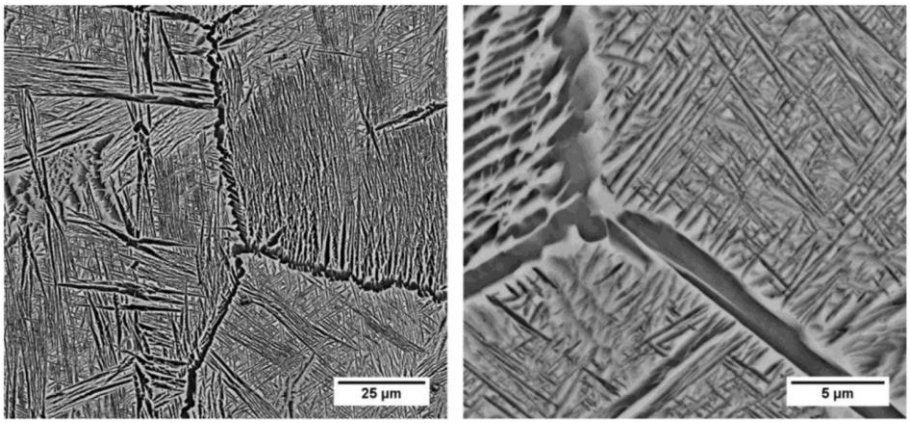

(a)

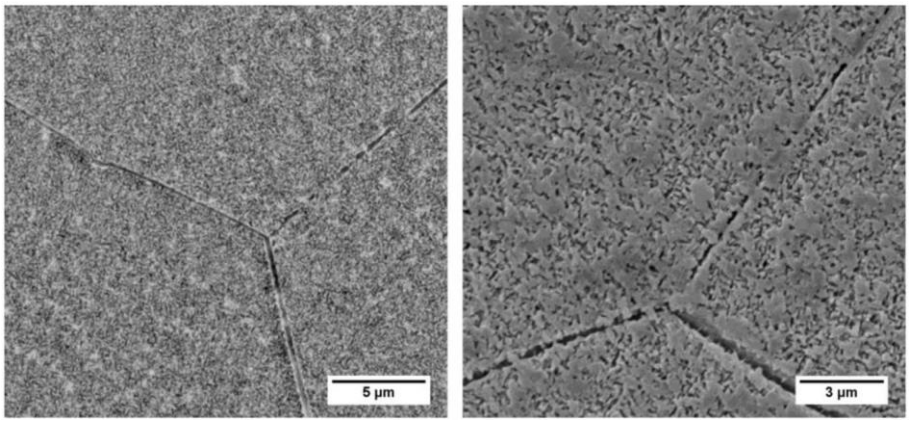

(b)

Figure 16: (a) SEM micrographs of Ti-5553 alloy treated through different heat treatment processes, BASCA and double ageing, captured at various magnifications: (a) BASCA microstructure (b) double aged microstructure [35]

Campanelli et al. also measured fatigue strength following the ISO 12107 standard and used Dixon-Mood statistics to determine fatigue limits [35]. Their results indicated that the double ageing process achieved a higher fatigue limit (708 MPa) compared to the BASCA process (658 MPa), with both conditions subjected to a consistent stress ratio of 0.1 and a 5×10^6 cycle count in fatigue tests (Figure 17). From a hardness point of view, the double ageing microstructure exhibited a higher hardness value of 467±10 HV than the BASCA microstructure's hardness value of 393±3 HV. This difference in hardness can be explained by the refinement of the microstructure achieved through the double ageing process.

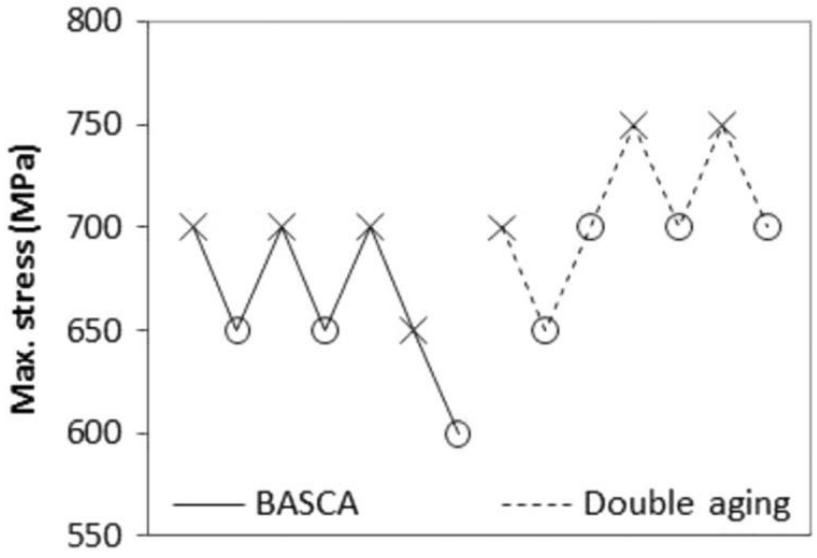

(a)

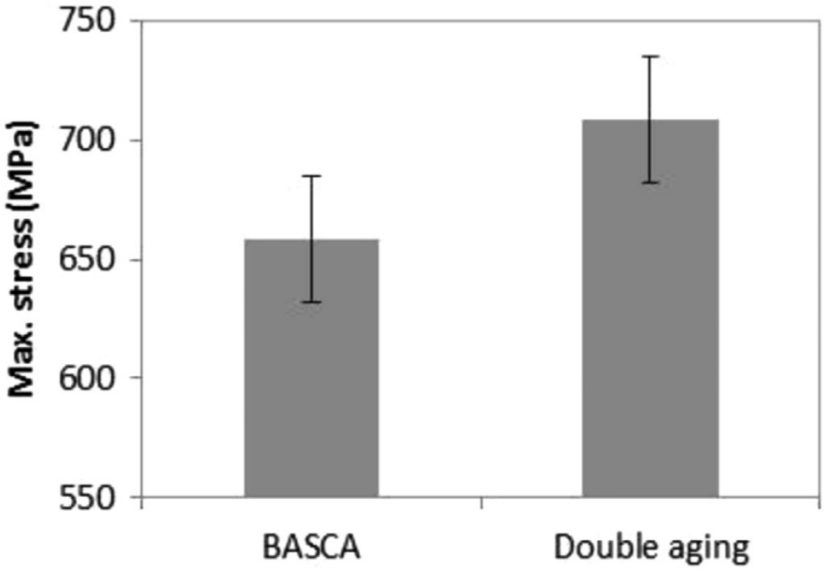

(b)

Figure 17: (a) Staircase results for 5×10^6 cycles endurance limits from BASCA and double ageing (b) Summary of the fatigue limit results for each condition [35]

The fracture surface analysis revealed differences in crack nucleation and propagation between the processes. For BASCA, cracks typically nucleated within α phases at grain boundaries, leading to transgranular fractures characterised by conventional fatigue crack features like striations and river patterns (Figure 18). In contrast, the double ageing process showed a dominance of transgranular fractures with shear lips and tear ridges, indicating a high degree of microstructural consistency across the fracture surfaces (Figure 19).

This study provides a deep insight into how heat treatment and α phase morphology influence the mechanical properties and fatigue behaviour of Ti5553, underlining the importance of microstructural control in enhancing the alloy's performance in demanding applications.

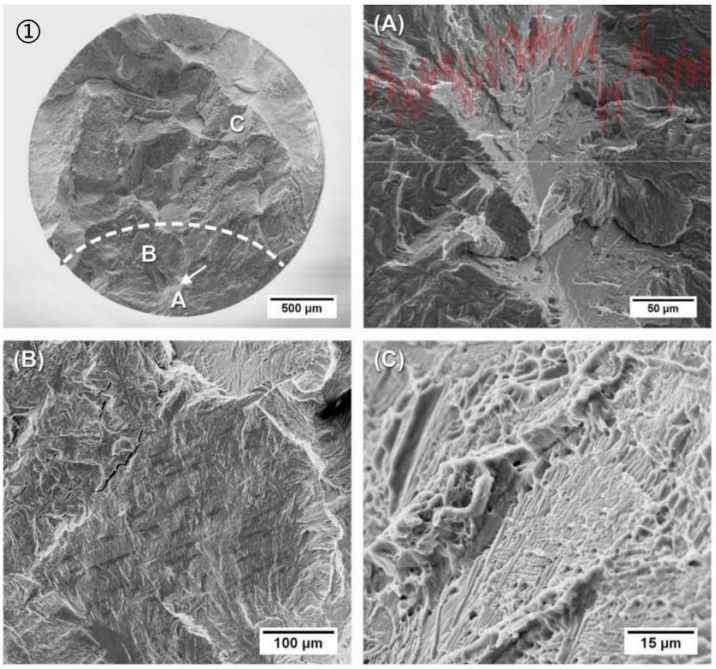

Figure 18: SEM micrographs of BASCA fracture surface. The upper right image contains the EDS line scan of Al content in the initiation region [35]

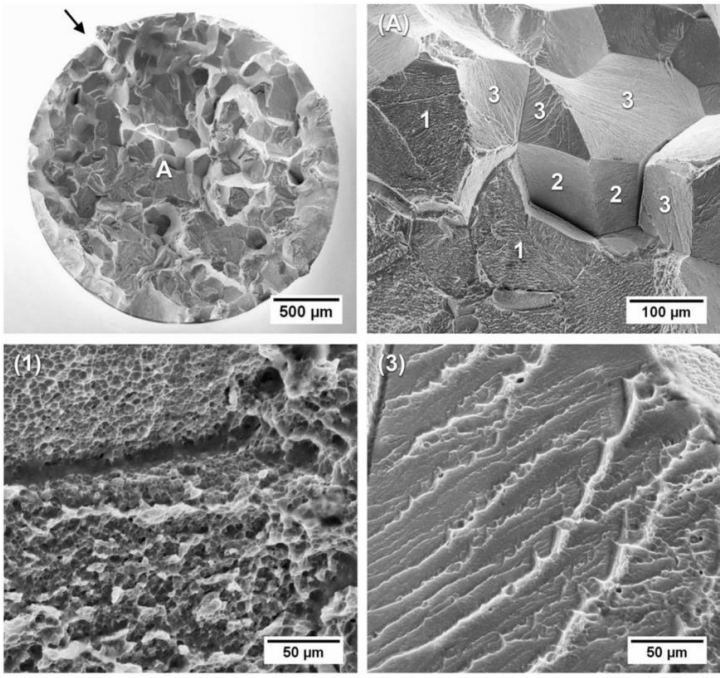

Figure 19: SEM micrographs of the double-aged fracture surface [35]

2.4 Critical Analysis and Gaps in Current Knowledge

The mechanical properties of Ti-5553 are significantly influenced by its microstructure, which is largely shaped by the heat treatment processes it undergoes. Among these processes, ageing treatment is crucial in determining the alloy's final properties, particularly by manipulating the α phase precipitations within the β matrix. Kar et al. have highlighted that the α phase volume fraction, which crucially determines the strength and ductility of the alloy, can be controlled by the parameters of heat treatment [36]. Specifically, the volume fraction of the α phase is dependent on the ageing temperature, which ranges from 450 to 700°C, and the heating rate applied to reach this temperature [37-39].

A vital aspect of ageing treatment is the heating rate, which has a profound impact on the microstructure and, consequently, the mechanical properties of the alloy. Slower heating rates often result in finer and more homogeneous α phase precipitations, thus enhancing the alloy's strength and fatigue behaviour. This microstructural refinement assists in obstructing dislocation movement, enhancing mechanical performance. However, the literature reveals a gap in comprehensive studies that correlate specific heating rates with precise microstructural outcomes, a deficiency that limits the development of optimised ageing processes for Ti-5553 alloys.

Moreover, while existing studies such as those by Jones et al. discuss the impact of heat treatments on the mechanical properties of Ti-5553, there is a notable absence of research integrating these findings into practical applications, especially in high-performance material-dependent industries like aerospace and automotive [8]. The optimisation of mechanical properties, particularly balancing strength, ductility, and toughness concerning specific ageing protocols, remains underexplored.

In summary, the research community has made significant strides in understanding the effects of heat treatments on Ti-5553. Yet, crucial aspects regarding optimising ageing heating rates and their impact on the microstructure remain underexplored. More detailed and targeted experimental studies could help refine the use of this alloy in critical applications, thus enhancing performance where it is most needed.

2.5 Conclusion of the Literature Review

Overall, the literature review establishes a solid foundation, demonstrating that the mechanical and fatigue properties of Ti-5553 can be optimised through specific heat treatments. However, to advance the application of Ti-5553 in demanding sectors such as aerospace, military, and industrial manufacturing, further research is needed to explore the effects of ageing treatments at varying heating rates on mechanical performance and fatigue behaviour. Such studies would not only address the current knowledge gap but also enhance our practical understanding of phase transformations and their impacts on material performance under operational conditions. This could lead to broader applications and significant advancements in materials engineering, benefiting both the scientific community and industry.

Chapter 3

3 Experimental Procedures

This chapter outlines the methodologies employed in the experimental investigation of this thesis. It begins with a brief description of the starting material's composition, processing history, and the extraction of samples specific to this study. The chapter then details the heat treatment conditions applied to the alloy, followed by the procedures for microstructural characterisation, including the techniques and equipment used for analysis. Additionally, it describes how mechanical testing was performed after extracting appropriate testing samples. The chapter concludes with a discussion of the analytical techniques and procedures utilised for the comprehensive evaluation of the alloy's properties.

3.1 Material

The material used in this thesis is Ti-5553 alloy, produced through ingot metallurgy. The alloy was received as part of a cogged billet, initially measuring 150 mm in diameter and 120 mm in height. The cogging process, a critical thermomechanical treatment, was applied to the billet to refine the microstructure and enhance the alloy's mechanical properties before further heat treatments. This process involved repeated deformation and cross-sectional reduction, which oriented the microstructure along the axial direction of the billet.

Blocks were extracted from the cogged billet for material characterisation and mechanical testing. These blocks were cut to dimensions of approximately 15 mm in thickness, 80 mm in width, and 120 mm in length using a wire-cut electronic discharge machine (EDM). The 120 mm length corresponds to the axial direction of the billet during cogging, and in this thesis, it is referred to as the longitudinal direction. The 80 mm width represents the direction perpendicular to the axial direction, referred to as the transverse direction. The subsequent experimental analysis and heat treatment processes detailed in this study were carried out on these blocks.

Table 3 outlines the primary alloying elements and their respective weight percentages, with titanium as the main constituent. X-ray Fluorescence (XRF) technique was employed to determine the elemental composition of Ti-5553 alloy.

Table 3: The nominal composition of the Ti-5553 alloy used in this study

Element	Composition (wt.%)
Aluminium (Al)	5.16
Molybdenum (Mo)	5.03
Vanadium (V)	5.01
Chromium (Cr)	3.10
Iron (Fe)	0.5
Titanium (Ti)	Balance

3.1.1 Heat Treatment

Four distinct heat treatments were employed to investigate their effects on the Ti-5553 alloy (Figure 20). Each treatment consisted of a common solution treatment step followed by an ageing step with varying heating rates. During the solution treatment, the material was heated to 810°C at a rate of 10°C/min, followed by a 2-hour isothermal hold. After this hold, the material was cooled to room temperature using ceramic blanket cooling to ensure a controlled cooling environment. This process was carried out in a muffle furnace to maintain consistent thermal exposure across all samples.

Following the solution treatment, the samples underwent an ageing process with four different heating rates. The samples were reheated to an ageing temperature of 610°C at rates of 1°C/min, 5°C/min, 10°C/min, and 15°C/min. Upon reaching 610°C, each sample was held isothermally for 8 hours, followed by air cooling to room temperature. This method was designed to produce variations in microstructure across the 120 mm x 80 mm x 15 mm blocks, which could influence the mechanical properties of the Ti-5553 alloy. For the remainder of this thesis, the terms Ageing Heating Rate (1°C/min), Ageing Heating Rate (5°C/min), Ageing Heating Rate (10°C/min), and Ageing Heating Rate (15°C/min) will be used to refer to the materials corresponding to each of these specific heat treatment conditions.

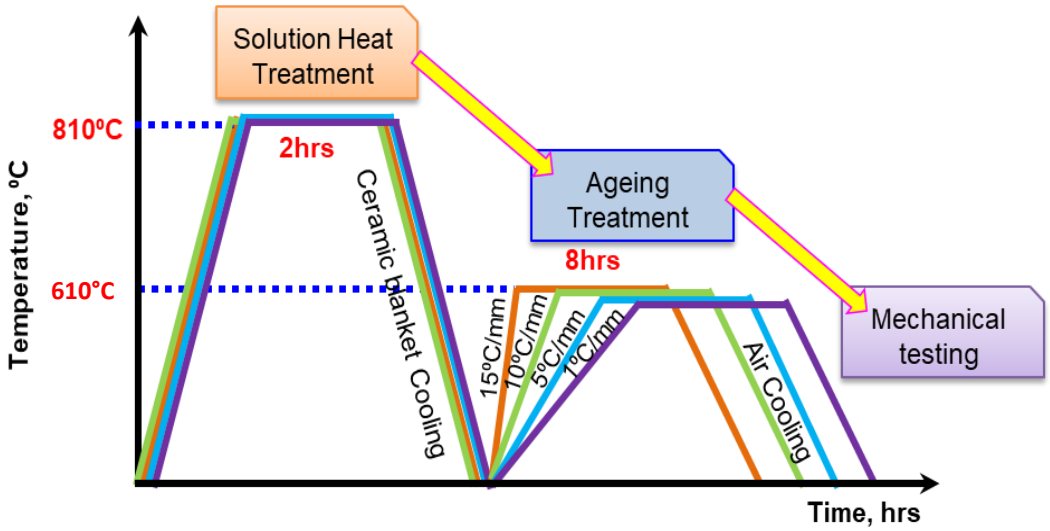

Figure 20: Schematic illustrating the time-temperature cycles for the solution treatment and the different ageing heating rates applied to the Ti-5553 alloy

3.1.2 Sample Extraction

Samples for microstructural analysis and various mechanical tests, including hardness, tensile, and fatigue, were carefully extracted from the blocks using EDM. The process began with material preparation for microstructural investigations, where slices were cut from the individual blocks. To observe microstructural evolution, 5 mm-thick slices were obtained from both the longitudinal and transverse directions (Figure 21). The longitudinal slices measured 120 mm x 80 mm x 5 mm, while the transverse slices measured 80 mm x 15 mm x 5 mm.

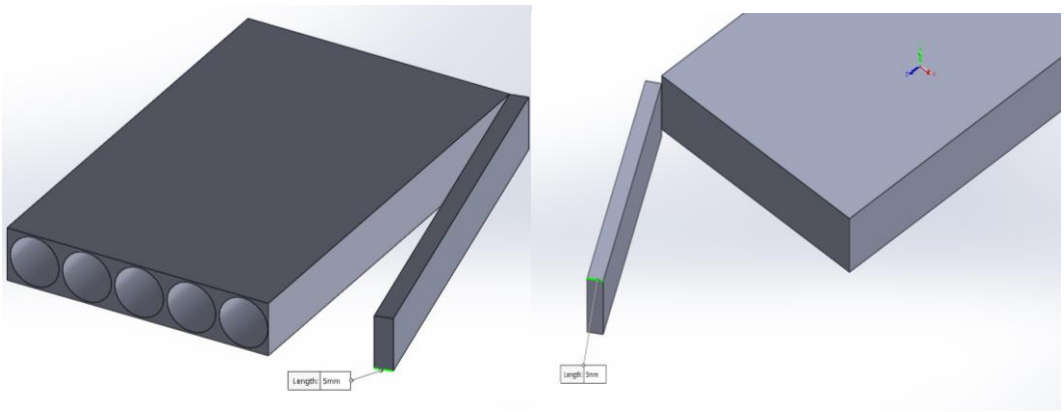

Figure 21: Diagram illustrating the extraction of 5 mm-thick slices for microstructure analysis from both the longitudinal (120 mm x 80 mm) and transverse (80 mm x 15 mm) directions of the Ti-5553 alloy blocks

For ease of microscopic sample preparation, the longitudinal slices were further divided into six equal segments, and the transverse slices were divided into four smaller pieces. Each sample's location was meticulously tracked to capture microstructural variations across the entire sample and to assess any anisotropy present within the material (Figure 22).

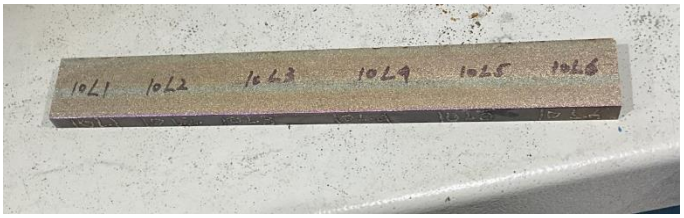

Figure 22: Sample labelling for tracking microstructural variations and assessing material anisotropy

The remaining block material was used to cut five cylindrical specimens for tensile and fatigue testing (Figure 23). Two cylinders were allocated for high-cycle fatigue testing, while the others were designated for tensile tests.

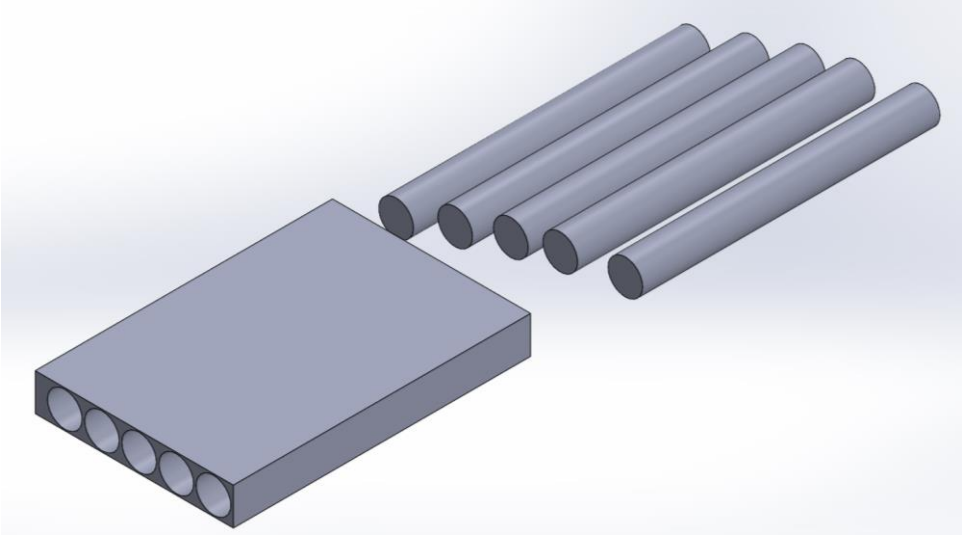

Figure 23: Diagram depicting the extraction of five cylindrical specimens for tensile and fatigue testing from the Ti-5553 block

During the wire-cutting process, it was crucial to frequently monitor the machine's voltage and current due to the high probability of the wire getting stuck, especially given the thickness of the blocks. This careful monitoring ensured the successful preparation of all samples without compromising their integrity.

3.2 Metallographic Sample Preparation

To prepare the Ti-5553 alloy samples for microstructural analysis, each sample was cut into 6 segments of 5 mm-thick slices in the longitudinal direction and 6 segments of 5 mm-thick slices in the transverse direction. These segments were then mounted in resin (Figure 24) to ensure their stability during the subsequent grinding, polishing, and imageing processes.

3.2.1 Mounting Process

The samples were mounted using a liquid mixture of epoxy resin and hardening agents in a ratio of 4:1. It is critical to ensure that these two components are thoroughly mixed to prevent inconsistencies in hardness and softness within the mounted samples. Once the mixture was homogenous, it was carefully poured into moulds containing the samples. The moulds were left overnight to allow the epoxy to harden completely, forming a solid mount that could withstand the mechanical stresses of polishing.

Figure 24: Microstructural samples of Ti-5553 alloy, segmented from 5 mm-thick longitudinal and transverse slices and mounted in resin

3.2.2 Grinding and Polishing

After the mounted samples had fully hardened, they were subjected to an initial grinding process to remove surface oxidation and achieve a flat, even surface suitable for metallographic analysis. Manual grinding was performed using 200, 350, 500 and 1000 grit silicon carbide (SiC) paper on a Struers RotoPol-21 manual

metallographic polisher. This step was essential for preparing the samples for subsequent polishing, further refining the surface.

Polishing was carried out using the Struers Tegramin-25 semi-automatic metallographic polisher (Figure 25). The samples were first polished with a 9µm diamond suspension to remove any remaining surface irregularities and scratches. This was followed by a final polishing step using a colloidal silica suspension (OP-S), which provided a mirror-like finish essential for high-quality optical and electron microscopy.

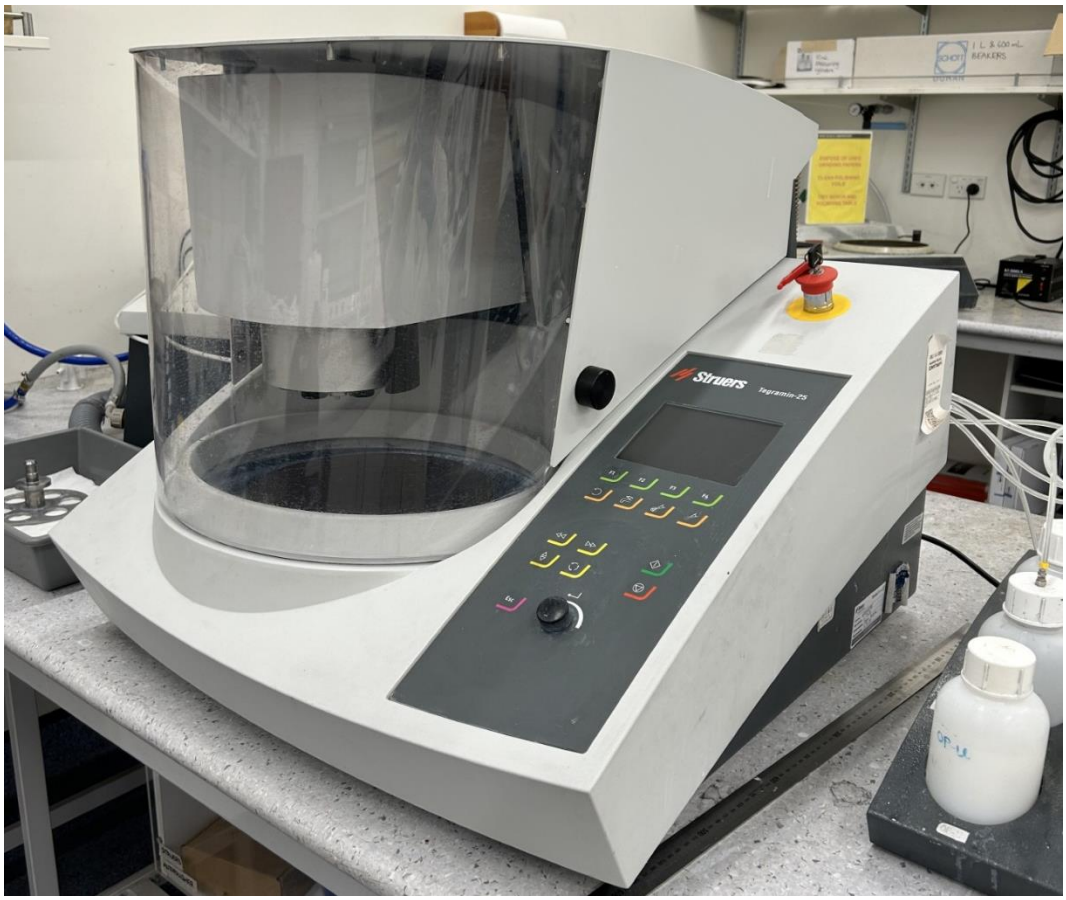

Figure 25: Struers Tegramin-25 semi-automatic metallographic grinder and polisher used for sample preparation

3.2.3 Etching

To enhance the visibility of the microstructural features, the polished samples were etched using Kroll's reagent, a chemical solution composed of 3% hydrofluoric acid

(HF), 10% nitric acid (HNO3), and distilled water. The samples were immersed in the etchant for 10-15 seconds, a process that selectively attacks certain microstructure phases, making them more distinguishable under microscopic examination.

3.3 Optical Microscopy

After etching, the samples were observed using an Olympus BX53 optical microscope (Figure 26) to gain a preliminary understanding of the microstructure under different heat treatment conditions. The optical microscope allowed for detailed observation of the metallographic morphology at various magnifications, including 50X, 100X, 200X, 500X, and 1000X. These magnifications provided a comprehensive view of the microstructural features, such as grain boundaries, phase distributions, and any anisotropies present within the material.

Figure 26: Olympus BX53 optical microscope used for microstructural analysis

3.4 Scanning Electron Microscopy (SEM)

Optical microscopy alone was insufficient for conducting a detailed analysis, particularly in characterising microstructural features highly sensitive to variations in heating rate during the ageing treatment. To overcome this limitation and to thoroughly investigate the microstructural differences between each condition, SEM was utilised. The SEM analysis was performed using a Hitachi S-4700 microscope (Figure 27), operating in both secondary electron (SE) mode for detailed topographical information and backscattered electron (BSE) mode for compositional contrast, which highlights differences in atomic number within the sample.

Figure 27: Hitachi S-4700 scanning electron microscope used for detailed microstructural analysis

To further investigate the microstructure, three SEM images at appropriate magnifications were analysed to measure the volume fractions and sizes of the globular primary α phases across selected samples, each subjected to different ageing heating rates. The analysis was conducted using Image J®, a widely used public-domain image processing software. The procedure in Image J® began by converting the SEM images to grayscale, enabling a clearer distinction between the

globular primary α phases and the surrounding matrix. Next, the images were thresholded to isolate the α phases, allowing for their differentiation from other microstructural features. The software's analysis tools were then employed to calculate the area percentages of this α phase, which were used to estimate their volume fractions. To measure the sizes of the globular primary α phases, the ruler tool within Image J® was utilised. This semi-manual approach involved selecting and measuring the dimensions of individual α phase features directly within the image. While this method provides valuable comparative data, it's important to note that these measurements are more suitable for relative comparisons rather than precise quantifications of microstructural features. This limitation should be considered when interpreting the results.

3.4.1 Energy Dispersive X-ray Spectroscopy (EDX) Analysis

In addition to SEM imageing, EDX analysis was employed to analyse the elemental distribution within the microstructure, providing insights into the effects of heat treatment on the Ti-5553 alloy (Figure 28). The EDX detector from Oxford Instruments, integrated with the SEM, enabled both the identification and mapping of elemental distributions across the microstructure. This technique was particularly valuable for assessing the chemical homogeneity and phase composition of the alloy, complementing the detailed microstructural observations obtained from SEM.

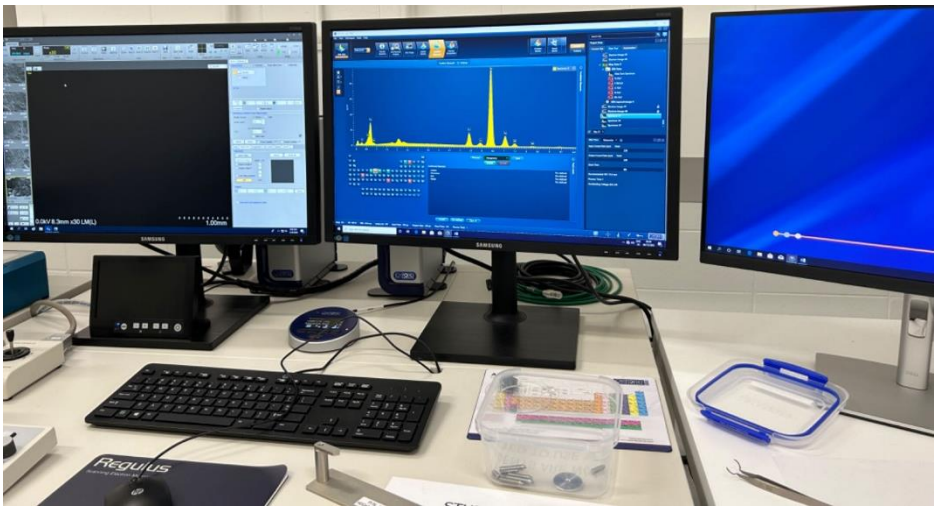

Figure 28: Software interface used for EDS analysis to perform elemental and chemical analysis

The elemental mapping focused on key elements Ti, Al, Mo, V, and Cr to evaluate how the different ageing heating rates influenced their distribution. In addition to mapping, semi-quantitative spot analysis was conducted at specific microstructural locations to obtain detailed elemental spectra. This analysis targeted critical microstructural features such as the globular primary α phase, grain boundary α phase, secondary α lamellar structure, and secondary α lath. Spectra were captured for each sample corresponding to the different ageing heating rates (1°C/min, 5°C/min, 10°C/min, 15°C/min), providing a comprehensive understanding of the elemental distribution and its correlation with the observed microstructural changes.

3.5 Mechanical Testing

3.5.1 Hardness Testing

Vickers hardness measurements were performed on the 5 mm-thick slices cut from the original blocks used for microstructural analysis. Before conducting the hardness tests, the target surfaces were meticulously prepared by grinding them to a 4000-grit finish and polishing them with OP-S gel. This preparation step was crucial to remove any oxide layers and residual stress, ensuring accurate hardness measurements. The hardness tests were carried out using a Leco FM-700 microhardness tester.

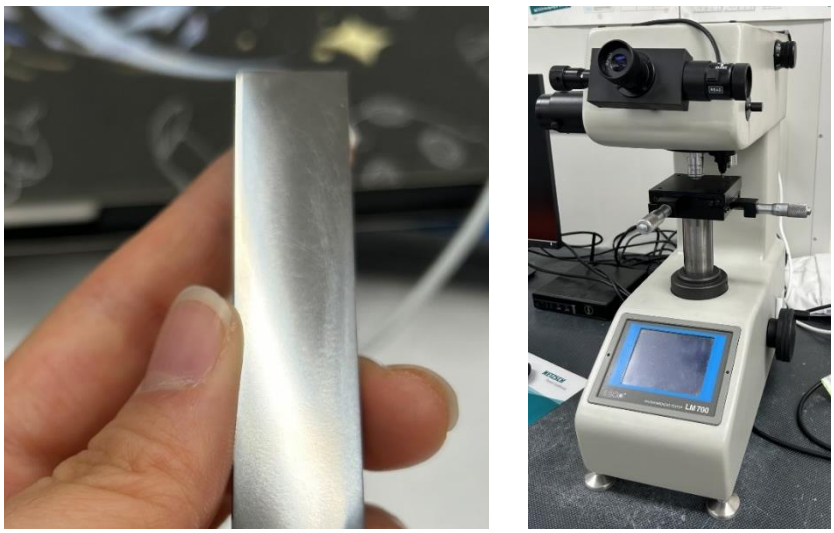

Figure 29: Polished sample and Leco FM-700 microhardness tester used for hardness measurement

To assess the effect of various ageing heating rates on hardness, a universal micro indentation hardness machine was employed with a 1000-g load and a dwell time of 10 seconds on each sample surface. Five indentations were made along a line on each sample, and the average hardness value, along with the standard deviation, was recorded to ensure the consistency and reliability of the results.

3.5.2 Tensile Testing

The tensile properties of the samples after heat treatments were evaluated in accordance with ASTM standard E8/E8M. To prepare the specimens, cylindrical cutouts obtained from the EDM process were machined into small-sized dog bone-shaped specimens. Each specimen was proportional to the standard tensile specimen, with a gauge length of 20 mm, a diameter of 6.007 mm, and a fillet radius of 6 mm at the corners. The ends of the specimen, located outside the gauge length, had a diameter of 8 mm and a suitable length to ensure a secure fit in the grips of the testing machine. The total length of each tensile specimen was 70.73 mm.

A lathe was used to machine the specimens to meet the required dimensions, as illustrated in Figure 30. The tensile tests were performed at room temperature using a 5982 INSTRON universal tensile testing machine equipped with a 100 kN load cell. A clip-on extensometer with a gauge length of 25 mm was used to measure strain. During the tensile testing, the strain rate was maintained at a constant 0.01/s. The samples were tested for fracture to obtain tensile properties under various heat treatment conditions.

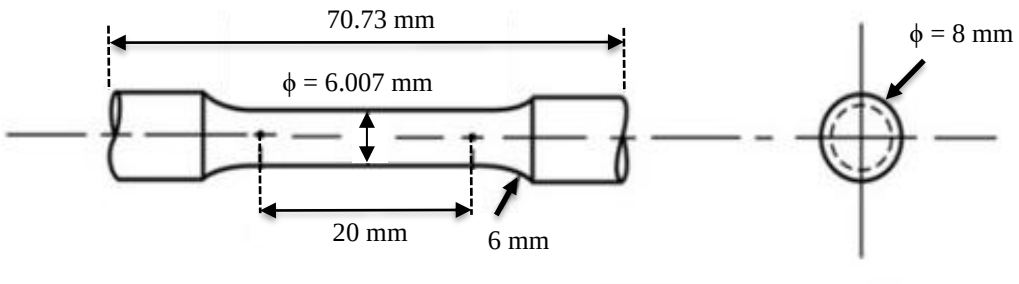

Figure 30: Dimensions of dog bone-shaped tensile samples

The raw data obtained from the tensile tests were recorded as load-extension curves.

This data was subsequently processed to calculate and plot both the engineering stress-strain curves and the true stress-strain flow curves. Engineering stress was calculated by dividing the applied load by the original cross-sectional area of the specimen (Equation 1). In contrast, engineering strain was determined by dividing the extension by the original gauge length (Equation 2).

$$\sigma = \frac{F}{A_0} \quad \text{Equation 1}$$

$$\varepsilon = \frac{\Delta L}{L_0} \quad \text{Equation 2}$$

where σ = engineering stress, F = applied load, A_0 = original cross-sectional area, ε = engineering strain, ΔL = change in gauge length, L_0 = original gauge length

To obtain the true stress-strain curve (also known as flow curves), the true stress was calculated by dividing the applied load by the instantaneous cross-sectional area of the specimen (Equation 3). In contrast, the true strain was determined by taking the natural logarithm of the change in length with respect to instantaneous gauge length (Equation 4).

$$\sigma_t = \frac{F}{A} = \sigma(e + 1) \quad \text{Equation 3}$$

$$\varepsilon_t = \int_{L_0}^{L} \frac{dL}{L} = \ln\frac{L}{L_0} = \ln(e + 1) \quad \text{Equation 4}$$

where σ_t = true stress, F = applied load, A = instantaneous cross-sectional area, ε_t = engineering strain, L = instantaneous gauge length, L_0 = original gauge length.

The tensile properties, including YS, UTS, and ductility, were derived from the processed data. YS was identified as the stress at which the material begins to deform plastically, typically using the 0.2% offset method on the engineering stress-strain curve. The UTS was determined as the maximum stress the material could withstand, represented by the peak stress on the engineering stress-strain curve.

Ductility was quantified by the elongation at fracture, indicated by the strain at the fracture point on the engineering stress-strain curve.

Figure 31: 5982 INSTRON universal tensile testing machine

3.5.3 Fatigue Testing

Two specimens were prepared for high-cycle fatigue testing, each featuring a 12 mm machined thread, as shown in Figure 32. These specimens were crafted from cylindrical cutouts obtained via the EDM process. To ensure precision in dimensions and a high-quality surface finish, the specimens were machined using computer numerical control (CNC) with carbide inserts. The material removal rate, or depth of cut, began at 0.5 mm/rev and was gradually reduced to 0.1 mm/rev during the final machining stages near the surface. A low feed rate was consistently maintained to minimise internal stress and achieve a lower surface roughness (Ra) value. The final machined specimens featured a uniform gauge length of 20 mm, a gauge diameter of 5 mm, and a total length of 90 mm, making them suitable for high-cycle fatigue testing.

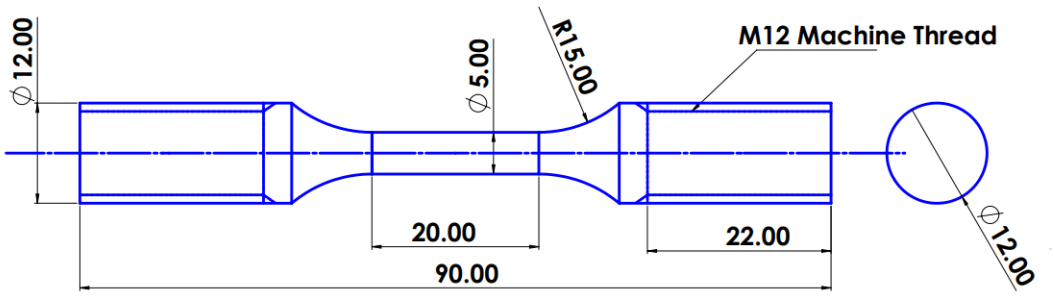

Figure 32: Schematic showing the dimensions of the high cycle fatigue test specimen

After machining, the specimens were uniformly polished in the gauge portion along the longitudinal direction to remove circular machining marks and achieve a smooth surface finish. The polishing process was manually performed using 500, 1000, 2000, and 4000 grit SiC paper. Each sample was subsequently examined using optical microscopy (Olympus BX 60) at 20X magnification to confirm the absence of circular lines or scratches. Figure 33 presents a representative example of the final prepared fatigue specimen.

Figure 33: High-cycle fatigue testing samples: original machined sample on the left and the same sample after polishing on the right

High-cycle fatigue testing was conducted in compliance with ASTM E466 standards, using sinusoidal stress control at a frequency of 40 Hz. The key parameter for each test was the maximum applied stress (P_{max}), determined based on the YS of the material under different heat treatment conditions. Using the stress ratio ($R = P_{min}/P_{max} = 0.1$), the minimum stress, mean stress and stress amplitude were calculated. The polished uniform gauge length specimens were loaded into an Instron 8801 Servo-hydraulic dynamic testing machine (Figure 34), with a stress ratio (R) of 0.1. The testing process was controlled via Wavematrix software to ensure the precise application of the loading conditions. An illustrative fatigue test cycle is shown in Figure 35.

Figure 34: Instron 8801 Servo-hydraulic dynamic testing machine used for fatigue testing

During testing, if a specimen reached 10^7 cycles without failure, the test was terminated, and the sample was considered unbroken. Given the limited number of test specimens available, any unbroken samples were subsequently retested at higher stress levels to further assess fatigue performance. After multiple tests, the fatigue limit under various conditions was determined. For the samples subjected to different ageing heating rates, the maximum stress levels were set as follows: for the 1°C/min ageing heating rate, the maximum stress levels were 750 MPa, 780

MPa, and 800 MPa; for the 5°C/min ageing heating rate, the maximum stress levels were 750 MPa and 700 MPa; for the 10°C/min ageing heating rate, the maximum stress levels were 750 MPa and 650 MPa; and for the 15°C/min ageing heating rate, the maximum stress levels were 600 MPa and 650 MPa. Upon completing the fatigue tests, S-N curves were constructed for each heat treatment condition, illustrating the relationship between maximum stress and the number of cycles on a logarithmic scale.

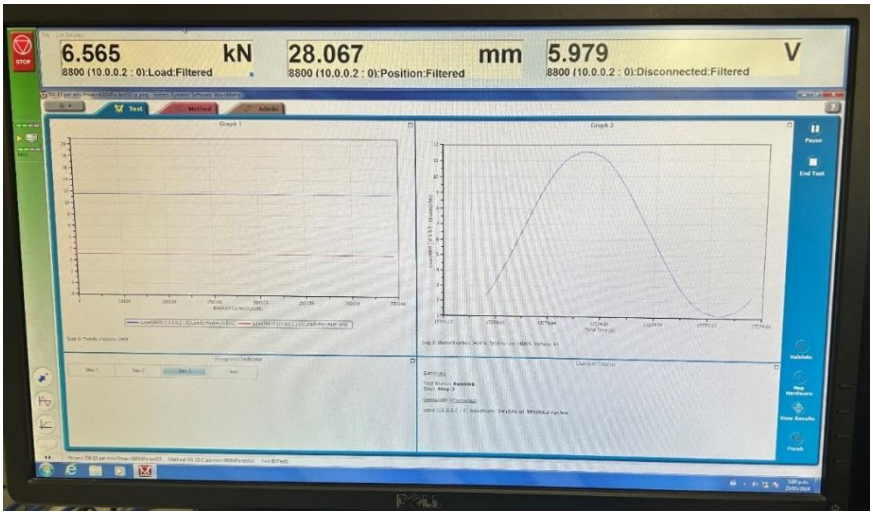

Figure 35: Illustrative fatigue test loading cycle

3.5.3.1 Fractography and crack path analysis of fatigue test specimens

Following the fatigue tests, the broken specimens were sectioned for detailed fracture analysis. Each specimen was sectioned along the testing direction to examine the vertical cross-section and identify the crack propagation path (Figure 36). The crack propagation paths were analysed using optical microscopy.

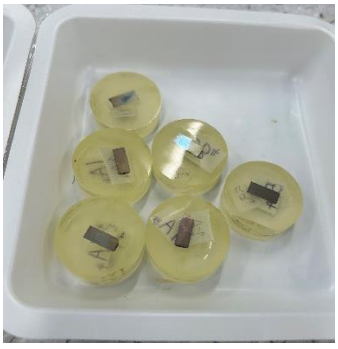

Figure 36: Fatigue crack path samples of Ti5553 alloy mounted in resin

Chapter 4

4 Results and Discussions

This chapter presents a comprehensive analysis of the microstructure and mechanical properties of the Ti-5553 alloy subjected to solutions and four different ageing heat treatment conditions. The chapter begins with a detailed microstructure investigation, utilising advanced characterisation techniques to reveal the phase transformations and grain structures that result from the various heat rates during ageing treatments. Following the microstructural analysis, the chapter reports the hardness measurements, providing insights into the material's resistance to localised plastic deformation under each condition. The alloy's strength and ductility are further explored through room-temperature tensile testing. High-cycle fatigue properties are also examined, focusing on the material's performance under cyclic loading. Additionally, a brief discussion of crack propagation behaviour in fatigue-tested samples is included to offer a deeper understanding of the failure mechanisms at play. The results are critically discussed in the context of existing literature, drawing connections between the microstructural features and the observed mechanical properties.

4.1 Microstructure

The following section presents the microstructure of the as-received alloy before any post-heat treatment, along with the microstructural changes resulting from each of the four different heat rates during the ageing process. Please note that due to time constraints, a detailed quantification of the microstructure was not possible, so a general comparison has been made.

4.1.1 Typical Microstructure of As-Received Ti-5553 Alloy

Figure 37 shows the typical bimodal microstructure of the Ti-5553 alloy in its as-received condition. The cogging process has shaped this microstructure, a forging technique that refines the alloy's grain structure. The micrographs reveal that the microstructure consists of globular primary α phase (α_p) within equiaxed β sub-grains, along with a fine secondary α lamellar structure (α_s lath). Additionally, a

continuous layer of grain boundary α phase (α_{GB}) is clearly visible around each grain.

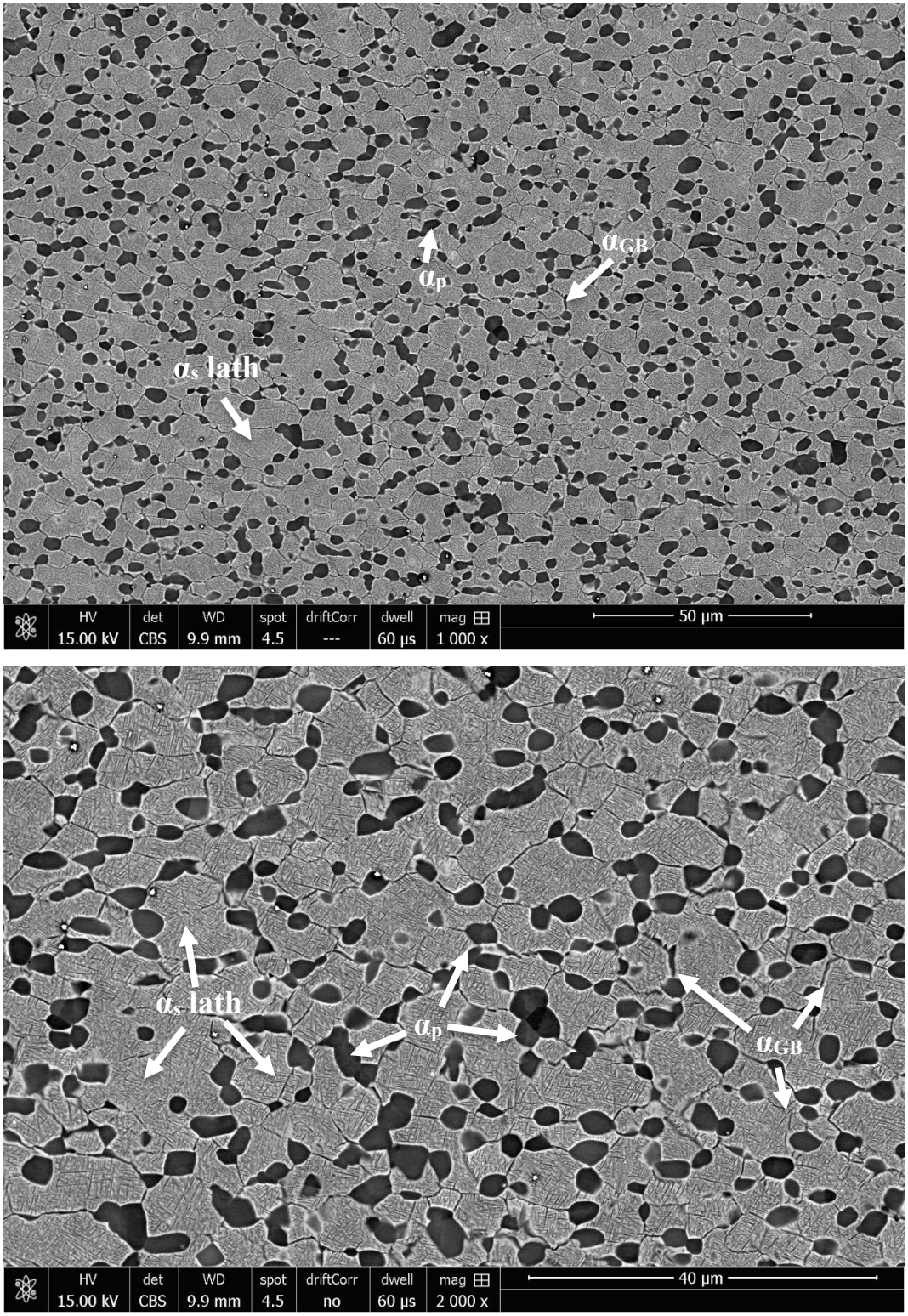

Figure 37: Fine bimodal microstructure of the Ti-5553 alloy in its as-received condition, after the cogging process

4.1.2 Typical Microstructure after Solution Treatment and Different Ageing Treatment

As shown in Figure 38, the Ti-5553 alloy blocks subjected to solution treatment and ageing conditions exhibit a typical bimodal microstructure. A comparison between the microstructure in its as-received condition (Figure 37) and after the heat treatments reveal some grain growth, although the equiaxed β sub-grains largely retain their shape. The globular primary α phase remains evenly distributed within the β matrix across all heat-treated conditions, with a noticeable increase in both its amount and size relative to the as-received microstructure. While all heat-treated microstructures show some changes in the secondary α lamellar structure compared to the as-received state, these low-magnification images do not fully capture the extent of these changes. A more detailed analysis of the secondary α lath structure will be provided in a later section of this thesis. Additionally, the grain boundary α phase appears to have undergone significant alterations, with the once continuous layer breaking down due to the varying heating rates applied during ageing. This indicates that the grain boundary α phase is less pronounced in the heat-treated microstructures.

Ageing heating rate (1°C/min)

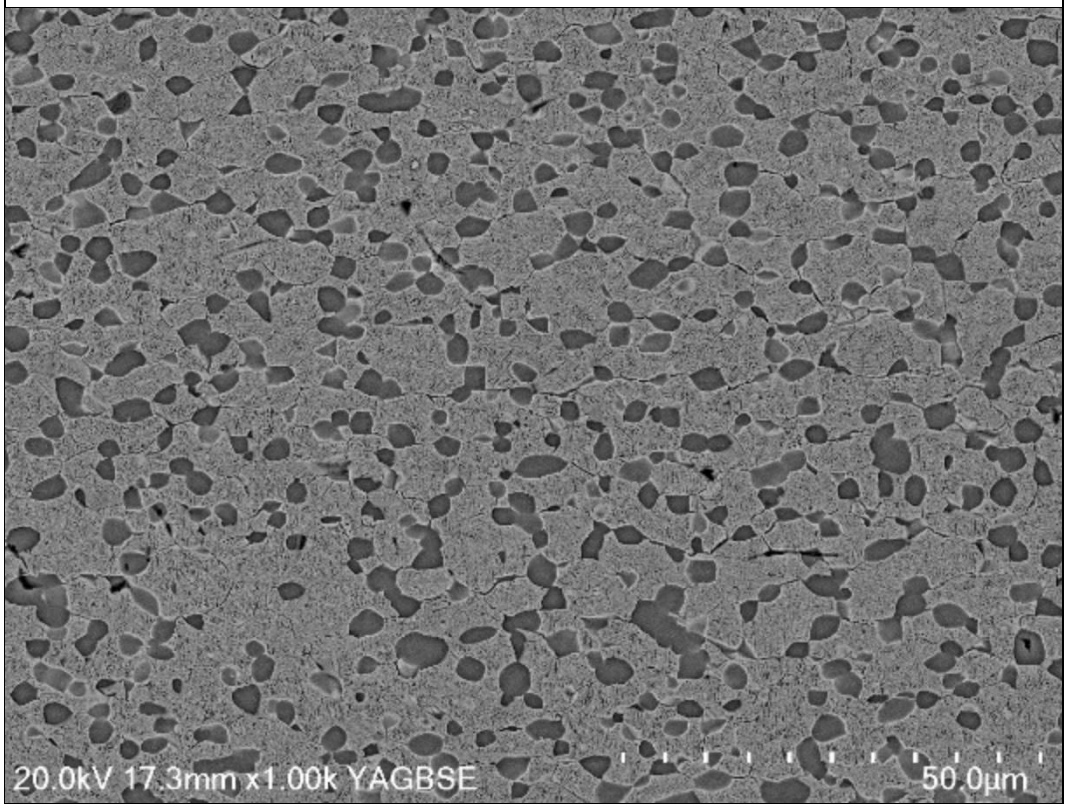

Ageing heating rate (5°C/min)
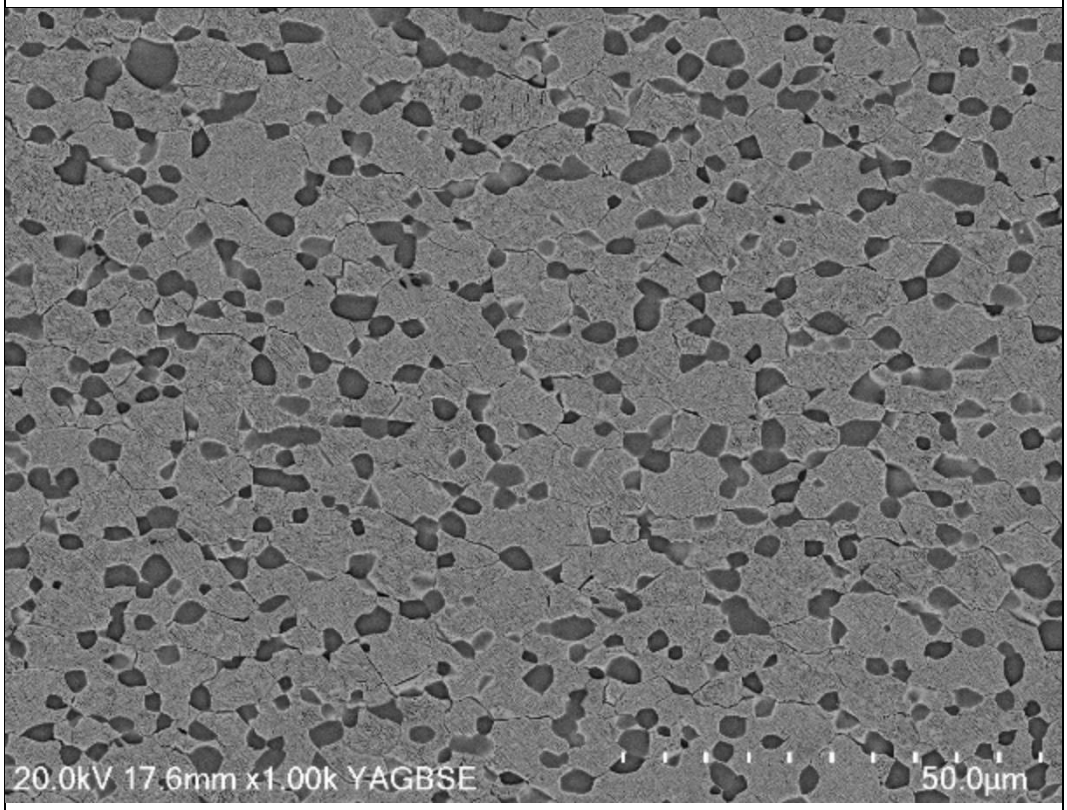
Ageing heating rate (10°C/min)
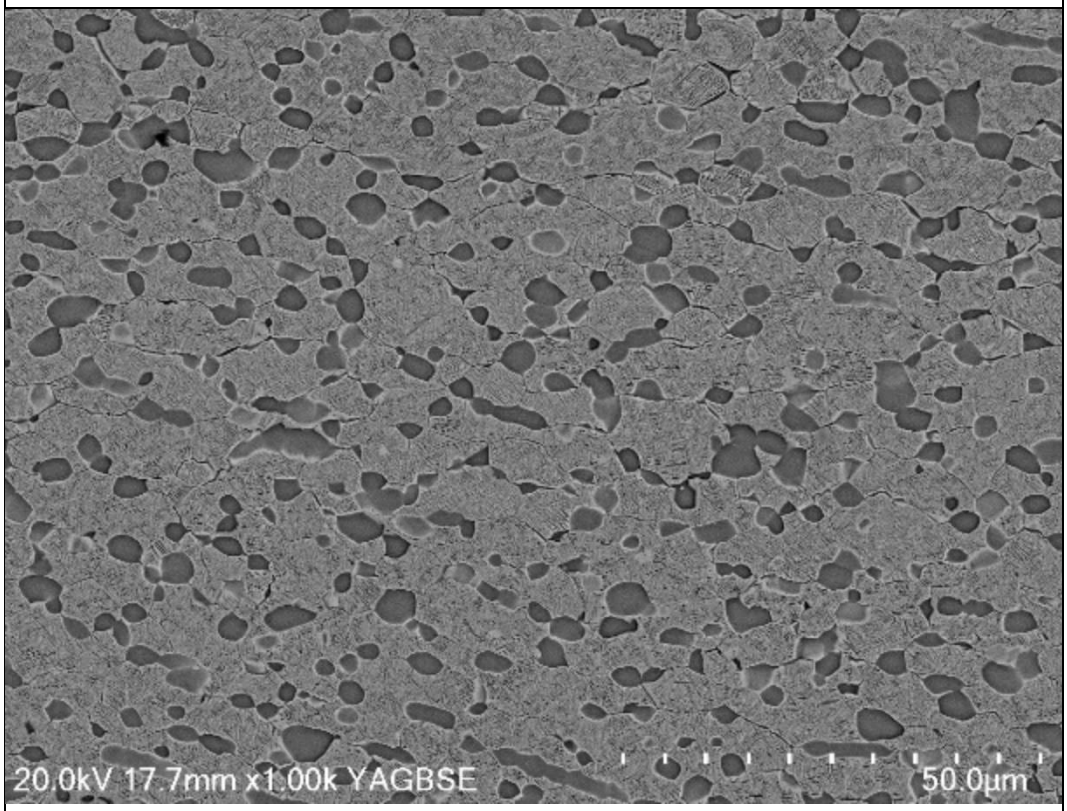

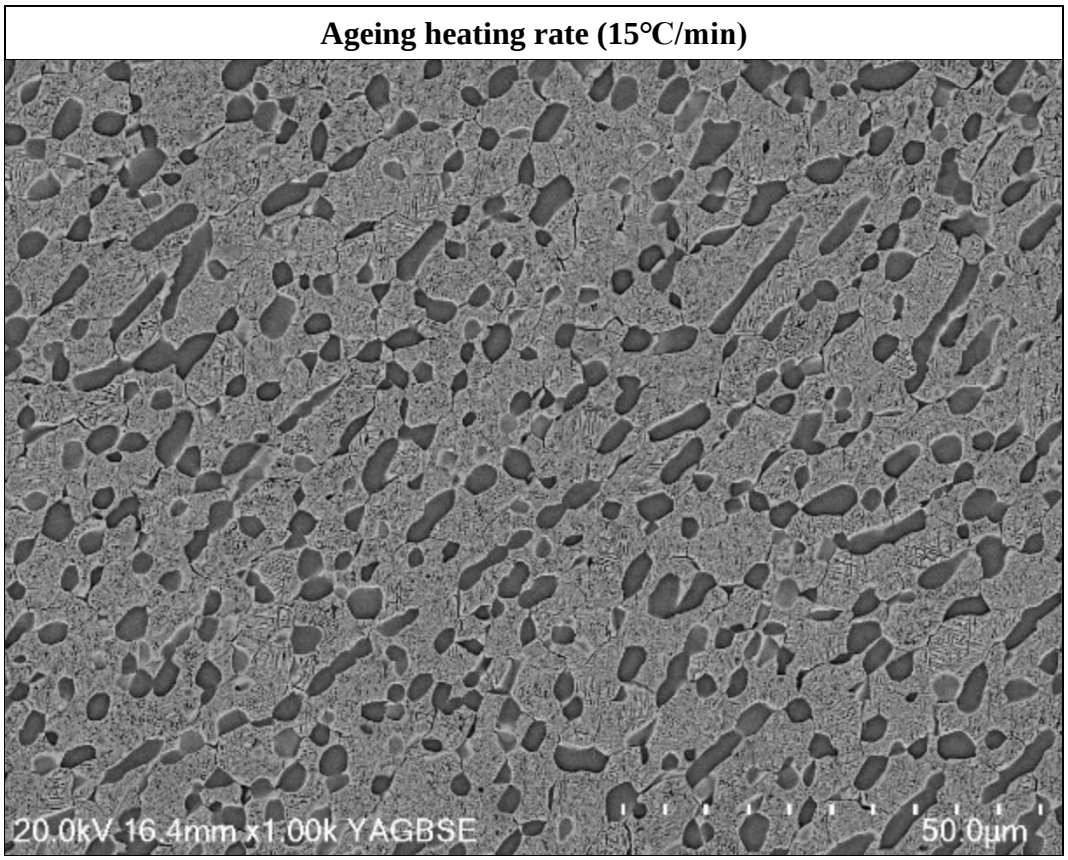

Figure 38: Typical bimodal microstructure of Ti-5553 alloy after solution treatment and various ageing treatments

The primary reason for the observed microstructural characteristics across all heat-treated conditions is the initial heat treatment stage, which includes solution treatment followed by ceramic blanket cooling. During the solution treatment at 810°C, which is within the α+β phase field, the microstructure of the Ti-5553 alloy typically develops as primary α particles dispersed within a β matrix. This observation is consistent with findings reported by Qingyun et al., who studied the microstructure of Ti-5553 alloy following a solution treatment at 815°C for 1.5 hours, followed by water quenching [40]. Their results revealed a bimodal microstructure consisting of equiaxed primary globular α particles (approximately 1-3 µm in size) within a β matrix, characterised by indistinct grain boundaries. This suggests that the solution treatment in the α+β field consistently produces a similar bimodal microstructure, irrespective of slight variations in temperature or treatment duration.

In the present study, after solution treatment, the samples were slowly cooled using

a ceramic blanket, an effective thermal insulator. This slow cooling process allows the primary α grains to grow significantly larger and also facilitates the precipitation of thin α layers around the β grain boundaries. The study by Jones et al. supports this conclusion, demonstrating that a slower cooling rate after solution treatment increases both the volume fraction and size of the primary α phase (3-5 μm) and promotes the formation of thin α layers at the grain boundaries [41]. This is attributed to the extended time available for diffusion during slow cooling, which provides the necessary driving force for the growth of globular α and the precipitation of grain boundary α [42].

While the initial solution treatment and slow cooling significantly influence the formation of the primary α phase and grain boundary α, the ageing process plays a critical role in refining and stabilising the microstructure. Different heat rates during ageing result in variable diffusion rates, phase transformations, and precipitation behaviours, all of which directly impact the microstructural features as observed in this study. Previous research has shown that the optimal ageing heat rate depends on the desired balance between strength and ductility in titanium alloys [43]. For example, Contrepois et al. demonstrated that intermediate ageing rates often provide a good balance, promoting a fine secondary α phase while maintaining sufficient grain boundary integrity [44]. The findings of this study align with current observations, suggesting that the chosen ageing heat rate has a direct impact on the resulting microstructure and, consequently, the mechanical performance of the alloy.

4.1.3 Microstructural Anisotropy after Heat Treatments - Comparison Between Longitudinal and Transverse Directions

The evaluation of microstructural anisotropy after heat treatments is critical, particularly for materials that have undergone significant deformation processes, such as the cogging process used in the initial preparation of the Ti-5553 alloy. The cogging process, involving repeated deformation and cross-sectional reduction, can potentially introduce directional variations in the microstructure, impacting the material's mechanical properties and overall performance. To assess the presence of any microstructural anisotropy in the Ti-5553 alloy post-heat treatment, identical

locations on each heat-treated sample were examined in detail. Both the longitudinal and transverse directions were analysed using Optical Microscopy and SEM, with micrographs captured at various magnifications to comprehensively assess any anisotropy. The micrographs included in the appendix provide a thorough visual comparison, while typical SEM images from each direction are presented in Figure 39.

Ageing heating rate (1°C/min)	
Longitudinal Direction	Transverse Direction
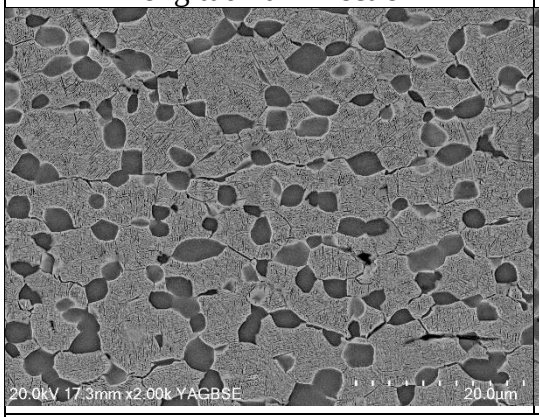	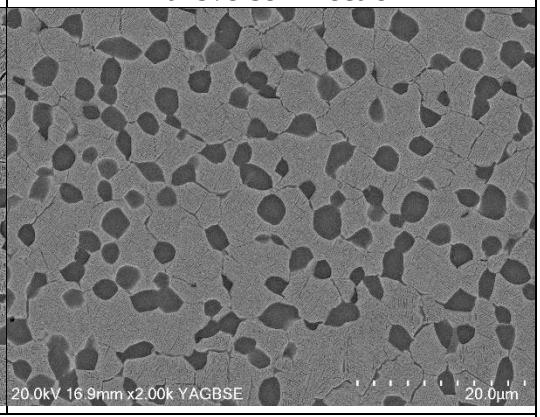
Ageing heating rate (5°C/min)	
Longitudinal Direction	Transverse Direction
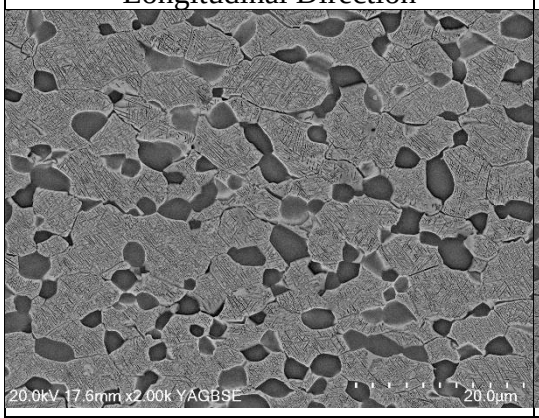	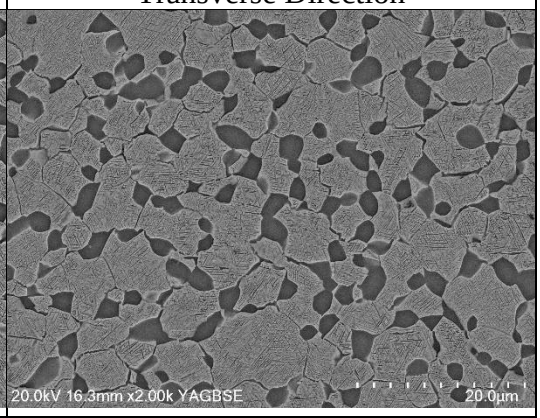
Ageing heating rate (10°C/min)	
Longitudinal Direction	Transverse Direction
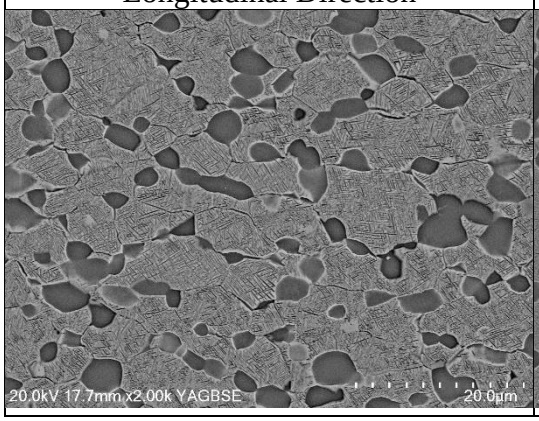	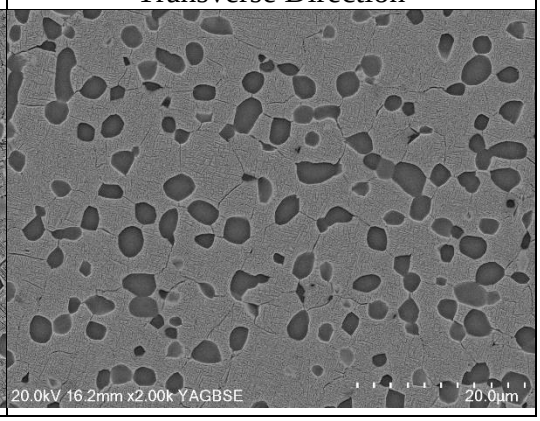

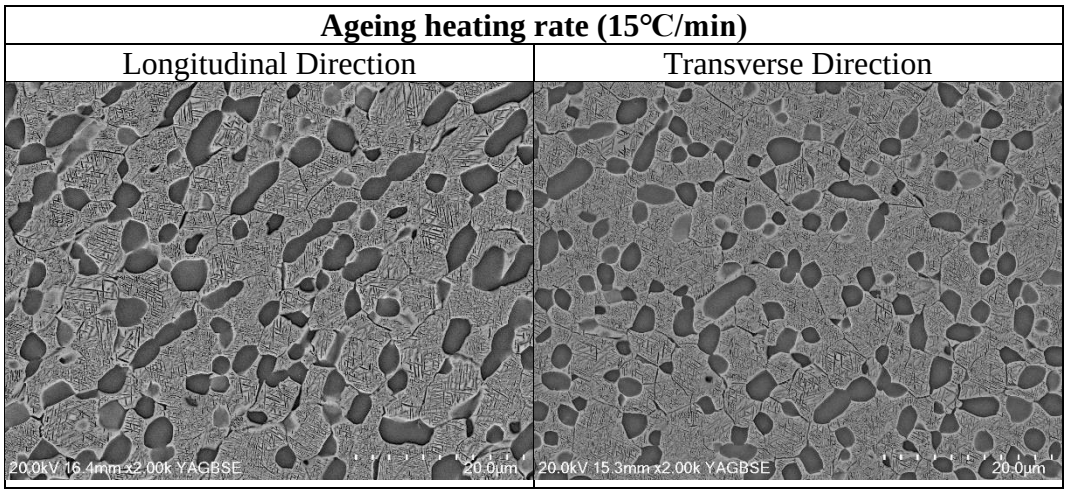

Figure 39: Microstructure variations in both longitudinal and transverse directions for each condition, observed under SEM at the same position

The analysis reveals a consistent bimodal microstructure across both longitudinal and transverse directions for all samples. Key microstructural features, including grain size and shape, the distribution of globular primary α phase, secondary α lamellar structure, and the grain boundary α phase, remain uniform in both directions. This consistency indicates that, despite the potential for anisotropy introduced by the cogging process, the heat treatments applied were effective in maintaining a homogeneous microstructure across the sample. In other words, these findings suggest that the Ti-5553 alloy retains a uniform microstructure across different directions after heat treatment, mitigating any potential anisotropy that could have arisen from the initial cogging process.

4.1.4 Microstructural Homogeneity after Heat Treatments - Variation Across the Samples

Similarly, understanding the microstructural homogeneity across the entire cross-section of a material is essential. To evaluate this in the Ti-5553 alloy after each heat treatment condition, the length of the individual samples was segmented into six parts. Each segment was then analysed using optical microscopy, with typical micrographs captured at various magnifications, which are included in the Appendix for a comprehensive evaluation of any variations. Selected micrographs at 1000x magnification are displayed in Figure 40 to provide a detailed view of the

microstructure across different regions of each sample after the different ageing heating rates.

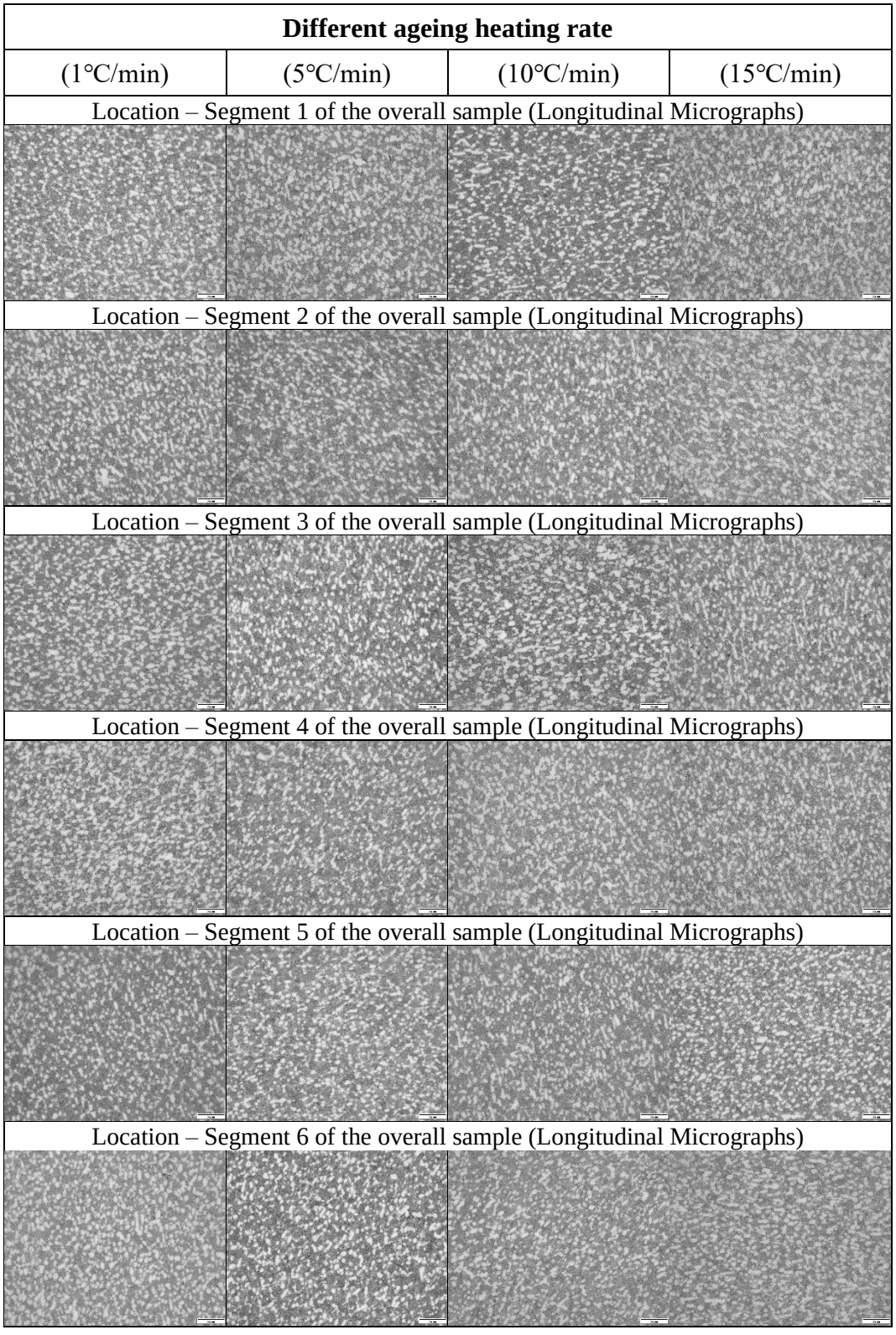

Figure 40: Optical micrographs illustrating microstructural homogeneity along the length of Ti-5553 alloy samples in the longitudinal direction after heat treatments

The optical micrographs for each condition reveal a high degree of similarity in the microstructure across all segments. The microstructure consistently shows a homogeneous distribution of globular α phase within the β matrix, indicating that any potential effects of the cogging process were effectively mitigated by the solution and ageing treatments, resulting in significant microstructural homogeneity. Overall, the findings suggest that the applied heat treatments did not significantly alter the microstructural homogeneity of the samples. However, subtle changes may be introduced to key microstructural features. A detailed analysis of these slight differences, which could have implications for the material's performance, will be elaborated upon in the next section.

4.1.5 Changes in microstructure due to different ageing heating rates

In the following section, we will compare the globular primary α phase, the size of equiaxed β sub-grains, the secondary α lamellar structure, and the grain boundary α phase morphology across the different heat-treated conditions. The analysis suggests that the varying ageing heating rates (1°C/min, 5°C/min, 10°C/min, and 15°C/min) have a noticeable impact on the overall morphology of the bimodal microstructure in the Ti-5553 alloy. Specifically, a very slow heating rate during ageing (1°C/min) appears to produce finer microstructural features and a more homogeneous distribution of precipitates. This observation is consistent with previous research further supporting the influence of heating rate on microstructural refinement [44].

4.1.5.1 Changes in Grain Size and Shape

Upon comparing the size and shape of equiaxed β sub-grains across the different ageing heating rates, a slight increase in grain size is observed; however, these changes are not significant (Figure 41). Notably, with increasing ageing heat rates, some grains exhibit more elongation or distortion, suggesting a minor impact on grain shape. This limited variation can likely be attributed to the ageing temperature of 610°C, which does not significantly accelerate grain growth kinetics. At this temperature, the movement of grain boundaries and the process of grain coalescence are constrained, preventing substantial grain growth. Overall, it can be stated that the impact of ageing heat rate on grain morphology is relatively minor.

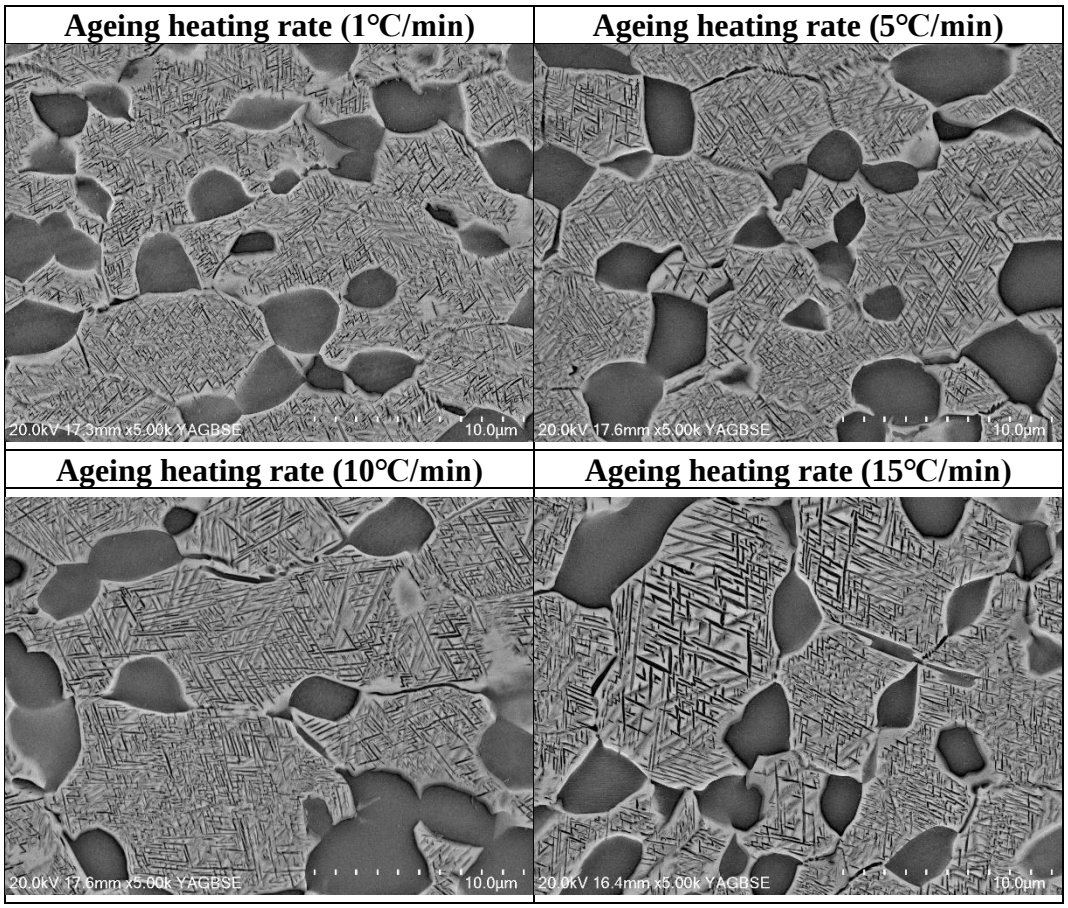

Figure 41: Variations in grain size and shape of equiaxed β sub-grains across different ageing heating rates

4.1.5.2 Changes in primary α phase morphology and distribution

Figure 42 illustrates the variations in the morphology and distribution of the primary α phase in the Ti-5553 alloy resulting from different ageing heating rates. It is evidence that the primary α phase remains uniformly distributed across all ageing heating rates, with no signs of concentration in specific areas. However, when comparing the morphology and distribution of the primary α phase at different ageing heating rates, it becomes evident that reduced ageing heating rates lead to finer and more homogeneous precipitates. At lower ageing heating rates, such as 1°C/min, the Primary α phase is more globular or round, indicating a more controlled and uniform precipitation process. In contrast, as the ageing heating rate increases, the morphology of the primary α phase becomes more elongated, with a noticeable coalescence of different precipitates. This change in morphology

suggests that higher ageing heating rates accelerate the growth and merging of α phase particles.

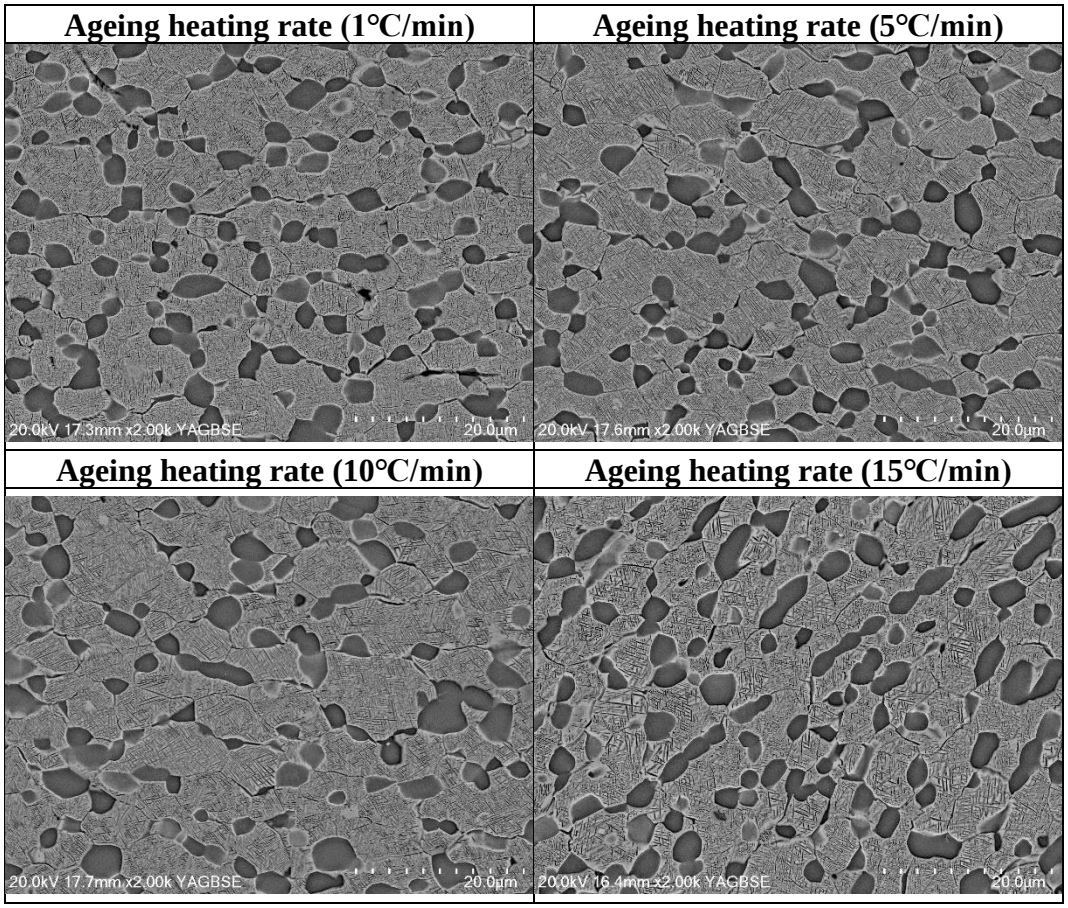

Figure 42: Variations in primary α phase morphology and distribution across different ageing heating rates

The results of the quantitative analysis revealed that the volume fraction of the globular primary α phase was observed to increase consistently with the increase in the ageing heating rate (Table 4). However, it is worth noting that the overall increase is rather limited. Specifically, at the lowest ageing heating rate of 1°C/min, the volume fraction was recorded at 25.4%. As the ageing heating rate increased to 5°C/min, there was a slight rise in the volume fraction to 25.8%. Further increases in the ageing heating rate to 10°C/min and 15°C/min resulted in volume fractions of 26.1% and 26.3%, respectively. These findings suggest a direct correlation between the ageing heating rate and the extent of α phase formation, with higher rates facilitating a slightly greater volume fraction of this phase.

Table 4: Volume fractions of the globular primary α phase (%) at different ageing heating rates

Sample	Volume fractions of the globular primary α phase (%)
Ageing Heating Rate (1°C/min)	25.4
Ageing Heating Rate (5°C/min)	25.8
Ageing Heating Rate (10°C/min	26.1
Ageing Heating Rate (15°C/min)	26.3

Similarly, the minimum and maximum sizes of the globular primary α phase were also influenced by the ageing heating rate. At an ageing heating rate of 1°C/min, the minimum size was 0.37 μm, while the maximum size was 7.5 μm. As the ageing heating rate increased to 5°C/min, the minimum size grew to 0.42 μm, and the maximum size increased to 7.8 μm. At 10°C/min, the minimum size was slightly reduced to 0.41 μm, with a corresponding decrease in the maximum size to 7.67 μm. Finally, at the highest ageing heating rate of 15°C/min, both the minimum and maximum sizes of the globular primary α phase increased to 0.43 μm and 8.07 μm, respectively.

Table 5: Sizes of the globular primary α phase (μm) under various ageing heating rates

Sample	Minimum size of globular primary α phase (μm)	Maximum size of globular primary α phase (μm)
Ageing Heating Rate (1°C/min)	0.37	7.5
Ageing Heating Rate (5°C/min)	0.42	7.8
Ageing Heating Rate (10°C/min	0.41	7.67
Ageing Heating Rate (15°C/min)	0.43	8.07

4.1.5.3 Changes in Secondary α Lamellar Structure

Figure 43 illustrates the variations in the secondary α lamellar structure across different ageing heating rates in the Ti-5553 alloy. It is evident that the secondary α lamellae are somewhat sensitive to the ageing heating rate. Slower ageing heating rates (1℃/min and 5℃/min) result in finer, more closely spaced lamellae with a needle-like morphology, likely due to the extended diffusion time at 610°C, which facilitates more controlled and gradual phase development. In contrast, faster-ageing heating rates (10℃/min and 15℃/min) produce coarser plate-like α lamellae as the rapid increase in temperature shortens the diffusion period, limiting refinement. These observations highlight the crucial role of the ageing heating rate in determining the fineness and uniformity of the secondary α structure, with slower rates promoting a more refined microstructure and faster rates leading to coarser formations. Overall, the secondary α phase consistently encapsulates the primary α phase in the same manner across all cases, regardless of the ageing heating rate.

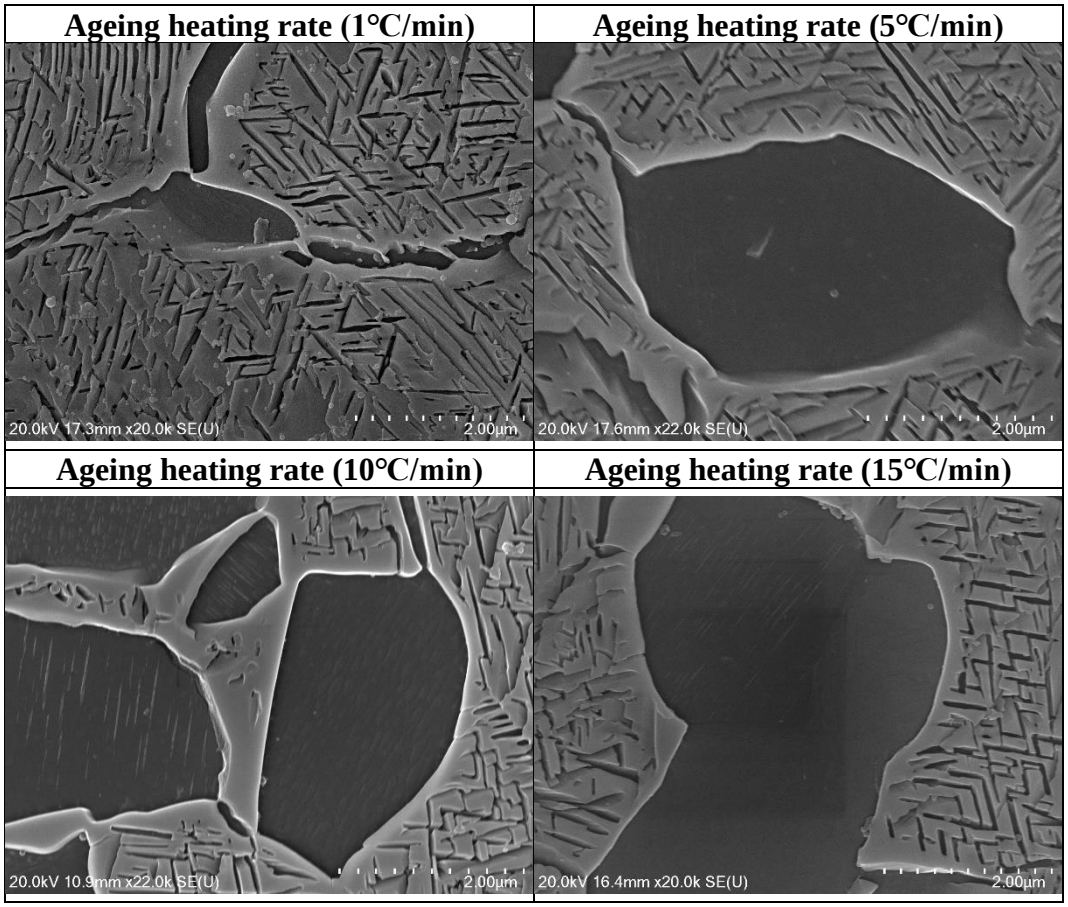

Figure 43: Variations in secondary α lamellar structure across different ageing heating rates

4.1.5.4 Changes in Grain Boundary α Phase

The grain boundary α phase in the Ti-5553 alloy is reasonably sensitive to the ageing heating rate, as displayed in Figure 44. Slower rates (1°C/min and 5°C/min) result in a more continuous, thick, and pronounced layer along the grain boundaries due to the prolonged diffusion time, which allows the α phase to fully develop and stabilise. As the ageing heating rate increases (10°C/min and 15°C/min), the thickness of the grain boundary α phase decreases, and its continuity becomes disrupted, leading to a more fragmented structure. This disruption is likely due to the reduced time for diffusion and phase stabilisation at higher ageing heating rates. The integrity of the grain boundary α phase is crucial for the alloy's mechanical properties, as a continuous layer enhances resistance to grain boundary sliding and crack initiation, whereas a fragmented structure may compromise these properties, potentially reducing the alloy's performance in applications requiring high structural integrity [45].

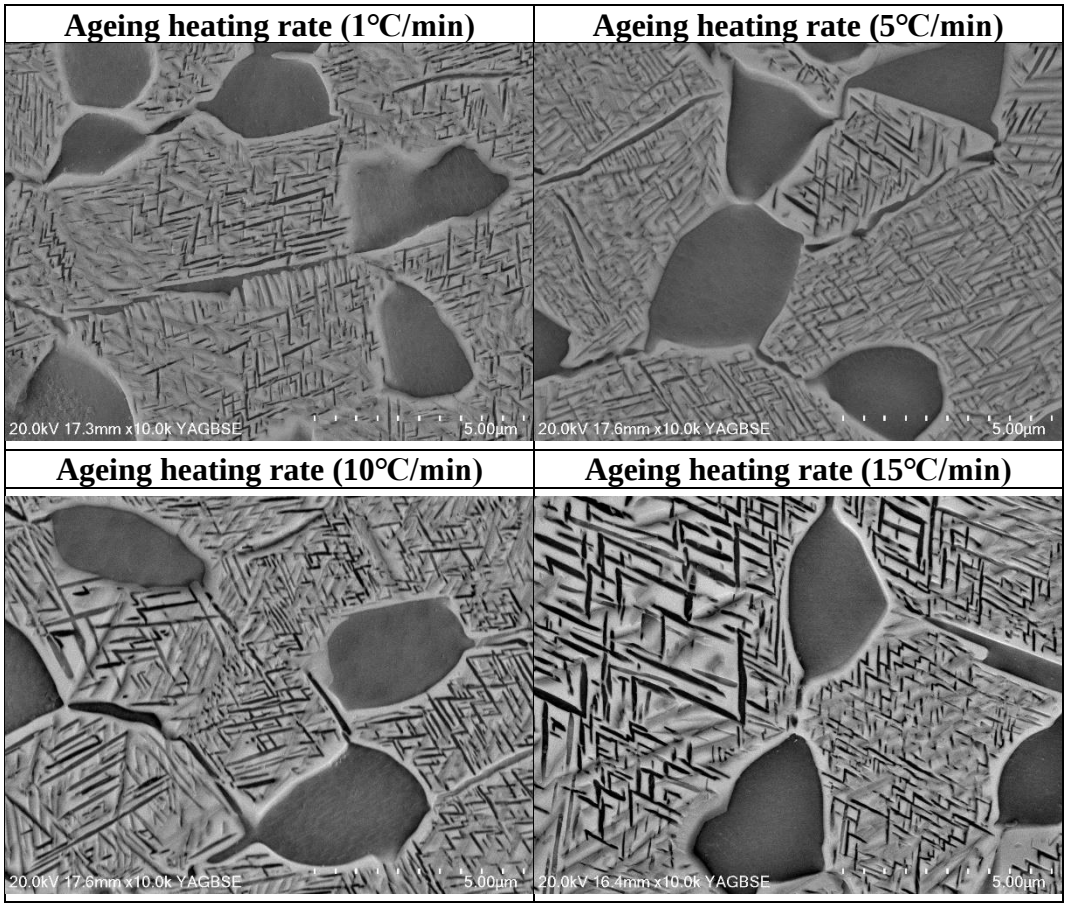

Figure 44: Variations in α phase layer along the grain boundaries across different ageing heating rates

In summary, the microstructural changes observed in the Ti-5553 alloy under varying ageing heating rates align closely with existing literature, which emphasises the importance of intermediate phase formation and diffusion kinetics. Our findings reveal that faster ageing heating rates, such as 15℃/min, lead to coarser α lamellae within some β grains, while slower rates (1℃/min, 5℃/min, and 10℃/min) result in finer, more uniformly arranged α lamellae. This observation is consistent with previous studies that highlight the role of ageing heating rates in the formation of intermediate phases, such as the ω phase, which serve as nucleation sites for α precipitation [44, 46]. The extended time at slower ageing heating rates facilitates ω phase formation, promoting a denser and more refined lamellar structure due to the increased number of nucleation sites. In contrast, faster-ageing heating rates limit ω formation, allowing α lamellae to grow larger and coarser within the β matrix. Additionally, the results from Zhao et al. indicate that the primary α phase in their study exhibits a significantly smaller size compared to that observed in this study [40]. This difference is likely due to the slower cooling process in the present study, which provides ample time for the growth of the primary α phase.

Moreover, our observations indicate that while the primary α phase remains uniformly distributed across different ageing heating rates, its morphology is influenced by the rate of heating. Slower ageing heating rates produce more globular and homogeneously distributed primary α particles, whereas faster ageing heating rates result in larger, more elongated α particles. This trend supports the findings of Sangali et al., who suggested that reduced ω phase formation at higher ageing heating rates leads to fewer nucleation sites, allowing the α particles to grow larger and coarser [43]. Additionally, it is observed that as the ageing heating rate increases, the grain boundary α phase becomes thinner and more fragmented, potentially weakening the material's resistance to grain boundary sliding and crack initiation. This finding is consistent with Contrepois et al. that slower ageing heating rates promote a more stable and continuous grain boundary α phase, while faster rates disrupt its formation [44].

Finally, the changes in grain size and shape following heat treatment may also be influenced by the initial microstructure. As highlighted by Settefrati et al., the presence of the primary α phase before ageing can alter the phase transformation

pathway, leading to different microstructural outcomes even under the same heating conditions. For instance, a β-solutionised microstructure may result in more significant α formation during ageing, while a structure containing some primary α phase may suppress intermediate phase formation, leading to different α morphologies [46].

4.1.6 Chemical Homogeneity after heat treatments - Element distribution

Assessing the chemical homogeneity of the Ti-5553 alloy after heat treatments is critical for understanding the stability and consistency of its microstructure. Ti-5553 is a complex alloy comprising 5 wt.% Al, 5 wt.% Mo, 5 wt.% V, and 3 wt.% Cr, where Mo, V, and Cr act as β-stabilisers, and Al serves as an α-stabiliser. The distribution of these elements within the microstructure is key in determining phase stability, mechanical properties, and overall alloy performance.

Figure 45 presents the EDX elemental mapping results used to evaluate chemical homogeneity across the heat-treated samples. The data clearly show that the distribution of elements within the microstructure aligns with their expected roles. Specifically, Mo and Cr are depleted in regions associated with the globular primary α phase and grain boundary α phase. At the same time, Al and Ti are concentrated in these areas, as anticipated. This consistent pattern across all samples indicates that each element is properly localised within the phases they stabilise.

4.1.6.1 Detailed Composition Analysis

Semi-quantitative EDX analyses were conducted to investigate the chemical composition and element distribution within the Ti-5553 alloy further after heat treatment. Spot analysis was performed at specific microstructural locations for each sample to obtain the elemental spectrum.

Ageing Heating Rate (1°C/min): For this sample, four spectra were captured, namely Spectrum 50 (globular primary α phase), Spectrum 51 (grain boundary α phase), Spectrum 52 (secondary α lamellar structure), and Spectrum 53 (secondary α lath) as shown in Figure 46.

Ageing heating rate (1°C/min)

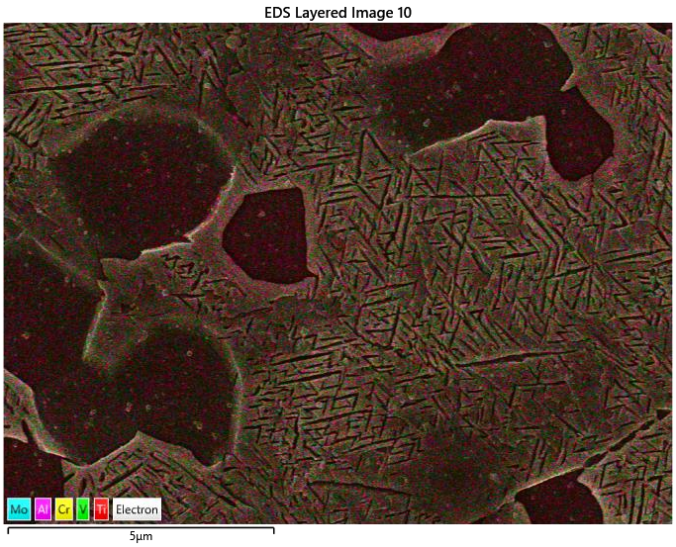

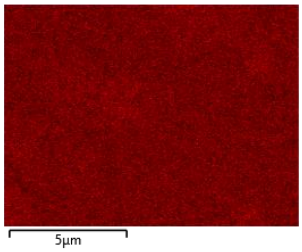

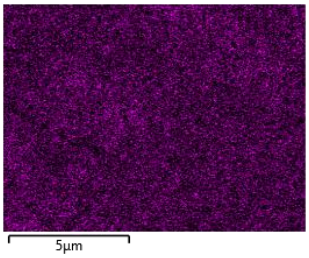

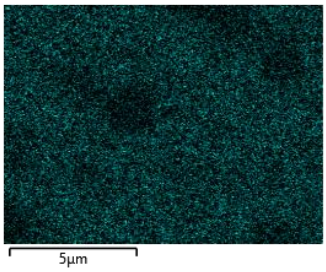

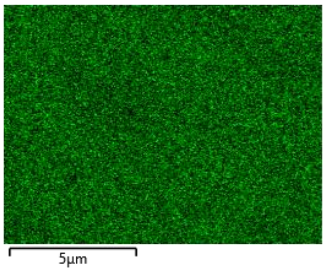

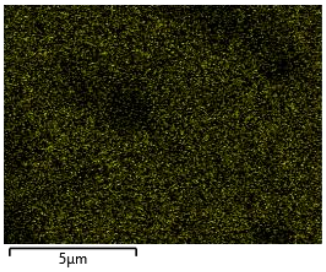

Ageing heating rate (5°C/min)

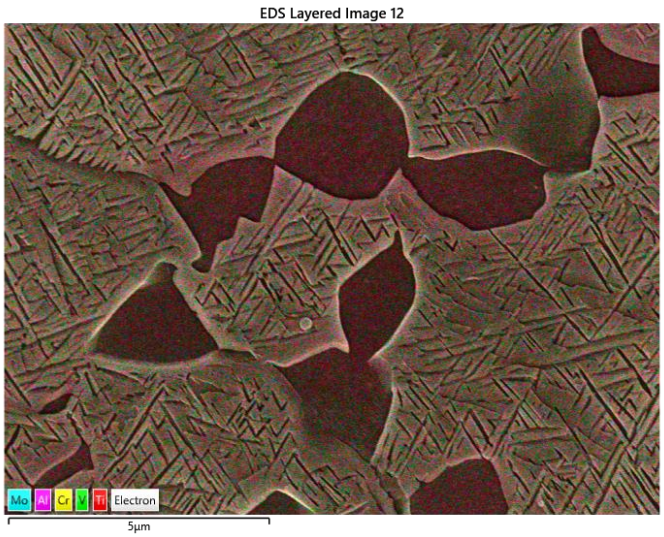

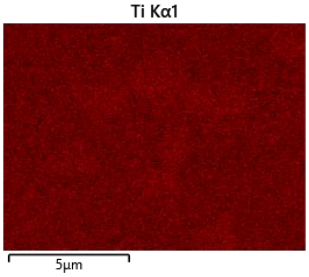

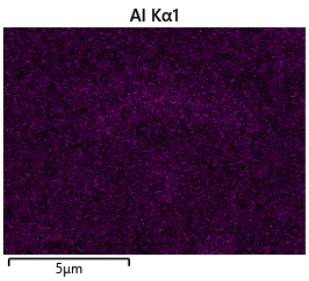

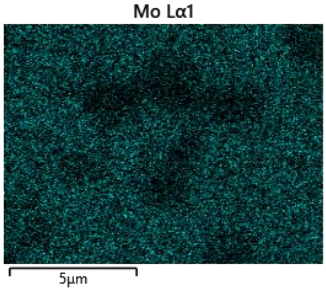

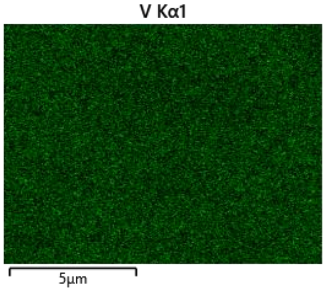

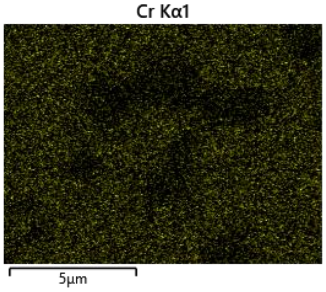

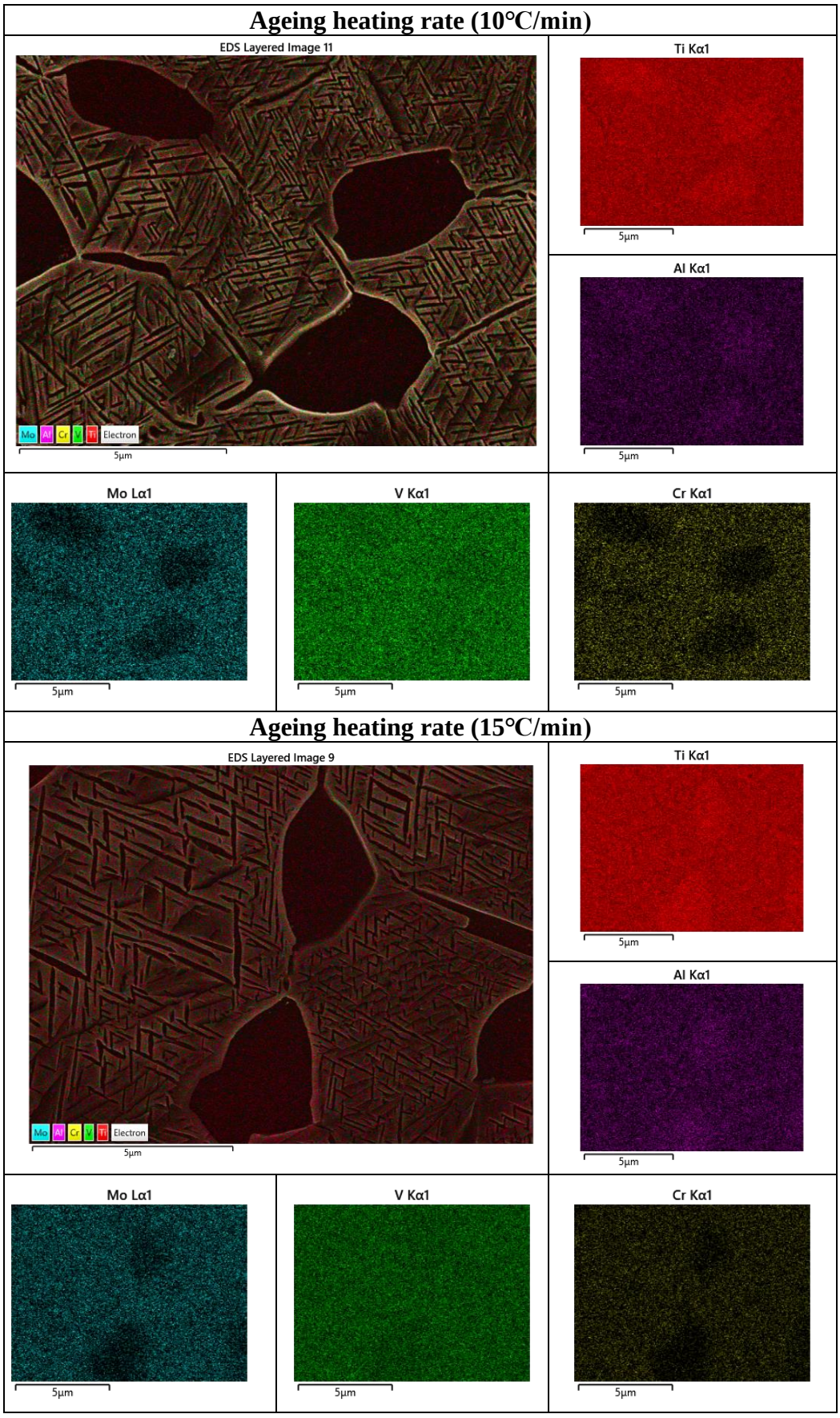

Figure 45: Element distribution within the microstructure of Ti-5553 alloy after each heat treatment

The results demonstrate a clear differentiation in elemental distribution among these features. The globular primary α phase (Spectrum 50) is characterised by high concentrations of Ti and Al, with moderate levels of V and Mo. The grain boundary α phase (Spectrum 51) shows a similar composition, reinforcing the stability of these α-rich regions. In contrast, the secondary α lamellar structure (Spectrum 52) and secondary α lath (Spectrum 53) exhibit higher concentrations of V and Mo, indicating their β-phase characteristics. The consistency in these findings suggests that the ageing heat treatment at 1°C/min effectively maintains chemical homogeneity and phase stability, preserving the alloy's microstructural integrity.

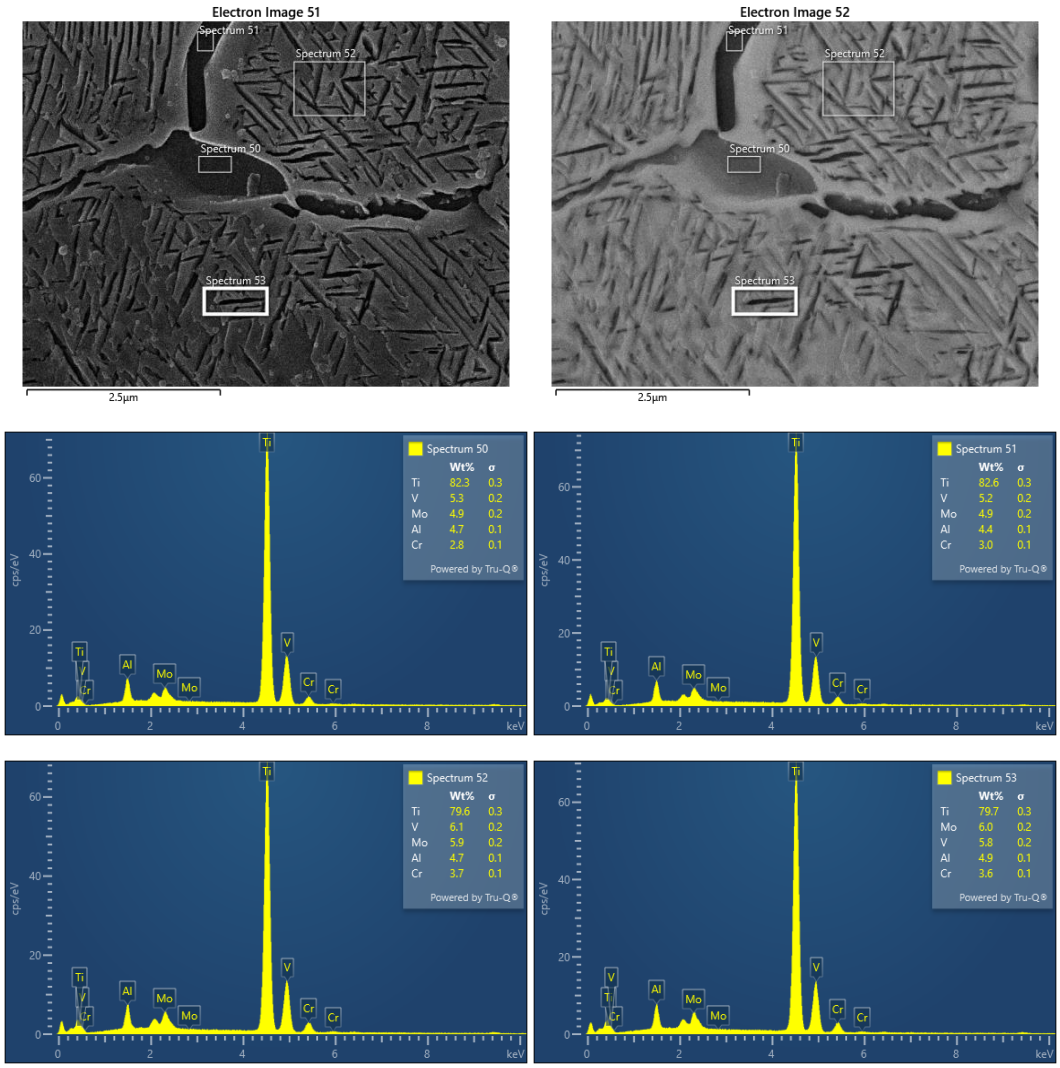

Figure 46: Semi-quantitative EDX analysis of the Ti-5553 alloy after heat treatment at an ageing heating rate of 1°C/min

Ageing Heating Rate (5°C/min): In this case, five spectra were captured, corresponding to different microstructural phases (Figure 47). The grain boundary α phases (Spectra 61 and 62) exhibit higher concentrations of V and Mo, indicative of β-stabilisers, while Al remains prominent as an α-stabiliser. The globular primary α phase (Spectrum 63) is rich in Ti and Al, with lower levels of V and Mo. The secondary α lamellar structures (Spectra 64 and 65) display a balanced distribution of both α- and β-stabilisers. These results confirm the expected distribution of elements within the microstructure, consistent with the alloy's known behaviour.

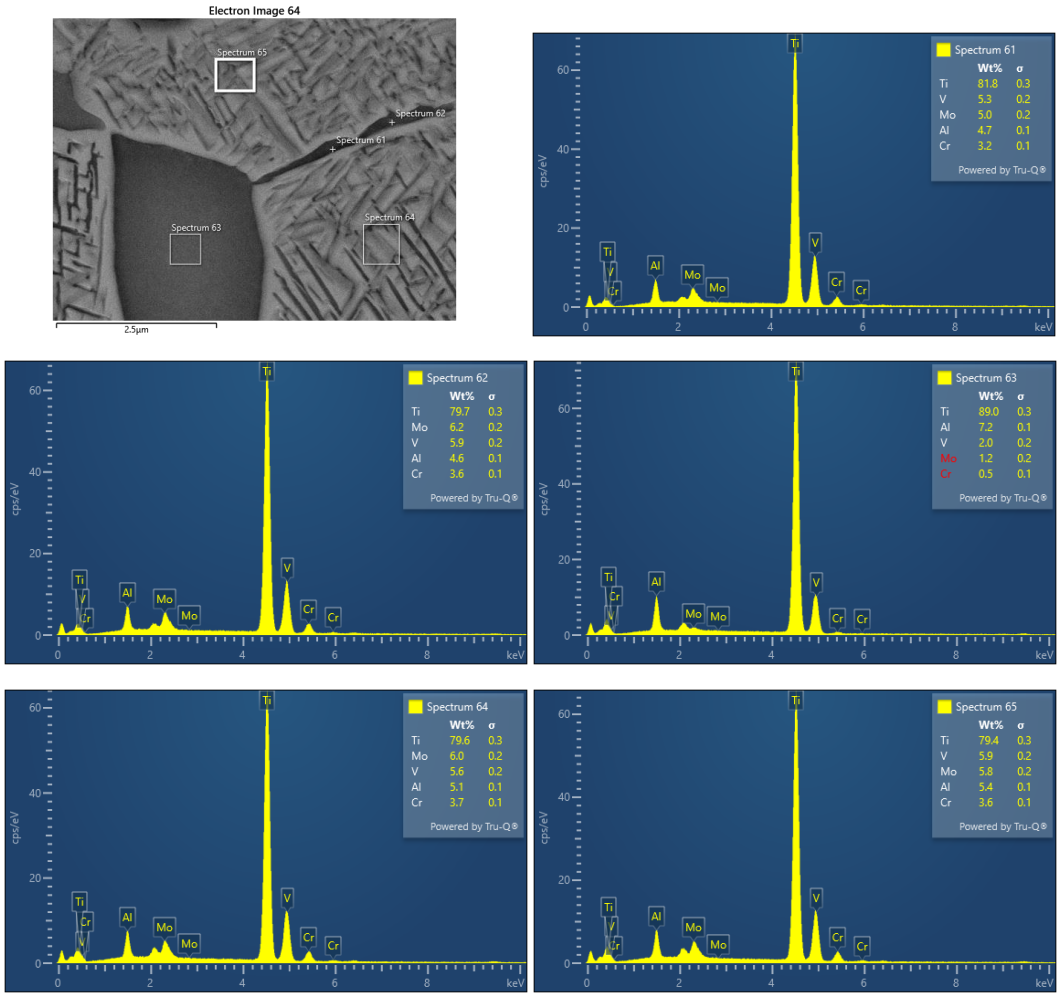

Figure 47: Semi-quantitative EDX analysis of the Ti-5553 alloy after heat treatment at an ageing heating rate of 5°C/min

Ageing Heating Rate (10°C/min): In this sample, four spectra were analysed, revealing distinct elemental distributions across the microstructure (Figure 48). Spectra 57 and 58, representing either the globular primary α phase or the grain

boundary α phase, reflect a balanced presence of α- and β-stabilisers. Spectrum 59, associated with the globular primary α phase, shows a higher Ti and Al content, indicating a more pronounced α-phase composition. Spectrum 60, related to the secondary α lamellar structure, displays a more even distribution of V and Mo, characteristic of the β-phase regions. These findings are consistent with the expected elemental differentiation between the α- stabilised and β-stabilised phases.

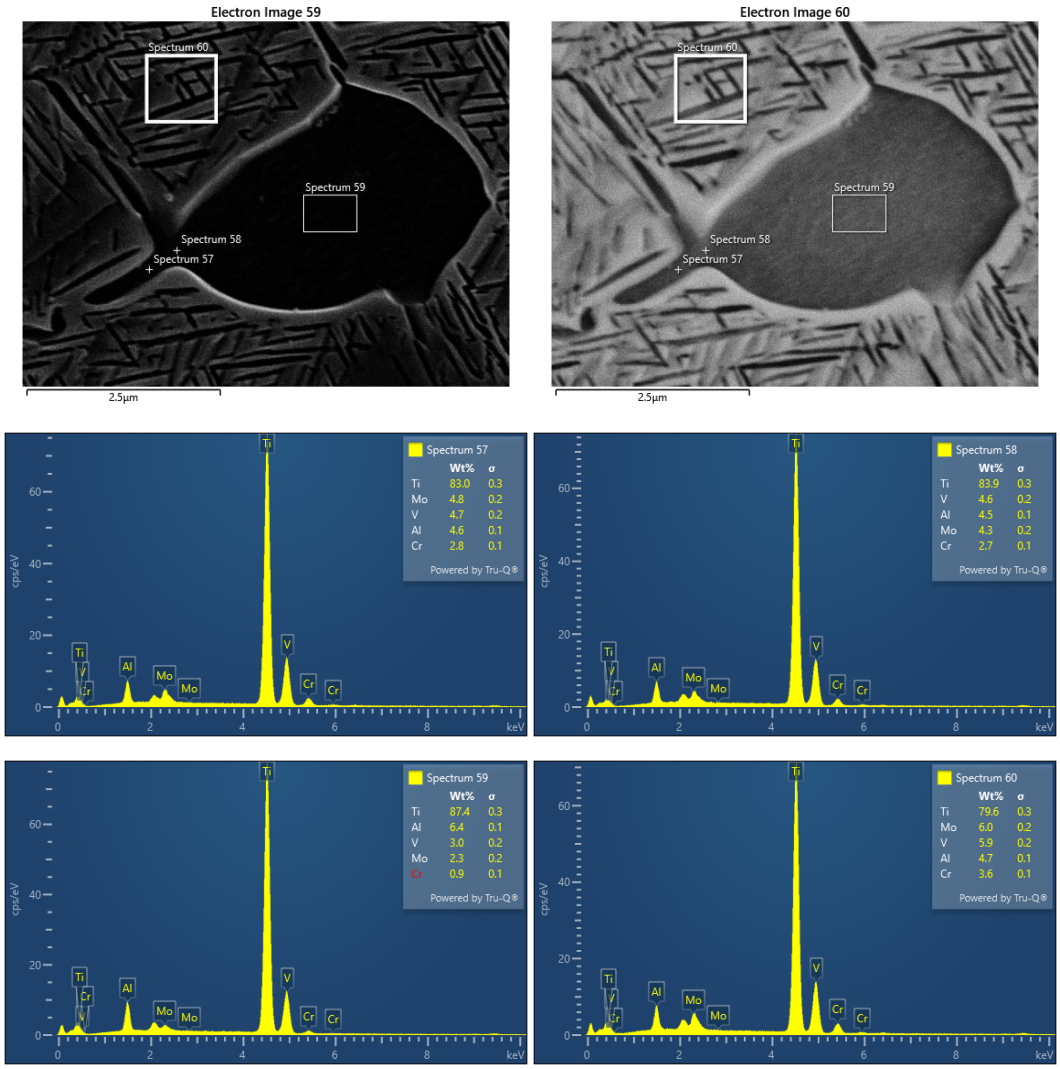

Figure 48: Semi-quantitative EDX analysis of the Ti-5553 alloy after heat treatment at an ageing heating rate of 10°C/min

Ageing Heating Rate (15°C/min): For the final sample, five spectra were recorded (Figure 49). The globular primary α phases (Spectra 39, 40, and 42) show high concentrations of Ti and Al, with lower amounts of V, Mo, and Cr, indicating strong α-stabiliser presence. Spectrum 39, in particular, stands out with the highest Ti and

Al content. The secondary α lamellar structures (Spectra 41 and 43) exhibit a balanced distribution of β-stabilisers, consistent with their expected role in the microstructure. These results confirm the effective maintenance of chemical composition and microstructural stability across the various phases.

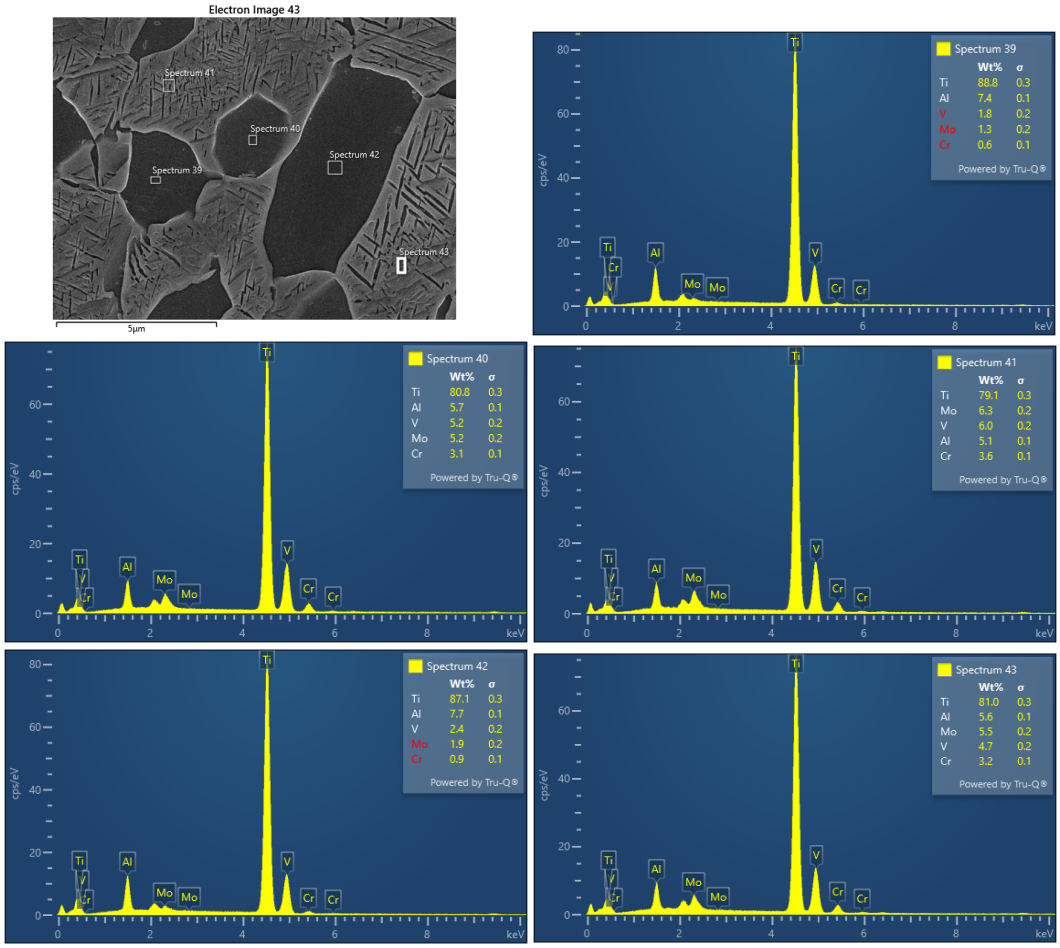

Figure 49: Semi-quantitative EDX analysis of the Ti-5553 alloy after heat treatment at an ageing heating rate of 15°C/min

Overall, across all samples subjected to different ageing heating rates, the semi-quantitative EDX analysis reveals a consistent elemental distribution within the Ti-5553 alloy's microstructure. The globular primary α phase and grain boundary α phase consistently show higher concentrations of α-stabilisers, such as Ti and Al, while the secondary α lamellar structure and grain boundary α phases exhibit higher concentrations of β-stabilisers, including V, Mo, and Cr. This distribution pattern aligns with the expected behaviour of the alloy, where α-stabilisers are localised in the α phases, and β-stabilisers are more concentrated in the β-associated regions.

The slight variations in composition observed between different samples and phases are consistent with the alloy's response to varying ageing heating rates. These differences do not contradict the overall chemical homogeneity and phase stability of the Ti-5553 alloy. The ageing treatments applied at different rates have successfully maintained the expected microstructural integrity.

4.2 Micro-Vickers Hardness Test Results

The Micro-Vickers hardness values (HV) for the Ti-5553 alloy measured after different ageing heating rates are displayed in the Table 6. The average hardness values varied slightly across the different ageing heating rates; however, the standard deviation associated with each condition clearly stated that change in hardness is statically insignificant (Figure 50). The 5°C/min and 10°C/min rates produced the highest average hardness values of 371.7 HV and 369.8 HV, respectively. In contrast, the 15°C/min heating rate resulted in the lowest average hardness of 357.4 HV. From average hardness values, it seems that moderate heating rates during the ageing process (5°C/min and 10°C/min) lead to slightly higher hardness in the Ti-5553 alloy compared to faster (15°C/min) rates. This may be due to the optimised microstructural changes that occur at these intermediate ageing heating rates, resulting in a more favourable balance of phase distributions that enhances hardness.

Table 6: Vickers hardness for each sample across different ageing heating rates

Hardness Values (HV)	**Different Ageing Heating Rate**			
	1°C/min	**5°C/min**	**10°C/min**	**15°C/min**
Reading 1	348.4	364.5	380.2	353.2
Reading 2	362.4	368.0	378.1	354.7
Reading 3	385.9	384.0	365.1	356.2
Reading 4	369.4	368.6	360.1	362.4
Reading 5	370.5	373.5	379.4	360.4
Average	**367.3**	**371.7**	**369.8**	**357.4**
Standard Deviation	**13.6**	**7.6**	**13.6**	**3.9**

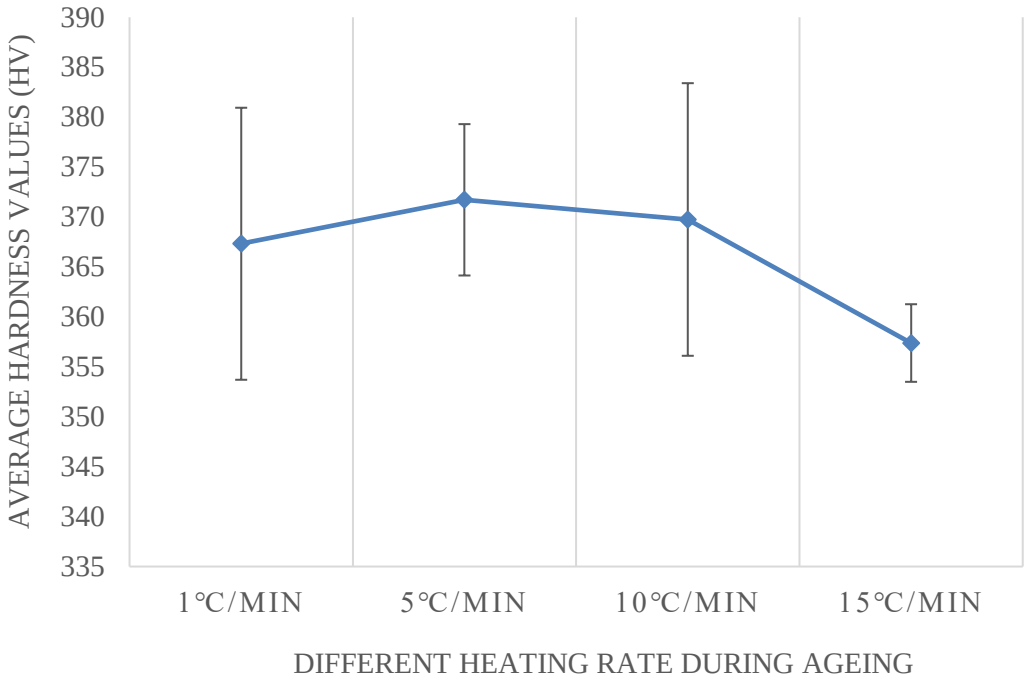

Figure 50: Overall trend of Micro-Vickers hardness values across different ageing heating rates

The hardness values observed in the Ti-5553 alloy under different ageing heating rates are closely linked to the microstructural characteristics revealed through SEM analysis. At slower ageing rates, the microstructure consists of a homogeneously distributed globular primary α phase and fine, needle-like secondary α lamellar structures within the β grains. This microstructural configuration contributes to relatively higher hardness values. The fine secondary α phase, formed during ageing, is harder than both the primary α and grain boundary α phases due to its smaller size and higher aluminium content. These fine α lamellae create numerous interphase boundaries that act as obstacles to dislocation motion, thereby enhancing the alloy's overall strength and hardness. This observation aligns with the findings of Qin et al. and Sadeghpour et al., who emphasise the critical role of secondary α phases in increasing hardness [47, 48]. Further support comes from Huang et al., who reported that the primary α phase exhibited a hardness of around 350 HV, while the transformed β grains, enriched with needle-like secondary α phases, demonstrated much higher hardness values [49].

In contrast, samples subjected to faster ageing heating rates display a microstructure

with coarser globular primary α phases and plate-like secondary α lamellar structures. These subtle microstructural changes are the primary reasons for the slight decrease in hardness observed at higher ageing heating rates. The coarser α lamellae reduce the number of α/β interphase boundaries, which serve as dislocation barriers during mechanical deformation [50]. The reduction in these barriers leads to decreased hardness, consistent with the observations [51]. Sukedai et al. study highlights that the hardness of an age-hardened material is significantly influenced by the size, strength, and distribution of α precipitate particles [51]. Fine primary α precipitates allow dislocations to shear through them, enhancing hardness. In contrast, larger primary α precipitates, as observed in the 15°C/min condition, cause dislocations to bypass them, forming dislocation loops and leading to reduced hardness due to the increased spacing between particles [28].

The trend of slightly decreasing hardness with increasing ageing heating rates is further supported by findings from previous studies (Figure 51) [43]. Their research suggests that higher ageing heating rates may limit the formation of the ω phase, a precursor that enhances nucleation density [43, 52]. A lower nucleation density results in fewer dislocation barriers, thereby reducing hardness.

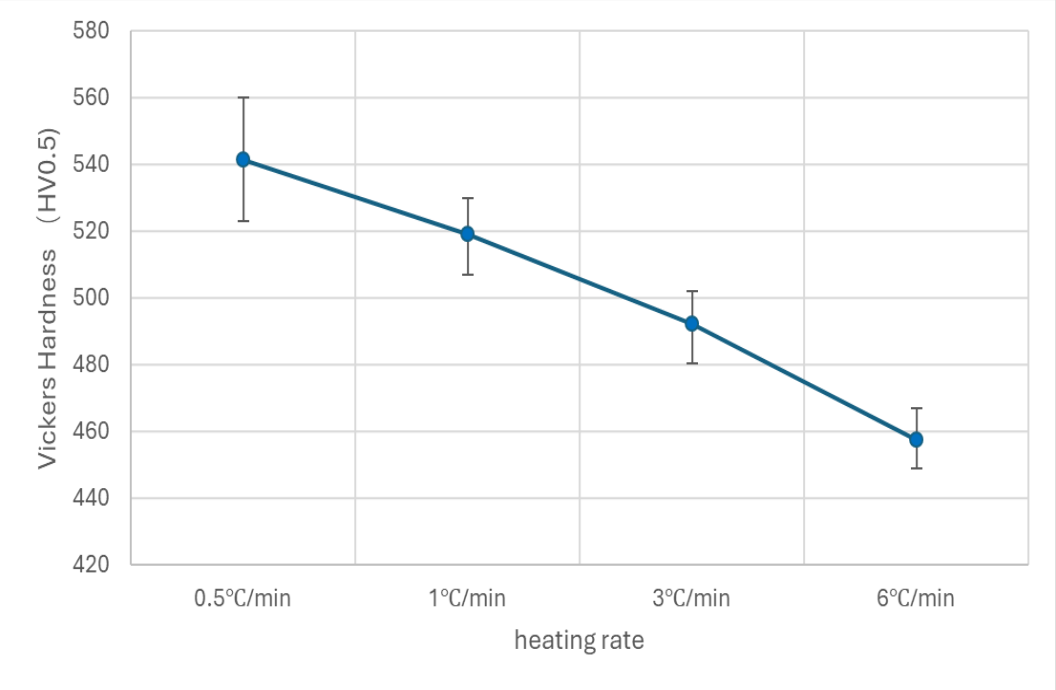

Figure 51: Vicker hardness value after ageing with different ageing heating rate [43]

Although the current study did not include in-depth Transmission Electron Microscopy (TEM) analysis to verify the presence and role of the ω phase in the microstructure of Ti-5553, it is plausible that under the processing conditions employed, particularly the ageing temperatures, the ω phase might not play a significant role. Future studies could aim to confirm the formation of this phase.

A comparison of the hardness values obtained in this thesis with those reported in the literature is presented in Table 7. The hardness values observed in this study are lower than those reported in studies featuring typical bimodal microstructures, such as the work by Opini et al. [53].

Table 7: Comparison of hardness values from the current study with values reported in the literature

Research study	**STA conditions**	**Typical Microstructure**	**Hardness**
Current study	810°C/2h/CBC + 610°C/8h/AC	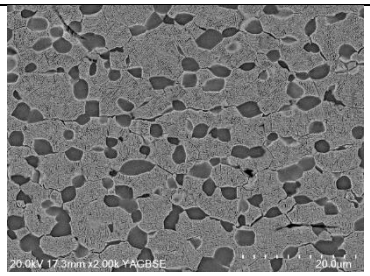	366.5±5.5 HV10
(Opini et al.) [53]	830°C/2h/AC + 600°C/10h/AC	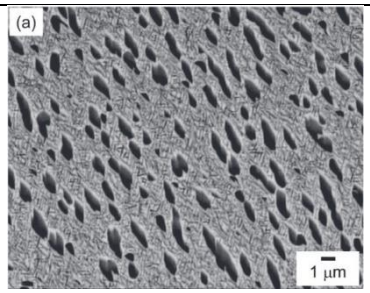	471±9 HV0.5
	900°C/1.5h/FC + 600°C/10h/FC	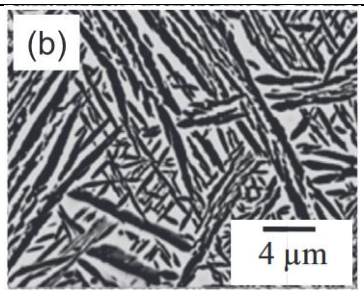	381±32 HV0.5

(Sahoo & Kabir) [28]	900°C/1h/WQ + 550°C/4h/WQ	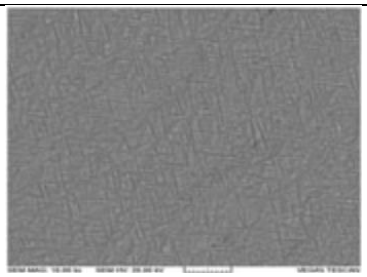	487.5±7.5 HV0.3
	900°C/1h/WQ + 600°C/4h/WQ	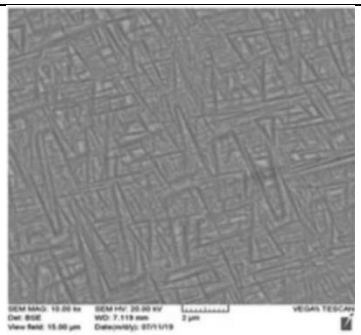	421±9 HV0.3
	900°C/1h/WQ + 650°C/4h/WQ	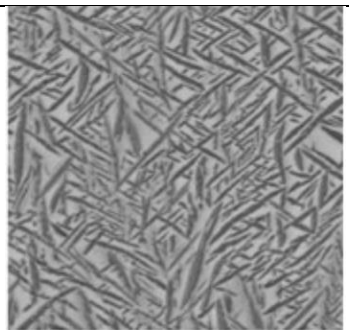	407±7 HV0.3
(Padmalatha & Chakkingal) [54]	800°C/4h/WQ	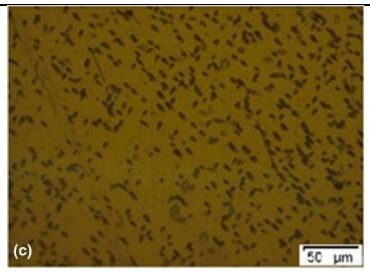	265±5 HV10
Please note that CBC stands for Ceramic Blanket Cooling, WQ is Water Quenching, AC is Air Cooling, and FC is Furnace Cooling			

Additionally, the hardness values are also lower than those found in fully lamellar structures but higher than those of a fully solutionised microstructure without ageing due to the contribution of needle-like secondary α particles within the β matrix. The discrepancies between this study and the broader literature could be attributed to differences in prior thermomechanical processing, heat treatment conditions, and the starting microstructure. These factors underscore the complexity of the processing-microstructure-property relationships in the Ti-5553 alloy and suggest areas for further investigation.

4.3 Tensile Test Results

The tensile properties of the Ti-5553 alloy, subjected to different ageing heating rates, reveal significant insights into the relationship between microstructural evolution and mechanical performance. The data presented in Table 8 highlight the variations in Young's Modulus, 0.2% YS, Ultimate Tensile Strength (UTS), and ductility across different ageing heating rates.

Table 8: Tensile properties obtained in the current thesis

Different Ageing Heating Rate	**Young's Modulus (GPa)**	**0.2%YS (MPa)**	**UTS (MPa)**	**Elongation to fracture (%)**
1°C/min	108.3	1295.9	1307.2	15.6
5°C/min	109.1	1287.4	1293.6	16.7
10°C/min	110.2	1278.9	1284.5	14.2
15°C/min	115.3	1259.0	1264.5	17.1
Average	**110.7**	**1280.3**	**1287.5**	**15.9**
Standard Deviation	**3.1**	**15.8**	**17.9**	**1.3**

Figure 52 illustrates the variation in Young's Modulus across different ageing heating rates. It is clear that Young's Modulus increased with higher ageing heating rates, ranging from 108 GPa at 1°C/min to 115 GPa at 15°C/min. This trend suggests a slight stiffening of the material as the ageing heating rate increases. The increase in modulus could be attributed to the distribution and morphology of the secondary α phase and the β matrix, where a more uniform distribution of β-stabilising elements (Mo, V, Cr) at higher ageing heating rates may contribute to the increased stiffness. However, the modest rise in modulus, with an average value of 110.7 GPa and a standard deviation of 3.1 GPa, indicates that the overall stiffness remains relatively stable across the different heat treatments.

Both the 0.2% YS and UTS exhibited a decreasing trend as the ageing heating rate increased (Figure 53). The YS dropped from 1296 MPa at 1°C/min to 1259 MPa at 15°C/min, while the UTS decreased from 1307 MPa to 1265 MPa over the same

range. The average YS was 1280.3 MPa, with a standard deviation of 15.8 MPa, and the average UTS was 1287.5 MPa, with a standard deviation of 17.9 MPa.

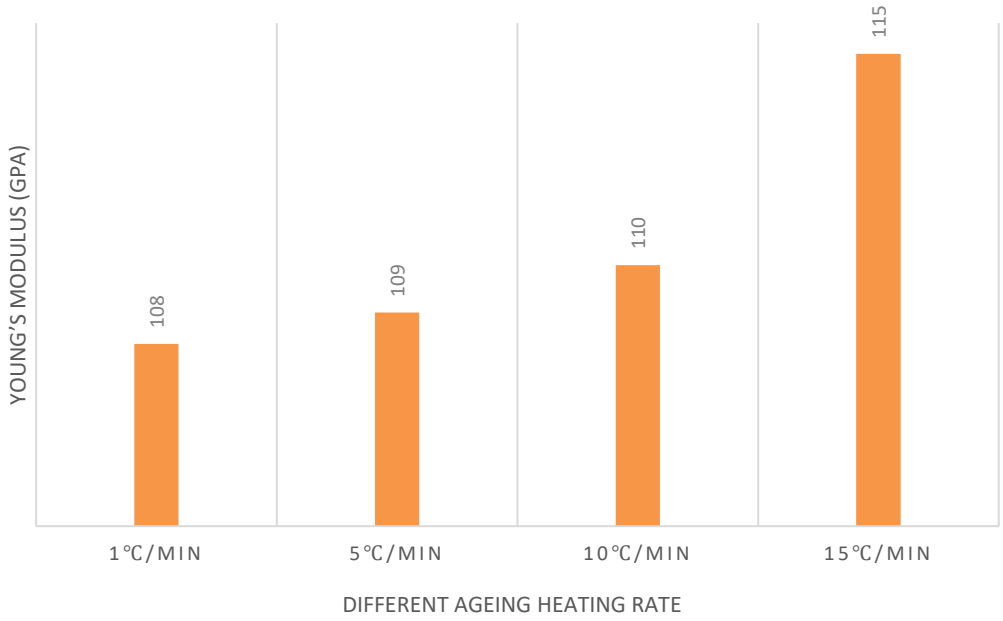

Figure 52: Variation in Young's Modulus across different ageing heating rates

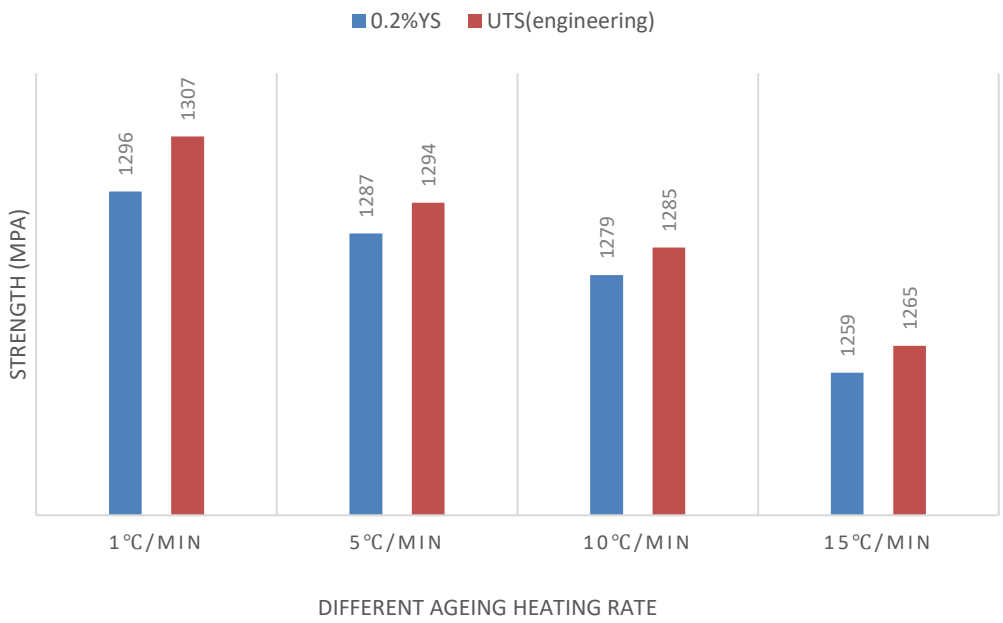

Figure 53: Variation in 0.2%YS and UTS across different ageing heating rates

This reduction in strength can be correlated with the microstructural changes observed at higher ageing heating rates. At lower ageing heating rates, the fine, well-distributed secondary α lamellae within the β grains act as effective barriers to

dislocation movement, resulting in higher strength. Conversely, at higher ageing heating rates, the coarser α lamellae reduce the density of these barriers, leading to lower strength. This observation is consistent with the understanding that finer microstructures generally enhance the material's yield and tensile strengths due to increased dislocation hindrance.

Change in ductility, measured as the elongation percentage, is displayed in Figure 54. It is very evident that there is a slight increase with increasing ageing heating rates, reaching its maximum at 15°C/min (17.1%). This inverse relationship between strength and ductility is a typical response in metallic materials where coarser microstructures, resulting from higher ageing heating rates, allow for greater plastic deformation before failure. The average ductility across the samples was 15.9%, with a standard deviation of 1.3%, indicating that while there is some variability, the ductility generally increases as the microstructure becomes coarser.

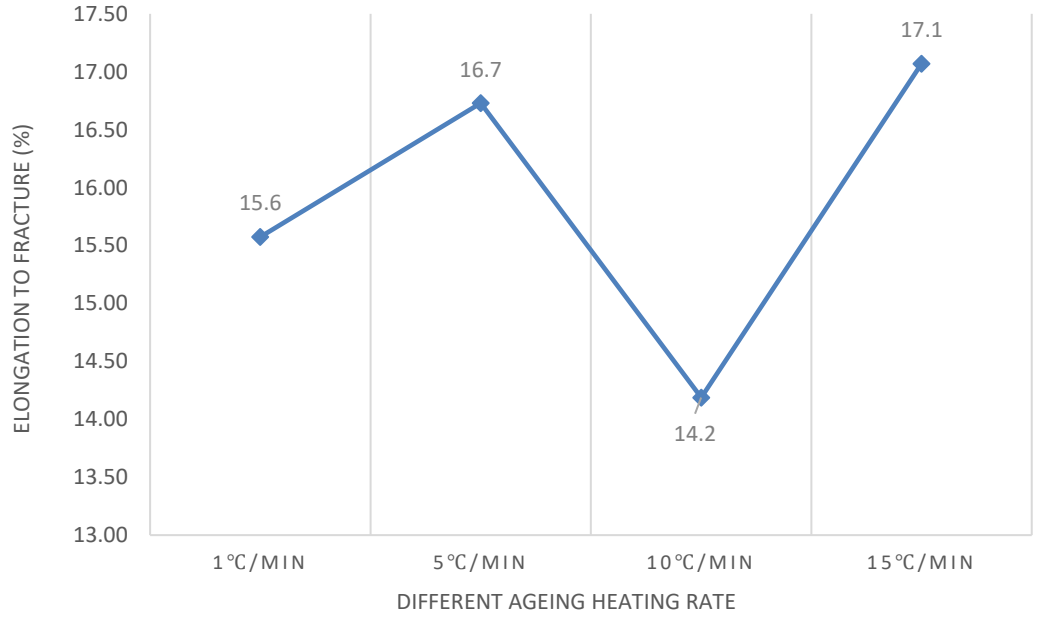

Figure 54: Variation in elongation to fracture across different ageing heating rates

The engineering stress-strain curves for the Ti-5553 alloy, aged at heating rates of 1°C/min, 5°C/min, 10°C/min, and 15°C/min are displayed in Figure 55. All curves show a typical metallic behaviour with a well-defined elastic region followed by yielding and plastic deformation. Also, it is clear that each curve exhibits a

significant amount of strain hardening before reaching the peak stress, followed by a gradual decline, suggesting good ductility.

Ageing heating rate (1°C/min)

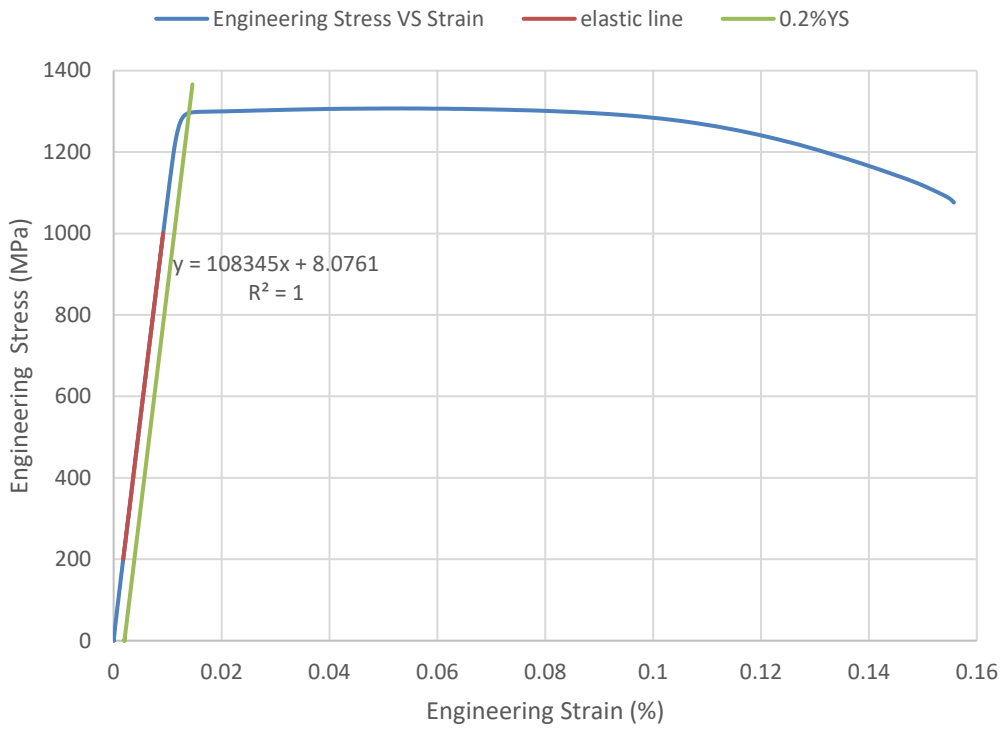

Ageing heating rate (5°C/min)

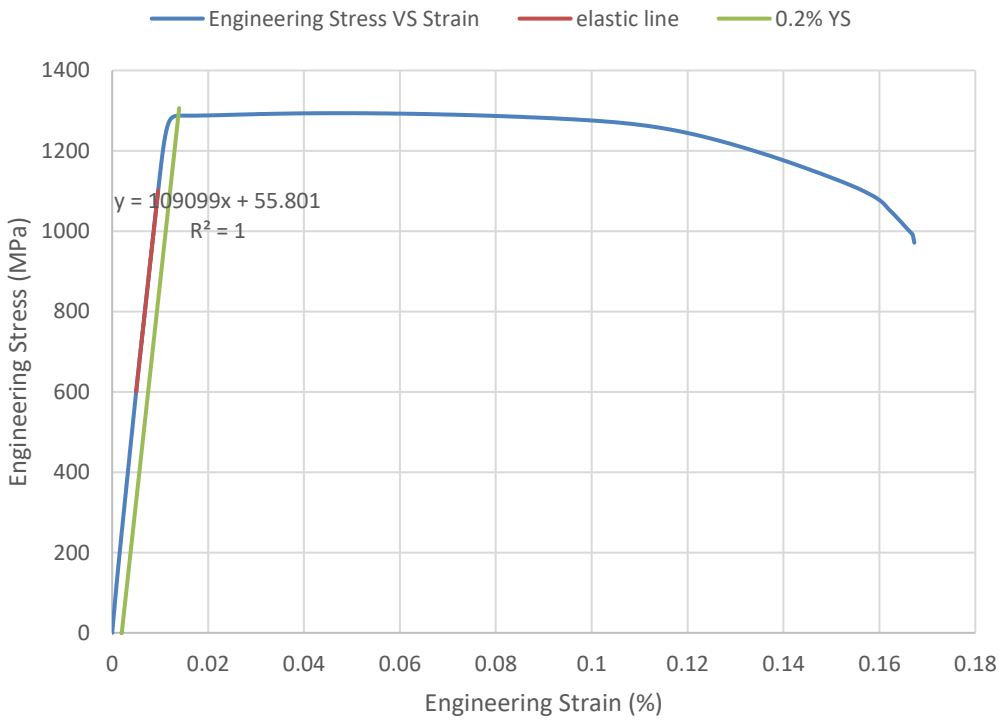

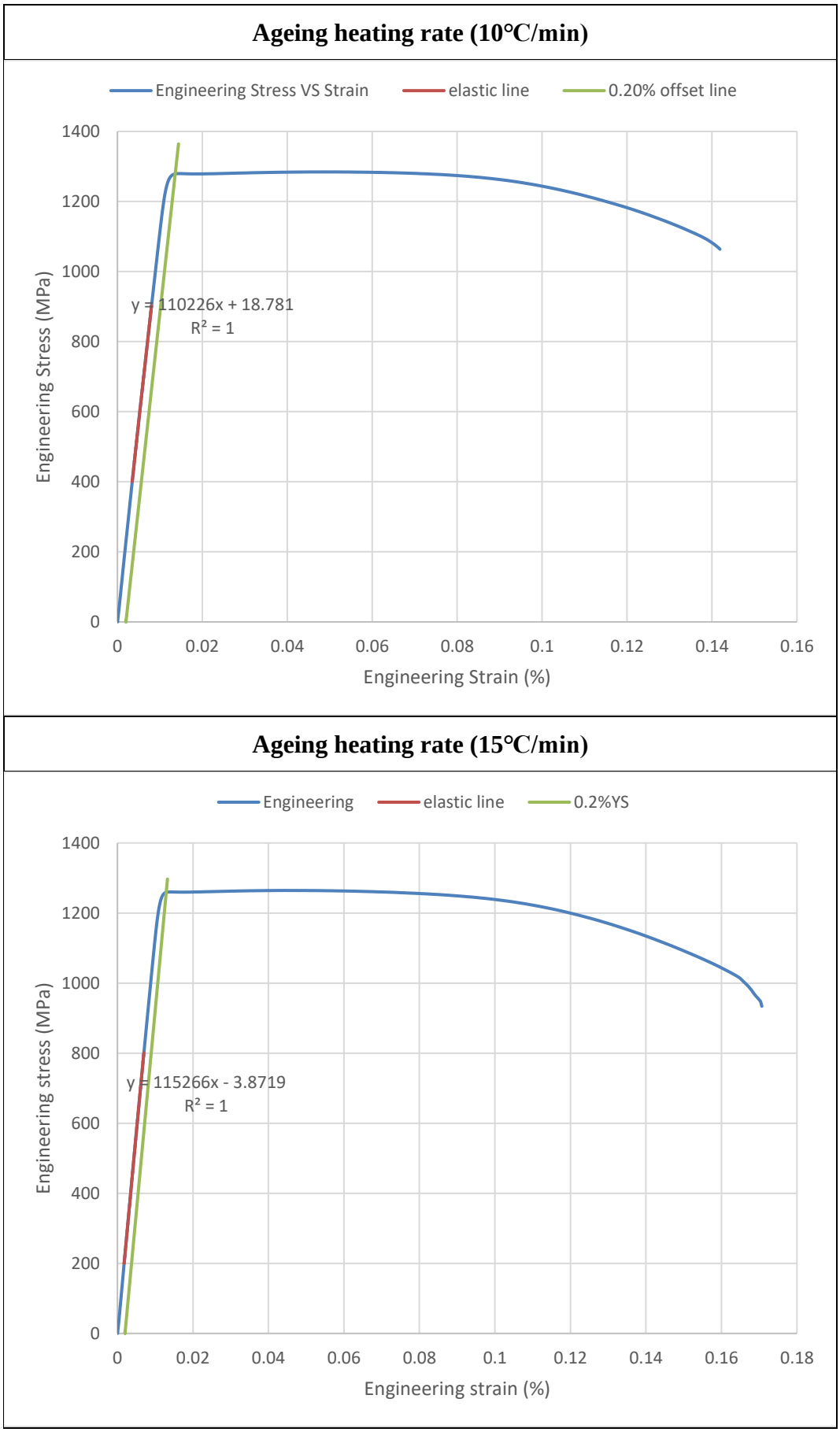

Figure 55: Typical engineering stress-strain curves for all four ageing heating rates

The true stress vs. true strain (flow) curves for the Ti-5553 alloy, aged at different heating rates, are shown in Figure 56. These curves demonstrate a steady increase in stress up to the yield point, followed by a gradual decrease after reaching the peak stress. This pattern indicates good ductility, with a well-balanced relationship between stress and strain, suggesting that the material can endure significant deformation before failure. Overall, increasing the ageing heating rate enhances the true stress (flow stress) of the material, resulting in greater strength. However, this increase in strength is accompanied by a reduction in ductility, as evidenced by the more rapid decline in stress after the peak in the flow curves at higher ageing heating rates.

Ageing heating rate (1°C/min)

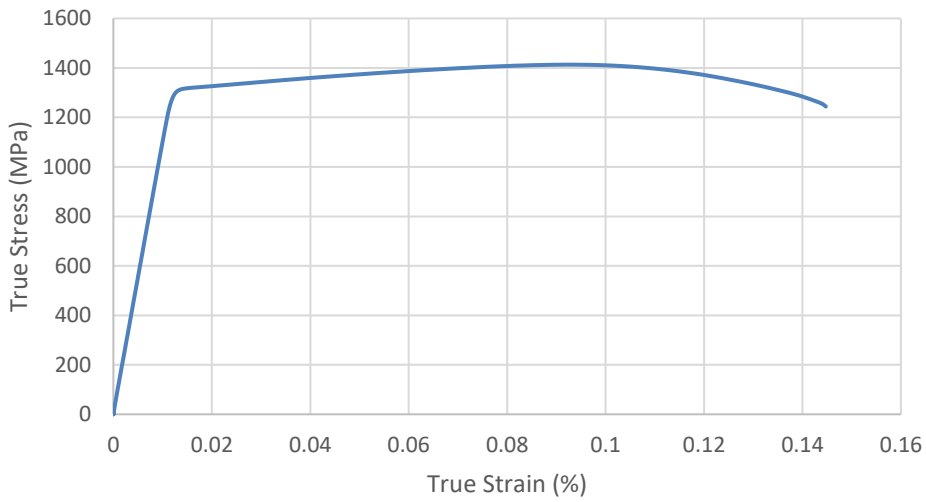

Ageing heating rate (5°C/min)

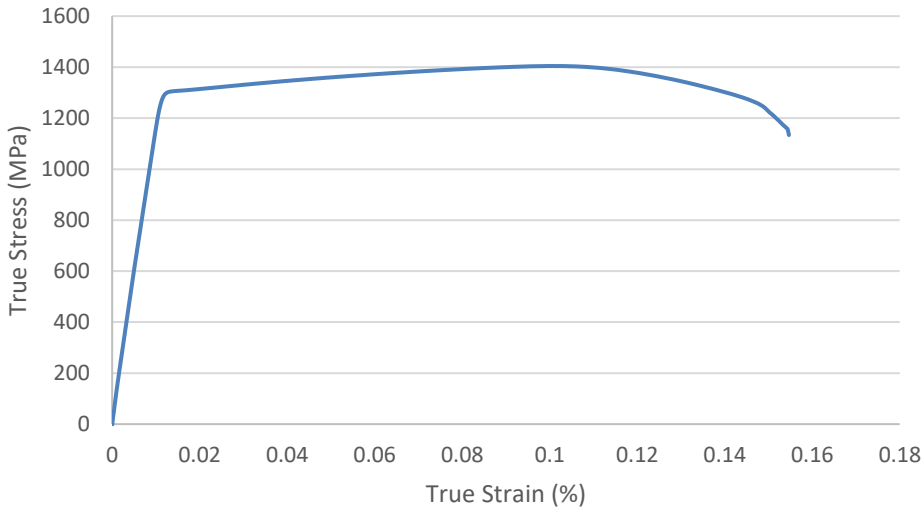

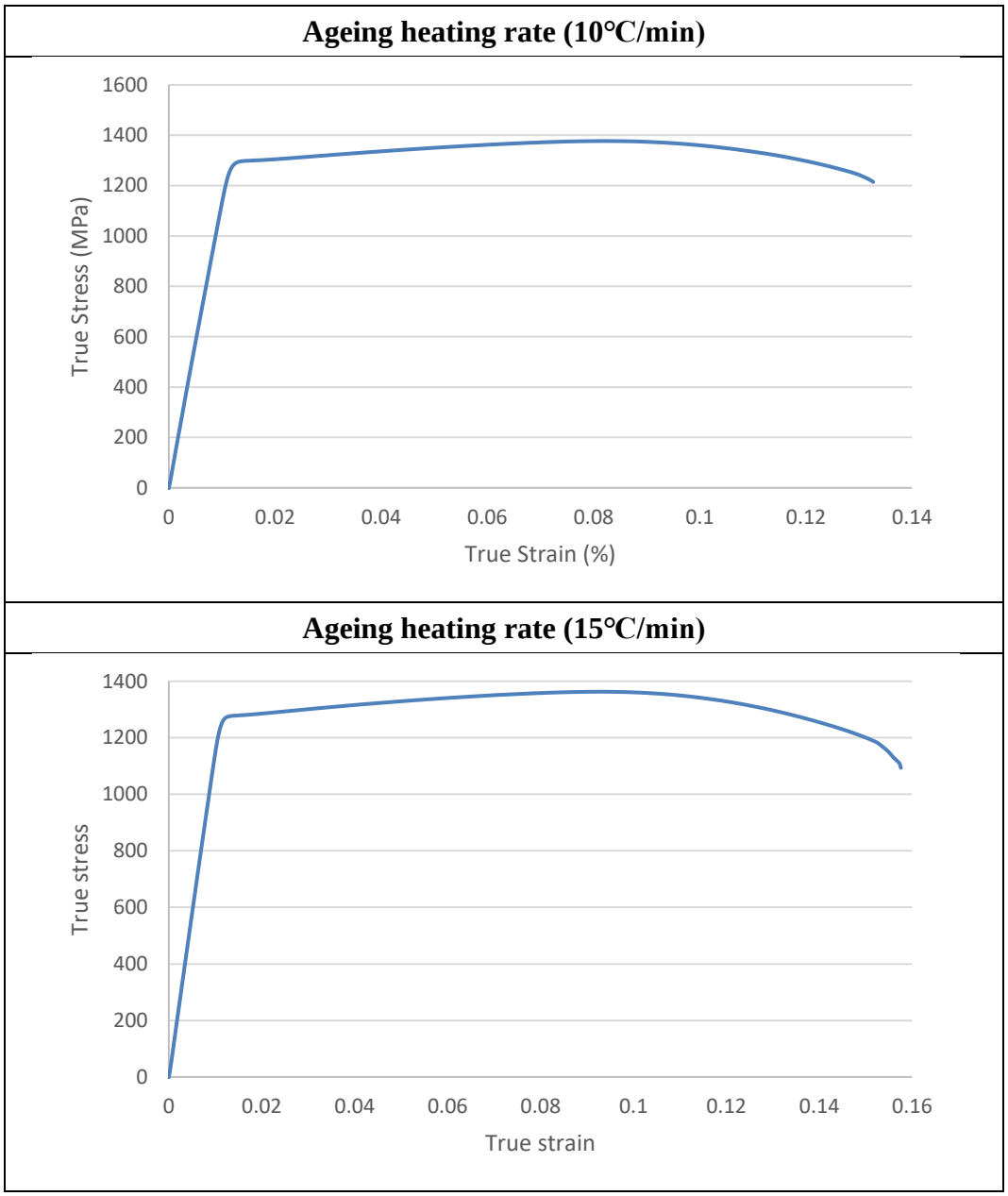

Figure 56: Typical true stress-strain curves for all four ageing heating rates

Overall, the tensile properties observed in the current study, which show a trade-off between strength and ductility across different ageing heating rates, align with findings from previous research, such as Sangali et al. [43]. This trend, where strength increases with slower ageing heating rates and ductility decreases, can be attributed to variations in microstructural features, particularly the size and distribution of the α lamellar phase.

Sangali's study draws parallels with Wang's investigation of a double-aged Ti-5Al-5Mo-5V-3Cr-1Zr alloy, where a microstructure combining fine and coarse α

precipitates was observed [43, 55]. Wang's key finding was that fine α regions primarily exhibited dislocation tangles, while coarse α regions showed deformation twinning, indicating that the dominant deformation mechanism shifts depending on the α phase morphology [55]. This observation is relevant to the current study, where fine α lamellae, produced at slower ageing heating rates, contribute to higher strength due to their ability to hinder dislocation motion effectively. Conversely, the coarse α lamellae formed at higher ageing heating rates facilitate twinning, which increases ductility but reduces strength.

Table 9: Strength variations in Ti-5553 alloy previously reported [43]

Alloy	Aging Heating rate (°C/min)	Tensile Test		
		YS (MPa)	UTS (MPa)	Elong. (%)
Ti-5553 (aged 600 °C/2h)	0.5	–	–	–
	3	1289 ± 10	1289 ± 10	1.7 ± 0
	6	1223 ± 12	1223 ± 11	1.1 ± 0.11

Further support for these findings comes from studies by Sen et al., who demonstrated that in titanium alloys, dislocation movement first occurs within the softer β matrix, with the α/β interface initially acting as a barrier [56]. In regions where α laths have favourable orientations, dislocations can transfer across the interface, allowing slip within the α phase (Figure 57). In other α lamellae, where slip transfer cannot occur, dislocations accumulate at the interface, leading to localised stress concentrations and eventually twinning. The coarse α lamellae, therefore, allow for greater plastic deformation before fracture, explaining the increased ductility observed in samples aged at higher ageing heating rates.

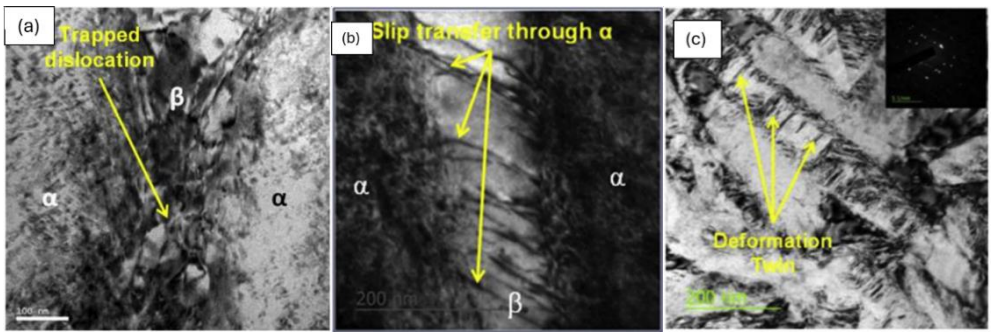

Figure 57: Evidence of trapped dislocation and twinning in α lamellae, promoting greater plastic deformation [56]

Moreover, the presence of the primary α phase in the microstructure plays a critical role in balancing strength and ductility. The globular primary α phase, often located at the grain boundaries of prior β grains, acts as a pinning agent that restricts grain growth during solution treatment. This pinning effect results in finer β grains, which deform more uniformly under tensile loading, contributing to the alloy's overall ductility. This effect has been observed by Li et al. and Sadeghpour et al., who noted that the presence of primary α phases prevents the formation of long shearing bands that could lead to premature failure, thereby enhancing the alloy's damage tolerance [48, 57].

Additionally, the current study's findings regarding the role of secondary α phases in strengthening the β matrix are consistent with the [37]. Qin et al. study suggests that the precipitation of intragranular α laths during ageing not only strengthens the β matrix by increasing dislocation density but also contributes to a finer β phase, which further enhances YS [37]. The current results support this mechanism, as the fine α lamellae observed at slower ageing heating rates result in a higher dislocation density within the β matrix, leading to increased strength.

However, this strengthening effect diminishes as the α lamellae coarsen with increasing ageing heating rates. The larger spacing between coarse lamellae reduces the dislocation density within the β phase, leading to lower overall strength. This trend is evident when comparing the microstructures of samples aged at different rates, where finer α lamellae correspond to higher strength and lower ductility, while coarser lamellae show the opposite trend.

The comparison of tensile properties with those reported in the literature, such as the work by Sadeghpour et al., highlights the complex interplay between microstructural features and mechanical properties in the Ti-5553 alloy [48]. While the current study observes lower strength values compared to some reports, these discrepancies can be attributed to differences in prior thermomechanical processing, initial microstructure, and ageing conditions. These findings underscore the importance of precisely controlling the ageing process to optimise the balance between strength and ductility in titanium alloys, particularly in those with a bimodal microstructure.

In conclusion, the tensile properties of the Ti-5553 alloy are significantly influenced by the ageing heating rate, which determines the size and distribution of α and β phases and the resulting deformation mechanisms. Fine α lamellae promote higher strength at the expense of ductility, while coarser lamellae enhance ductility but reduce strength. The presence of the primary α phase further contributes to the alloy's ductility by ensuring more uniform deformation. These insights emphasise the critical role of microstructural control in achieving the desired mechanical properties in advanced titanium alloys.

4.4 Fatigue Test Results

The fatigue properties of Ti-5553 alloy were investigated under various ageing heating rates, with testing performed under different stress amplitudes. Two samples were tested under each condition, and if a sample survived the first fatigue test without breaking, it was considered a non-broken sample and continued to be tested under the next higher stress amplitude level. However, the testing process encountered technical issues, including random fluctuations in load that resulted in overloading some samples instead of applying the intended cyclic loading. This issue particularly affected the data at a stress amplitude of 315 MPa and a heating rate of 5°C/min, which should be considered when interpreting the results.

Despite these challenges, the summary in Table 10 provides an overview of the fatigue properties observed under different stress amplitudes and ageing heating rates. At the lowest ageing heating rate of 1°C/min, the alloy exhibited a relatively high fatigue endurance, surviving over 10 million cycles at a stress amplitude of 337.5 MPa. However, as the stress amplitude increased to 351 MPa and 360 MPa, the number of cycles to failure decreased significantly to approximately 7.9 million and 4 million cycles, respectively. This trend is consistent with the general understanding that higher stress amplitudes lead to a reduction in fatigue life.

For the 5°C/min heating rate, the fatigue life showed some variability. At a stress amplitude of 315 MPa, the sample endured approximately 8.1 million cycles before failure, while at 337.5 MPa, the number of cycles to failure decreased slightly to around 7.6 million cycles. This indicates that the 5°C/min condition provides a good

balance between stress amplitude and fatigue life, although the endurance limit appears to be lower than that of the 1°C/min condition.

Table 10: Summary of fatigue test results obtained in the current thesis

Ageing Heating Rate	Max Stress (MPa)	Stress Amplitude (MPa)	Total Cycles to Failure
1°C/min	750	337.5	10000001
1°C/min	780	351	7869243
1°C/min	800	360	4029077
5°C/min	700	315	8086978
5°C/min	750	337.5	7586004
10°C/min	650	292.5	10000000
10°C/min	700	315	9328072
15°C/min	600	270	10000000
15°C/min	650	292.5	4186502

The 10°C/min ageing heating rate exhibited a notable improvement in fatigue life at lower stress amplitudes. At 292.5 MPa, the sample survived the full 10 million cycles, indicating a high endurance limit. Even at a higher stress amplitude of 315 MPa, the fatigue life remained relatively high, with the sample enduring approximately 9.3 million cycles. This suggests that the microstructure developed under the 10°C/min condition is more resistant to fatigue failure compared to the lower heating rates, particularly at moderate stress levels.

The highest ageing heating rate of 15°C/min revealed a mixed response in terms of fatigue life. At a lower stress amplitude of 270 MPa, the sample also survived 10 million cycles, indicating a strong endurance limit. However, as the stress amplitude increased to 292.5 MPa, the fatigue life sharply decreased to approximately 4.2 million cycles. This steep decline suggests that the microstructure resulting from the highest ageing heating rate may have increased sensitivity to higher stress amplitudes, leading to earlier failure.

The stress amplitude versus the number of cycles to failure (S-N) curve generated from the data indicates some trend in the fatigue behaviour of the alloy under different ageing heating rates. For the 1°C/min heating rate, the S-N curve (Figure 58) indicates a relatively steep decline in maximum stress as the number of cycles increases, with failure occurring after approximately 4 million to 10 million cycles, depending on the applied stress. This suggests that under lower stress amplitudes, the alloy can endure a higher number of cycles, but its endurance limit is reached more quickly as the stress increases.

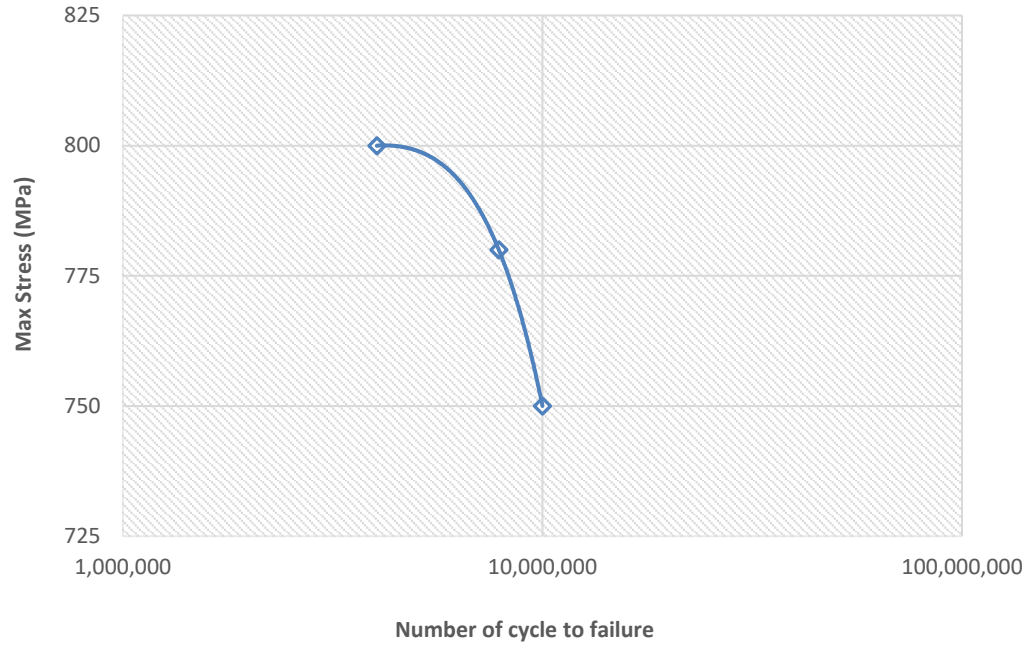

Figure 58: S-N curve for Ti-5553 alloy aged at a 1°C/min heating rate

The 5°C/min heating rate exhibits a similar pattern (Figure 59), but the total cycles to failure are generally lower compared to the 1°C/min condition. The rapid decline in the S-N curve here emphasises that even moderate increases in stress amplitude significantly reduce the fatigue life, which aligns with the previously discussed data indicating compromised data points due to technical issues.

Figure 59: S-N curve for Ti-5553 alloy aged at a 5°C/min heating rate

For the 10°C/min heating rate, the S-N curve (Figure 60) shows a less steep decline compared to the 1°C/min and 5°C/min conditions, with the alloy sustaining higher cycles before failure at lower stress amplitudes. This suggests a more stable fatigue performance under moderate stress levels, with the alloy demonstrating better endurance at this particular heating rate.

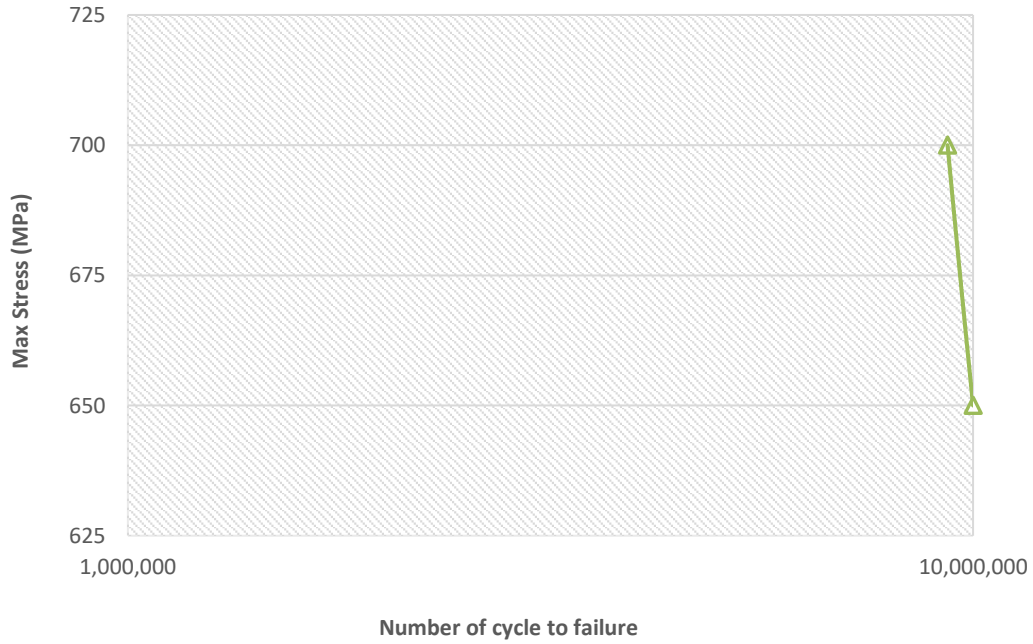

Figure 60: S-N curve for Ti-5553 alloy aged at a 10°C/min heating rate

Finally, the 15°C/min heating rate curve (Figure 61) shows a more pronounced drop in cycles to failure as the stress amplitude increases, with a marked decline when the stress is raised from 600 MPa to 650 MPa. This steep drop indicates that the alloy's fatigue life is significantly reduced at higher stress amplitudes when subjected to a faster heating rate during ageing.

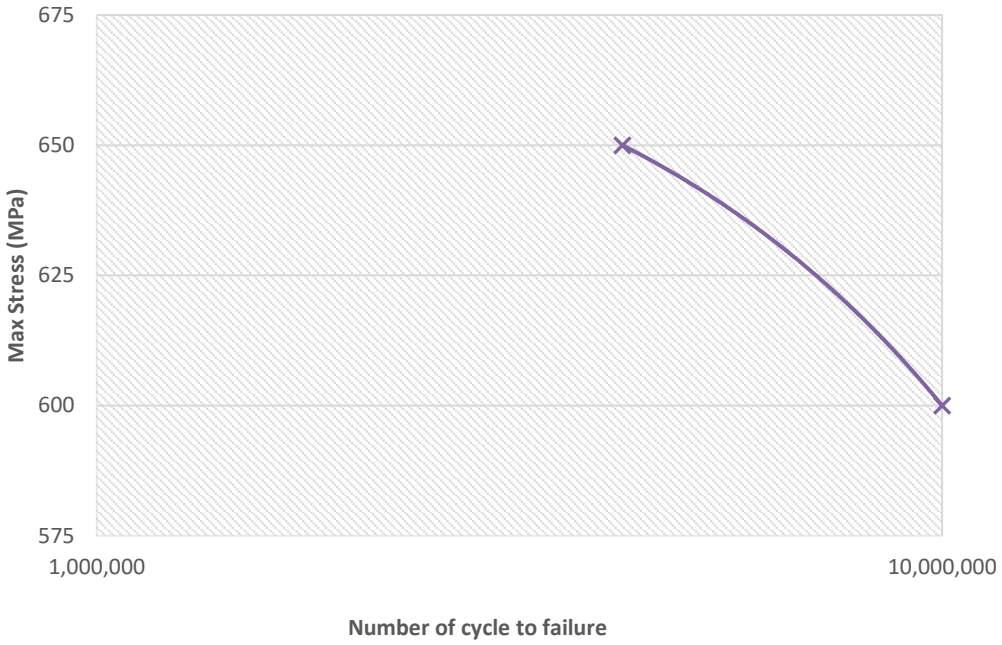

Figure 61: S-N curve for Ti-5553 alloy aged at a 15°C/min heating rate

The fatigue behaviour observed in the current study reveals a clear trend where the endurance limit of the Ti-5553 alloy decreases as the ageing heating rate increases. This trend mirrors the observations made for tensile strength and hardness, where a slower heating rate during ageing results in finer secondary α lamellar structure, leading to improved mechanical properties across the board. Specifically, the fatigue resistance is highest in samples aged at the slowest heating rate (1°C/min) and decreases progressively with faster heating rates (up to 15°C/min).

This relationship between fatigue performance and microstructure can be explained by the critical role of secondary α lamellar structure in hindering dislocation movement, thereby delaying crack initiation. As discussed previously, the finer secondary α lamellar structure formed at slower heating rates creates more effective

barriers to dislocation motion, which is a crucial factor in both delaying the onset of plastic deformation and extending the fatigue life of the alloy. Huang et al. support this finding, showing that fine a secondary α lamellar structure is associated with higher tensile and fatigue strengths [34, 49].

During cyclic loading, even when the macroscopic stress levels are well below the alloy's yield point, localised plastic deformation can occur, particularly at microstructural interfaces such as the α/β interface [58]. The globular primary α phase, which is softer and exhibits lower YS compared to the β matrix containing embedded secondary α lamellar structure, is particularly susceptible to these localised stresses. This leads to the accumulation of dislocations within the primary α phase, which can act as nucleation sites for fatigue cracks.

In summary, the fatigue performance of the Ti-5553 alloy is closely linked to the microstructural features developed during ageing. The fine secondary α lamellar structure formed at slower ageing heating rates provides superior resistance to dislocation motion and delays crack initiation, leading to enhanced fatigue properties. In contrast, faster-ageing heating rates result in a coarser microstructure that is less effective in hindering dislocation movement, thereby reducing fatigue life. These observations are consistent with the tensile and hardness results discussed earlier, highlighting the crucial role of microstructural control in optimising the mechanical performance of titanium alloys.

When generating the overall S-N curve (Figure 62) for the Ti-5553 alloy by carefully selecting and plotting fatigue data from different ageing heating rate conditions, it is evident that the general shape aligns with the trends reported in previous studies [21, 34]. The data clearly illustrates the trade-offs between maximum stress and fatigue life at different ageing heating rates, reinforcing the notion that slower heating rates generally improve fatigue performance while faster rates lead to diminished endurance. This behaviour is consistent with the trends observed in the tensile properties, where slower heating rates produced finer microstructures that contributed to better fatigue resistance. These findings collectively emphasise the importance of carefully controlling the ageing process

to achieve the desired balance between strength, ductility, and fatigue performance in titanium alloys. Future studies should aim to eliminate the technical issues encountered in this investigation and explore these trends further with a larger sample size to provide more robust conclusions.

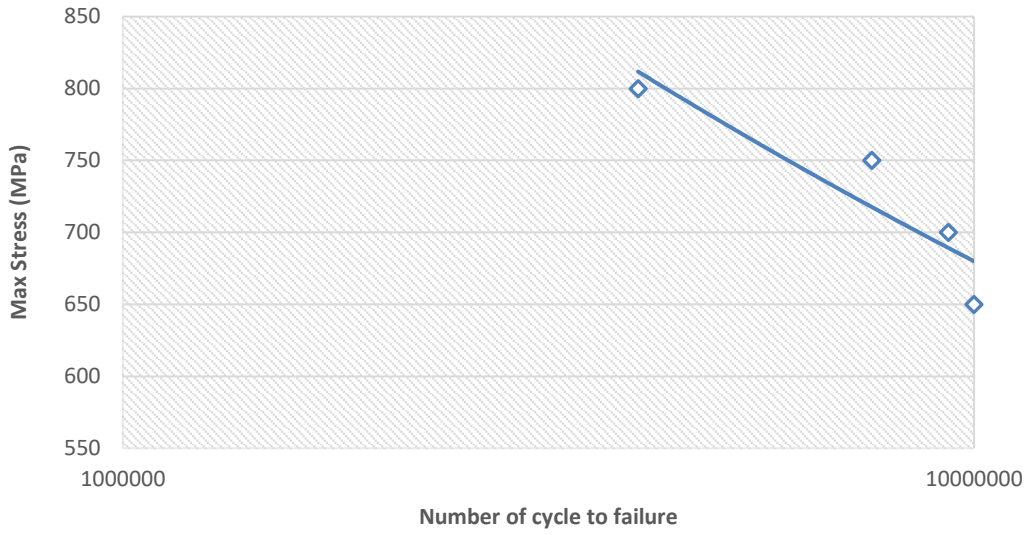

Figure 62: Overall S-N curve for the Ti-5553 alloy, generated by carefully selecting and plotting fatigue data from different heating rate conditions

As shown in Figure 63, the crack paths varied significantly across different conditions depending on the ageing heating rates. At lower heating rates, such as 1°C/min and 5°C/min, which facilitated the formation of a finer secondary α lamellar structure, the fracture surfaces displayed notable characteristics in line with those reported by [59, 60]. In these cases, cracks predominantly initiated at deformed primary α phases located just below the surface. The propagation of these cracks was primarily along the planes of maximum shear stress, with crack paths inclined at approximately 45° relative to the vertical load. In contrast, at higher heating rates of 10°C/min and 15°C/min, which led to the development of a coarser microstructure, the fracture surfaces became flatter and exhibited less pronounced surface features. This trend highlights how coarser microstructures, associated with higher heating rates, facilitate more straightforward crack propagation paths, ultimately compromising the alloy's fatigue performance.

Ageing heating rate (1°C/min)	
50X	**1000X**
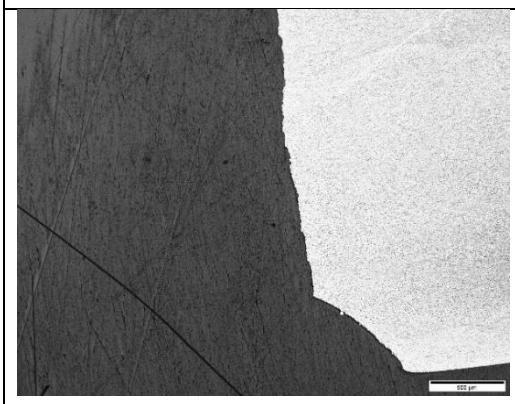	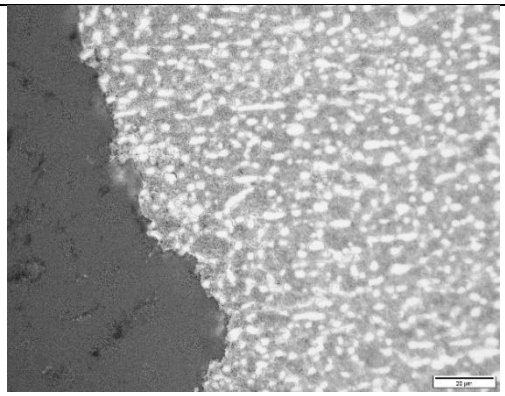
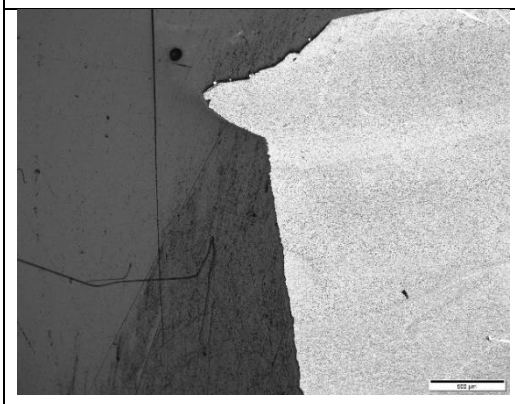	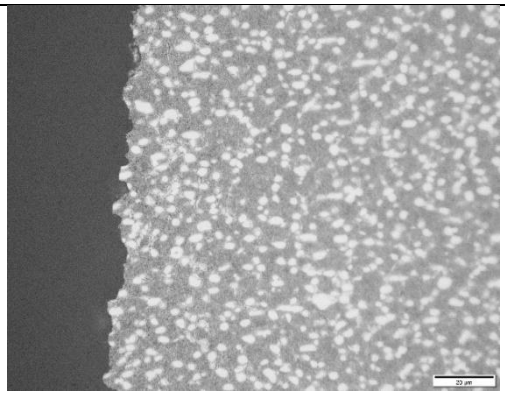
Ageing heating rate (5°C/min)	
50X	**1000X**
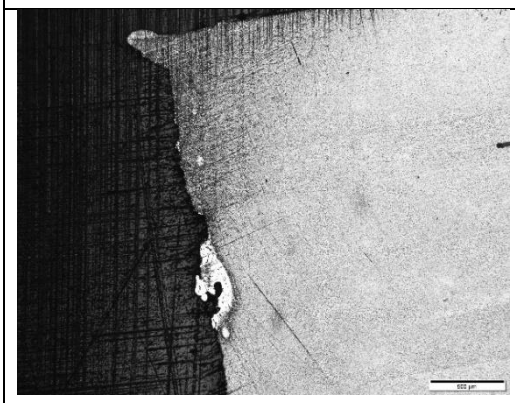	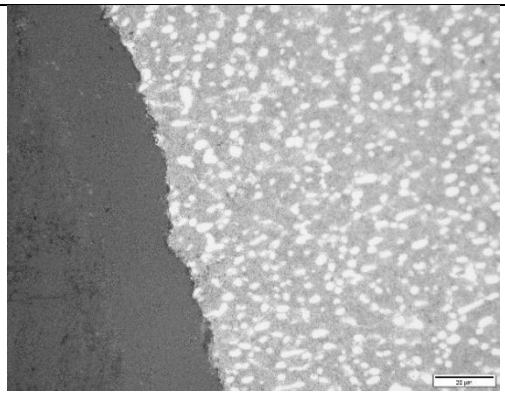
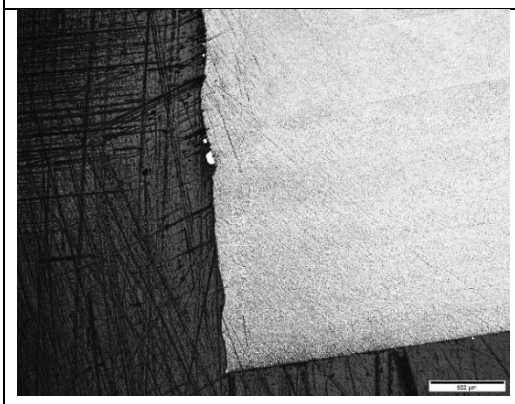	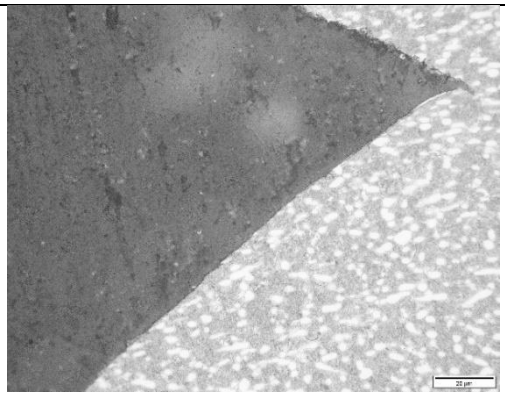

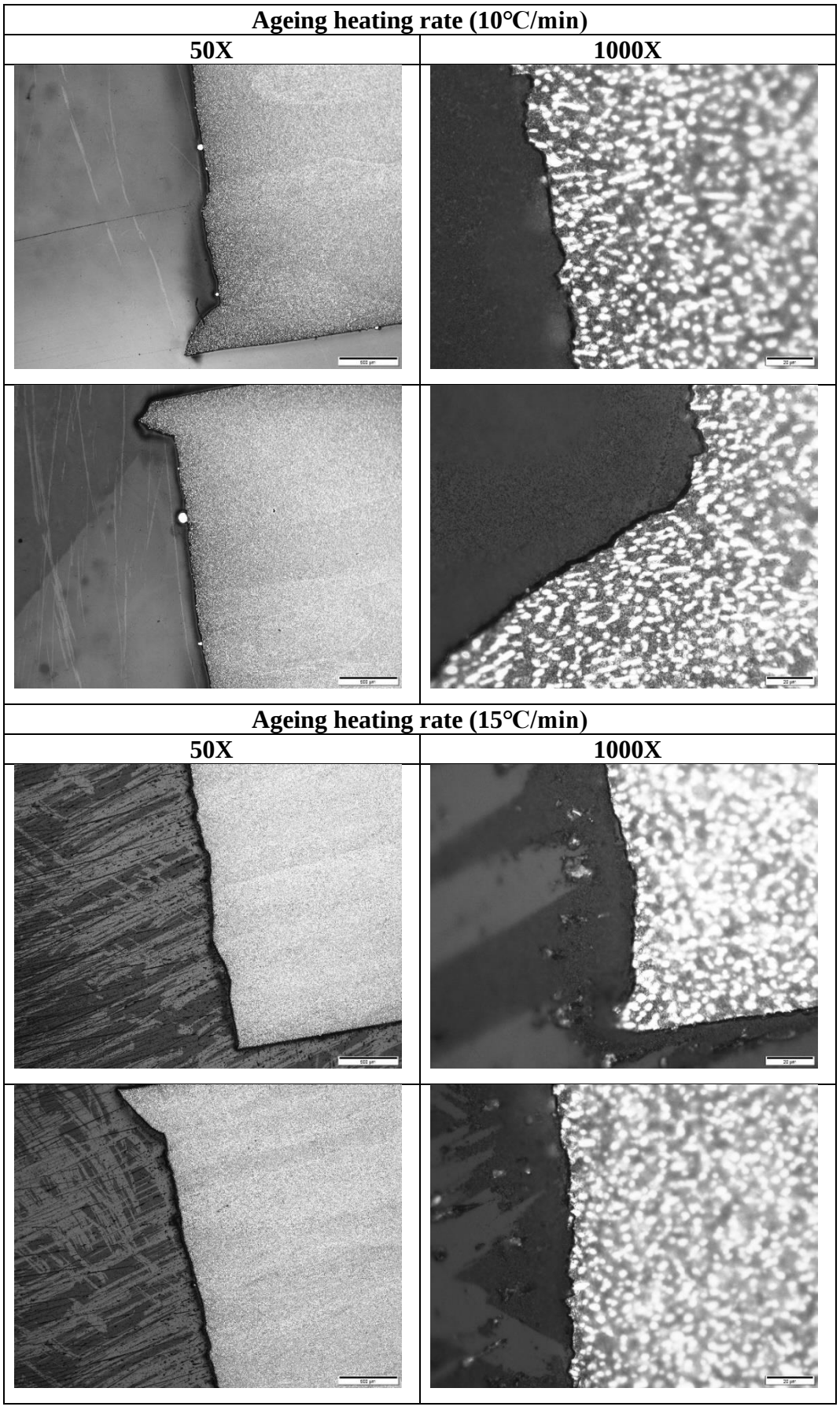

Figure 63: Fractography of fatigued specimens at different heating rates

The fatigue fracture surfaces observed in this study align with established fatigue failure mechanisms. Cracks were predominantly initiated at the α/β interfaces, particularly in regions where the primary α phase was present. This is consistent with findings from previous research, which also identified the primary α phase as a common site for crack initiation under cyclic loading conditions [59, 60]. The shorter fatigue life observed at higher ageing heating rates can be explained by the coarser secondary α lamellar structure and the wider spacing between lamellae. This coarsening reduces the effectiveness of dislocation barriers, facilitating earlier crack initiation and faster crack propagation.

Chapter 5

5 Conclusions and Future Work

This chapter summarises the key findings from the study, focusing on the effects of different ageing heating rates (1°C/min, 5°C/min, 10°C/min and 15°C/min) employed during overall solution treatment and ageing process on the microstructure and mechanical properties of the Ti-5553 alloy. Following is the key findings and overall trends observed in hardness, tensile strength, and fatigue resistance, and their relationship to the microstructural features developed under each ageing condition:

5.1 Key Findings

- The as-received microstructure of the Ti-5553 alloy, which originated from a cogged billet, primarily consisted of a bimodal structure featuring a mixture of equiaxed primary α phase distributed within a matrix of transformed β phase. This initial microstructure served as the foundation for the subsequent heat treatments, influencing the evolution of microstructural features during ageing.

- The different ageing heat rates applied to the Ti-5553 alloy resulted in some changes in the bimodal microstructure morphology. The slower ageing heating rates promoted the formation of finer, more uniformly distributed secondary α lamellae, while faster heating rates led to a coarser microstructure with less evenly distributed α phases. Despite the variations in ageing conditions, the microstructural changes were relatively slight, leading to only minor differences in mechanical performance.

- The investigation into the anisotropy of the Ti-5553 alloy's microstructure, comparing the longitudinal and transverse directions, showed that the subsequent heat treatments effectively homogenised any initial anisotropy introduced by the cogging process.

- The examination of the microstructure across the entire cross-section of an individual sample confirms the uniformity of key microstructural features,

indicating that the heat treatment process applied was effective in homogenising the microstructure.

- The chemical homogeneity analysis, including EDX elemental mapping and spot analysis, revealed a consistent and uniform distribution of key elements across all heat-treated samples. The α stabilisers, such as aluminium and titanium, were predominantly concentrated within the primary α phase, while the β stabilisers, including molybdenum and vanadium, were primarily located within the β phase. This precise elemental positioning within the respective phases ensured stable phase compositions, effectively preserving chemical homogeneity regardless of the specific ageing treatment applied.

- Micro-Vickers Hardness results showed that the Ti-5553 alloy maintained consistent hardness across all ageing heating rates, with only minor variations. The hardness values ranged from 357.4 HV at the fastest heating rate of 15°C/min to 371.7 HV at the heating rate of 5°C/min. The fine microstructure, particularly the secondary α lamellar structure, contributed to slightly higher hardness at slower heating rates, while coarser structures at higher rates resulted in marginally lower hardness.

- The tensile properties of the alloy exhibited only slight variations with changes in the ageing heating rate, reflecting the subtle differences in microstructure. The trade-off between strength and ductility observed across the different heating rates was insignificant. For example, the UTS for the 1°C/min condition was 1307 MPa with a ductility of 15.6%, compared to 1265 MPa UTS and 17.1% ductility for the 15°C/min condition. These results suggest that while slower heating rates may produce slightly finer microstructures that contribute to marginally higher strength, the overall impact on tensile properties remains limited, with only a minor decrease in strength and a slight increase in ductility at faster heating rates.

- The fatigue performance of the Ti-5553 alloy followed similar trends to those observed in hardness and tensile properties, with only minor variations in fatigue life observed across different heating rates. The alloy showed better fatigue resistance at slower heating rates, which produced finer

secondary α lamellae. For example, at a stress amplitude of 337.5 MPa and a heating rate of 1°C/min, the material withstood over 10 million cycles, indicating excellent fatigue resistance. However, as the stress amplitude increased to 360 MPa, the fatigue life significantly decreased, with failure occurring after approximately 4 million cycles. Similar trends were observed across different heating rates, with the material generally exhibiting decreased fatigue life as the heating rate and stress amplitude increased.

Overall the findings from this thesis underscore the relationship between ageing heating rate, microstructure, and mechanical properties in the Ti-5553 alloy. While slower ageing heating rates do lead to a slightly finer secondary α lamellar structure, which in turn offers marginal improvements in hardness, tensile strength, and fatigue resistance, the differences observed are relatively minor. This suggests that the Ti-5553 alloy's mechanical performance is not highly sensitive to variations in ageing heating rates, allowing for some flexibility in heat treatment without significantly compromising the material's overall properties. These insights provide valuable guidance for optimising the heat treatment process in applications where a balance between strength, ductility, and fatigue life is required without necessitating stringent control over the heating rate.

5.2 Future Work

- Explore additional ageing heat treatments with a broader range of heating and cooling rates, as well as varied holding times, to further refine the microstructure for enhanced mechanical properties.

- Utilise TEM analysis to investigate the influence of microstructural features, such as the ω phase and dislocation structures, on mechanical properties, focusing on low-cycle fatigue performance.

- Conduct further fatigue testing with expanded sample size and without technical difficulties to ensure more reliable and statistically robust results.

- Investigate the low-cycle fatigue behaviour of the Ti-5553 alloy to gain an understanding of its performance under high-strain, low-cycle conditions, which are critical for its potential applications in demanding environments.

6 References

[1] G. Welsch, R. Boyer, E. Collings, Materials properties handbook: titanium alloys, ASM International1993.

[2] L. Wang, X. Zhao, X. Wang, S. Shang, Z. Xiu, Y. Xi, H. Jia, S. Xu, H. Liu, L. Wen, Current Status Review of Corrosion Resistance Applications of Titanium Alloys in the Petroleum Industry, Coatings 14(8) (2024) 941.

[3] I.T. Association, Titanium: The Ultimate Choice, 1999. http://www.alliedtitanium.com/technical/Titanium%20-%20The%20Ultimate%20Choice.pdf.

[4] C. Leyens, M. Peters, Titanium and Titanium Alloys: Fundamentals and Applications, Wiley2003.

[5] M.J. Donachie, Titanium: a technical guide, ASM international2000.

[6] J.M. Sánchez-Amaya, T. Pasang, M.R. Amaya-Vazquez, J.D.D. Lopez-Castro, C. Churiaque, Y. Tao, F.J. Botana Pedemonte, Microstructure and Mechanical Properties of Ti5553 Butt Welds Performed by LBW under Conduction Regime, Metals 7(7) (2017) 269.

[7] H.A. Kishawy, A. Hosseini, H.A. Kishawy, A. Hosseini, Titanium and titanium alloys, Machining Difficult-To-Cut Materials: Basic Principles and Challenges, Springer International Publishing, Cham, 2019, pp. 55-96.

[8] J.C. Williams, R.R. Boyer, Opportunities and issues in the application of titanium alloys for aerospace components, Metals 10(6) (2020) 705.

[9] J.D. Destefani, Introduction to titanium and titanium alloys, Properties and selection: nonferrous alloys and special-purpose materials, ASM International1990, pp. 586-591.

[10] G. Lütjering, J.C. Williams, Titanium, 2. Aufl. ed., Berlin, Heidelberg: Springer-Verlag, Berlin, Heidelberg, GERMANY, 2007.

[11] S. Saroja, M. Vijayalakshmi, B. Raj, Ti–5Ta–1.8 Nb: an advanced structural material for high performance application in aggressive oxidising environments, Transactions of the Indian Institute of Metals 65 (2012) 111-133.

[12] A. Biesiekierski, K. Munir, Y. Li, C. Wen, Titanium alloys, Structural Biomaterials, Elsevier2021, pp. 157-187.

[13] I. Polmear, D. StJohn, J.-F. Nie, M. Qian, 7 - Titanium Alloys, in: I. Polmear, D. StJohn, J.-F. Nie, M. Qian (Eds.), Light Alloys (Fifth Edition), Butterworth-Heinemann, Boston, 2017, pp. 369-460.

[14] K. Gao, Y. Zhang, J. Yi, F. Dong, P. Chen, Overview of Surface Modification Techniques for Titanium Alloys in Modern Material Science: A Comprehensive Analysis, Coatings 14(1) (2024) 148.
[15] C. Veiga, J.P. Davim, A. Loureiro, Properties and applications of titanium alloys: a brief review, Rev. Adv. Mater. Sci 32(2) (2012) 133-148.
[16] M. Kaur, K. Singh, Review on titanium and titanium based alloys as biomaterials for orthopaedic applications, Materials Science and Engineering: C 102 (2019) 844-862.
[17] R.P. Kolli, A. Devaraj, A review of metastable beta titanium alloys, Metals 8(7) (2018) 506.
[18] M. Sen, S. Suman, S. Mukherjee, T. Banerjee, S. Sivaprasad, S. Tarafder, A. Bhattacharjee, S. Kumar Kar, Low cycle fatigue behavior and deformation mechanism of different microstructures in Ti-5Al-5Mo-5V-3Cr alloy, International Journal of Fatigue 148 (2021) 106238.
[19] W. Yonggang, L. Honglang, Summary and Analysis of the Aging Aircrafts' Failure, Procedia Engineering 17 (2011) 303-309.
[20] S.K. Lok, J.M. Paul, V. Upendranath, Prescience Life of Landing Gear Using Multiaxial Fatigue Numerical Analysis, Procedia Engineering 86 (2014) 775-779.
[21] R.R. Boyer, R.D. Briggs, The Use of β Titanium Alloys in the Aerospace Industry, Journal of Materials Engineering and Performance 14(6) (2005) 681-685.
[22] J.D. Cotton, R.D. Briggs, R.R. Boyer, S. Tamirisakandala, P. Russo, N. Shchetnikov, J.C. Fanning, State of the Art in Beta Titanium Alloys for Airframe Applications, JOM 67(6) (2015) 1281-1303.
[23] J.D. Cotton, R.R. Boyer, R.D. Briggs, R.G. Baggerly, C.A. Meyer, M.D. Carter, W. Wood, G. Tewksbury, V. Li, X. Yao, Phase transformations in Ti-5Al-5Mo-5V-3Cr-0.5 Fe, 2007.
[24] S. Nyakana, J. Fanning, R. Boyer, Quick reference guide for β titanium alloys in the 00s, Journal of Materials Engineering and Performance 14 (2005) 799-811.
[25] J. Fanning, Properties of TIMETAL 555 (Ti-5Al-5Mo-5V-3Cr-0.6 Fe), Journal of Materials Engineering and Performance 14(6) (2005) 788-791.
[26] A.C. Arohi, S. Shekhar, I. Sen, Effect of thermomechanical processing on microstructure evolution and mechanical properties of metastable β Ti–5Al–5V–5Mo–3Cr alloy, Materials Chemistry and Physics 314 (2024) 128809.
[27] N. Ramachandiran, H. Asgari, F. Dibia, R. Eybel, W. Muhammad, A. Gerlich, E. Toyserkani, Effects of post heat treatment on microstructure and mechanical

properties of Ti5553 parts made by laser powder bed fusion, Journal of Alloys and Compounds 938 (2023) 168616.
[28] R. Sahoo, A.S. Kabir, Effect of heat treatments on microstructures and mechanical properties of Ti-5553 alloy, TMS 2020 149th Annual Meeting & Exhibition Supplemental Proceedings, Springer, 2020, pp. 1799-1807.
[29] B.A. Welk, Microstructural and property relationships in β-titanium alloy Ti-5553, The Ohio State University, 2010.
[30] N. Chanfreau, D. Poquillon, A. Stark, E. Maawad, C. Mareau, M. Dehmas, Phase transformation of the Ti-5553 titanium alloy subjected to rapid heating, Journal of Materials Science 57(9) (2022) 5620-5633.
[31] S. Veeck, D. Lee, R. Boyer, R. Briggs, The microstructure and properties of cast titanium alloy Ti-5553 were evaluated in a joint program by Howmet and Boeing, Advanced Materials & Processes 162(10) (2004) 47-49.
[32] J. Gao, Understanding the relationship between microstructure and mechanical properties in HIPped Ti-5Al-5Mo-5V-3Cr, University of Birmingham, 2018.
[33] J. Cotton, R. Boyer, R. Briggs, R. Baggerly, C. Meyer, M. Carter, W. Wood, G. Tewksbury, V. Li, X. Yao, Phase Transformations in Ti-5Al-5Mo-5V-3Cr-0.5Fe, 2007.
[34] M. Bettaieb, A. Lenain, A. Habraken, Static and fatigue characterization of the Ti5553 titanium alloy, Fatigue & Fracture of Engineering Materials & Structures 36(5) (2013) 401-415.
[35] L.C. Campanelli, P.S.C.P. da Silva, C. Bolfarini, High cycle fatigue and fracture behavior of Ti-5Al-5Mo-5V-3Cr alloy with BASCA and double aging treatments, Materials Science and Engineering: A 658 (2016) 203-209.
[36] S.K. Kar, A. Ghosh, N. Fulzele, A. Bhattacharjee, Quantitative microstructural characterization of a near beta Ti alloy, Ti-5553 under different processing conditions, Materials Characterization 81 (2013) 37-48.
[37] D. Qin, F. Zhao, Y. Li, The conflicts between strength and ductility of bimodal Ti-5553 alloy with fine equiaxial prior β grains, Materials Science and Engineering: A 841 (2022) 143074.
[38] S. Shekhar, R. Sarkar, S.K. Kar, A. Bhattacharjee, Effect of solution treatment and aging on microstructure and tensile properties of high strength β titanium alloy, Ti–5Al–5V–5Mo–3Cr, Materials & Design 66 (2015) 596-610.

[39] M.G. de Mello, F.H. Costa, V. Opini, A. Resende, A. Cremasco, R. Caram, Isothermal omega assisted alpha phase precipitation and microstructural evolution of an aged Ti-30Nb-3Fe alloy, Materials Research 23 (2020) e20200026.
[40] Z. Qing-yun, Y. Yang, W. Li-dong, D. Li-min, L. Feng-lei, Microstructure and Properties of Ti-5553 Alloy for Aerospace Fasteners, Journal of Materials Engineering 45 (2017) 95-102.
[41] N. Jones, R. Dashwood, D. Dye, M. Jackson, Thermomechanical processing of Ti–5Al–5Mo–5V–3Cr, Materials Science and Engineering: A 490(1-2) (2008) 369-377.
[42] Y. Lin, L.-H. Wang, Q. Wu, Y.-W. Xiao, H. Cheng, X.-Y. Zhang, Effects of solution temperature and cooling rate on α phases and mechanical properties of a forged Ti-55511 alloy, Materials Research Express 6(11) (2019) 1165h2.
[43] M. Sangali, V.C. Opini, A.Z. Fatichi, M.G. Mello, L. Fanton, R. Caram, A. Cremasco, Nb modified Ti-5553 alloy: Effects of heating rate on mechanical properties, corrosion behavior, and crystallographic texture, Journal of Materials Research and Technology 23 (2023) 5310-5317.
[44] Q. Contrepois, C. Marc, J. Lecomte-Beckers, Characterization of the β phase decomposition in Ti-5Al-5Mo-5V-3Cr at slow heating rates, Open Journal of Metal 1 (2011).
[45] C. Liu, Y. Lu, X. Tian, D. Liu, Influence of continuous grain boundary α on ductility of laser melting deposited titanium alloys, Materials Science and Engineering: A 661 (2016) 145-151.
[46] A. Settefrati, E. Aeby-Gautier, M. Dehmas, G. Geandier, B. Appolaire, S. Audion, J. Delfosse, Precipitation in a near beta titanium alloy on ageing: Influence of heating rate and chemical composition of the beta-metastable phase, Solid State Phenomena 172 (2011) 760-765.
[47] D. Qin, Y. Lu, D. Guo, L. Zheng, Q. Liu, L. Zhou, Tensile deformation and fracture of Ti–5Al–5V–5Mo–3Cr–1.5 Zr–0.5 Fe alloy at room temperature, Materials Science and Engineering: A 587 (2013) 100-109.
[48] S. Sadeghpour, S. Abbasi, M. Morakabati, S. Bruschi, Correlation between alpha phase morphology and tensile properties of a new beta titanium alloy, Materials & Design 121 (2017) 24-35.
[49] J. Huang, Z. Wang, K. Xue, Cyclic deformation response and micromechanisms of Ti alloy Ti–5Al–5V–5Mo–3Cr–0.5 Fe, Materials Science and Engineering: A 528(29-30) (2011) 8723-8732.

[50] S.-W. Xin, Y.-Q. Zhao, Discussion about the heat treatment and precipitated phases of titanium alloy, Heat Treatment of Metals(China) 31(9) (2006) 39-42.
[51] E. Sukedai, E. Aeby-Gautier, M. Dehmas, TEM observation of precipitates and their role to mechanical properties in Ti-5553 alloy heated to some temperatures up to 923 K, MATEC Web of Conferences, EDP Sciences, 2020, p. 11035.
[52] Y. Ohmori, T. Ogo, K. Nakai, S. Kobayashi, Effects of ω-phase precipitation on β→ α, α″ transformations in a metastable β titanium alloy, Materials Science and Engineering: A 312(1-2) (2001) 182-188.
[53] V.C. Opini, C.A. Salvador, K.N. Campo, E.S. Lopes, R.R. Chaves, R. Caram, α phase precipitation and mechanical properties of Nb-modified Ti-5553 alloy, Materials Science and Engineering: A 670 (2016) 112-121.
[54] T. Padmalatha, U. Chakkingal, The effect of heat treatment and the volume fraction of the alpha phase on the workability of Ti-5Al-5Mo-5V-3Cr alloy, Journal of Materials Engineering and Performance 28 (2019) 5352-5360.
[55] Y. Wang, M. Hao, D. Li, P. Li, Q. Liang, D. Wang, Y. Zheng, Q. Sun, Y. Wang, Enhanced mechanical properties of Ti-5Al-5Mo-5V-3Cr-1Zr by bimodal lamellar precipitate microstructures via two-step aging, Materials Science and Engineering: A 829 (2022) 142117.
[56] M. Sen, S. Suman, T. Banerjee, A. Bhattacharjee, S.K. Kar, Tensile deformation mechanism and failure mode of different microstructures in Ti5Al5Mo5V3Cr alloy, Materials Science and Engineering: A 753 (2019) 156-167.
[57] C.-L. Li, X.-J. Mi, W.-J. Ye, S.-X. Hui, Y. Yu, W.-Q. Wang, Effect of solution temperature on microstructures and tensile properties of high strength Ti–6Cr–5Mo–5V–4Al alloy, Materials Science and Engineering: A 578 (2013) 103-109.
[58] H. Luo, W. Yuan, W. Xiang, H. Deng, H. Yin, L. Chen, S. Cao, High-Cycle Fatigue Behavior and Corresponding Microscale Deformation Mechanisms of Metastable Ti55511 Alloy with A Basket-Weave Microstructure, Materials 15(20) (2022) 7144.
[59] C. Huang, Y. Zhao, S. Xin, W. Zhou, Q. Li, W. Zeng, C. Tan, High cycle fatigue behavior of Ti–5Al–5Mo–5V–3Cr–1Zr titanium alloy with bimodal microstructure, Journal of Alloys and Compounds 695 (2017) 1966-1975.
[60] C. Huang, Y. Zhao, S. Xin, C. Tan, W. Zhou, Q. Li, W. Zeng, Effect of microstructure on high cycle fatigue behavior of Ti–5Al–5Mo–5V–3Cr–1Zr titanium alloy, International Journal of Fatigue 94 (2017) 30-40.

7 Appendix 1

Comparison of Longitudinal vs Transverse micrographs

Ageing heating rate (1°C/min)	
Longitudinal Direction	Transverse Direction
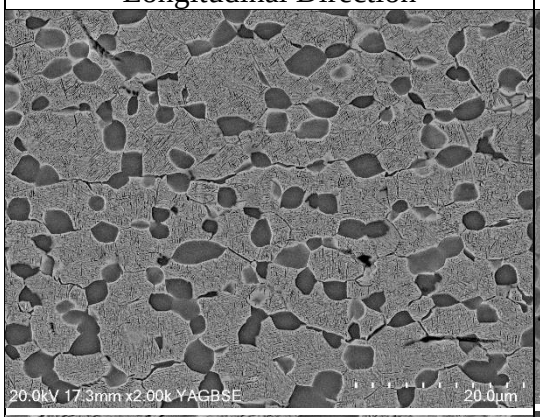	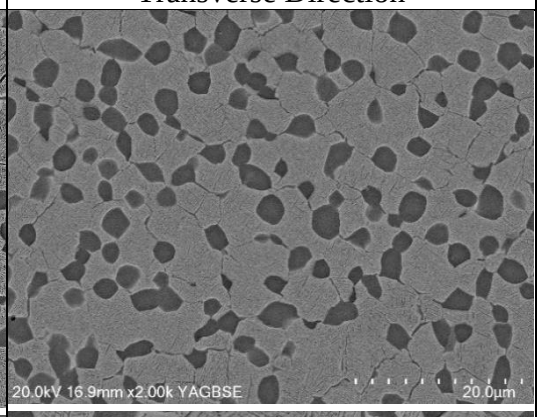
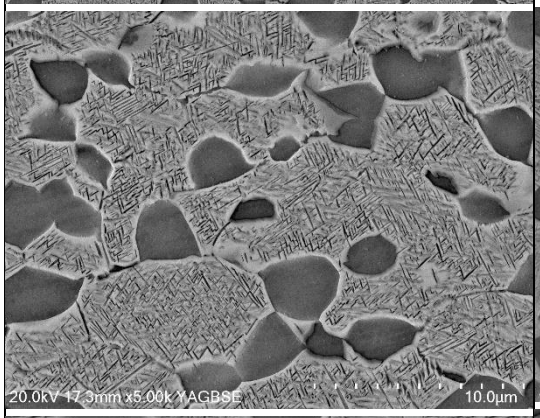	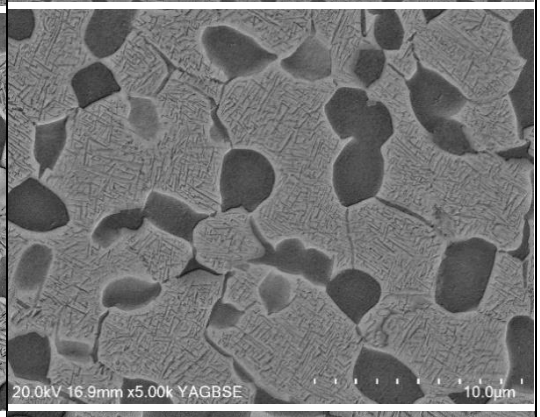
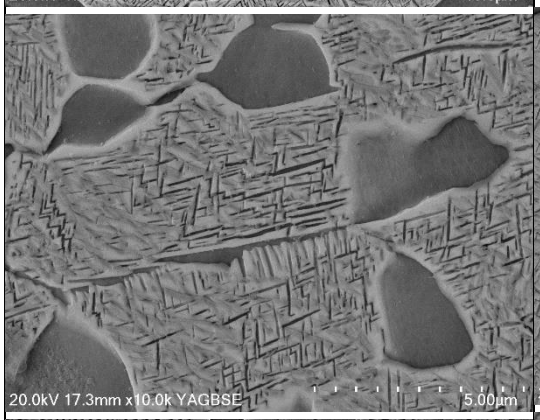	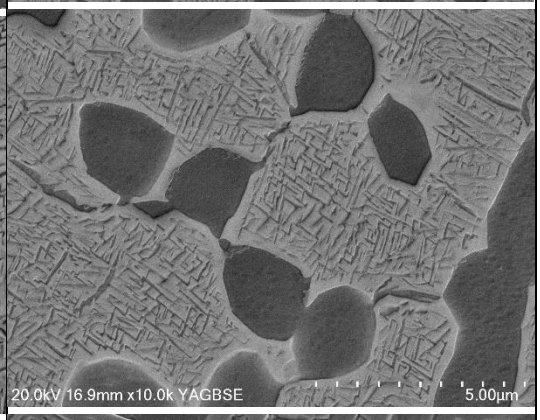
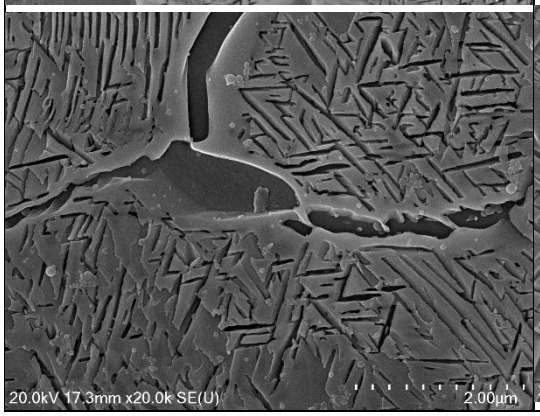	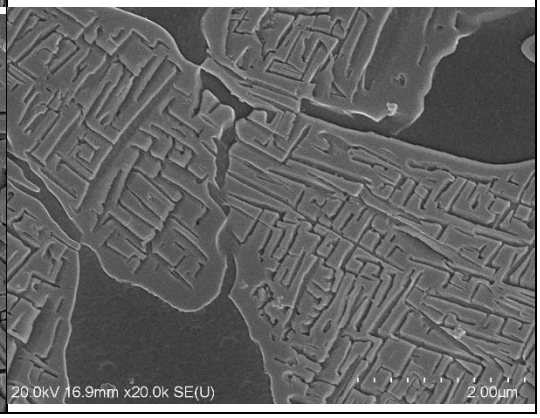

Ageing heating rate (5°C/min)	
Longitudinal Direction	Transverse Direction
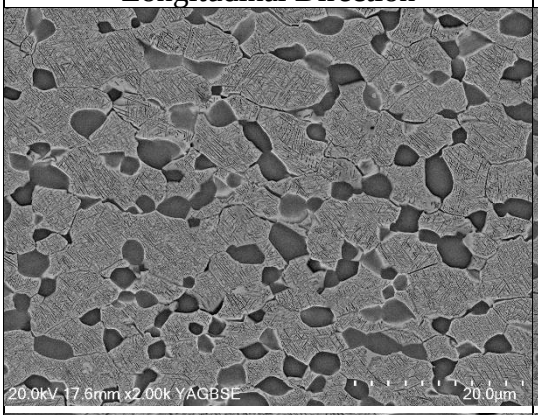	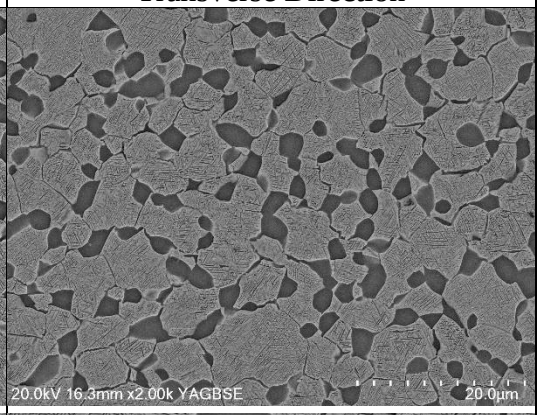
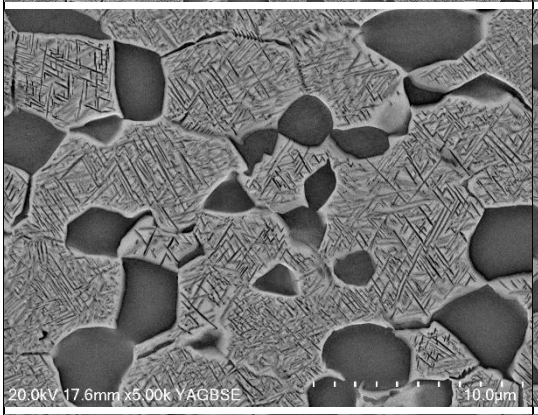	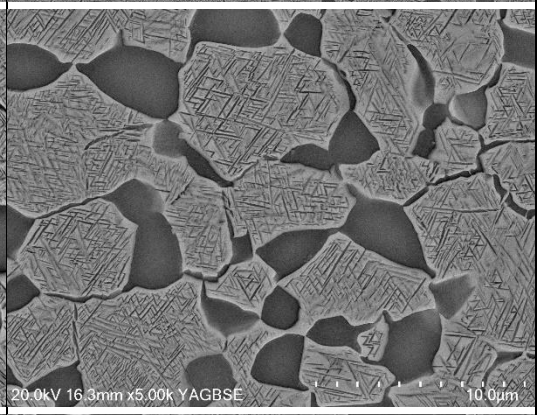
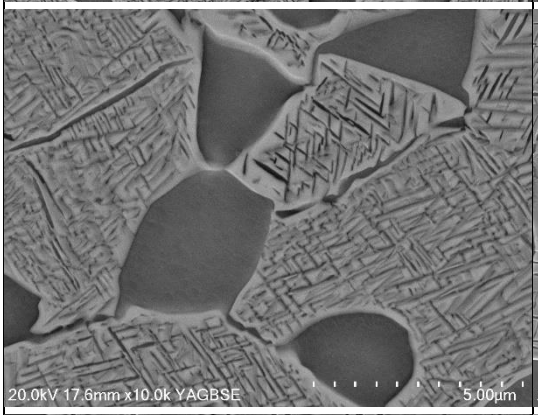	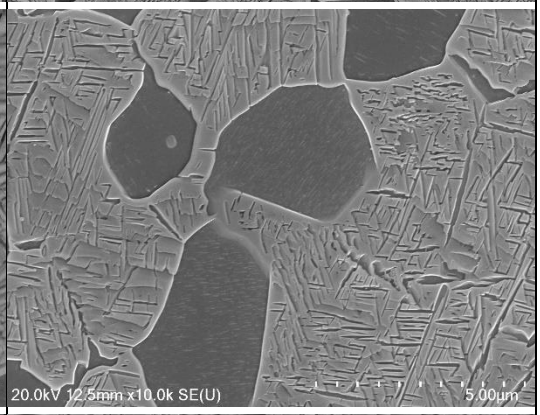
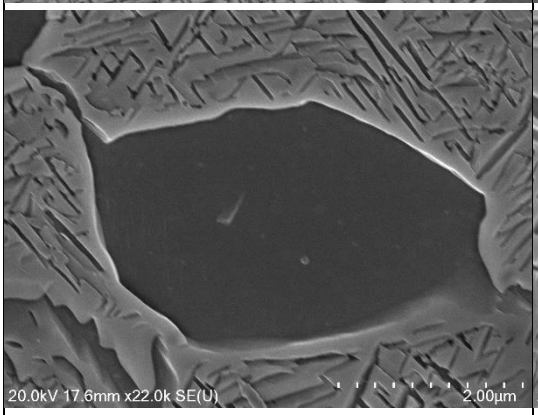	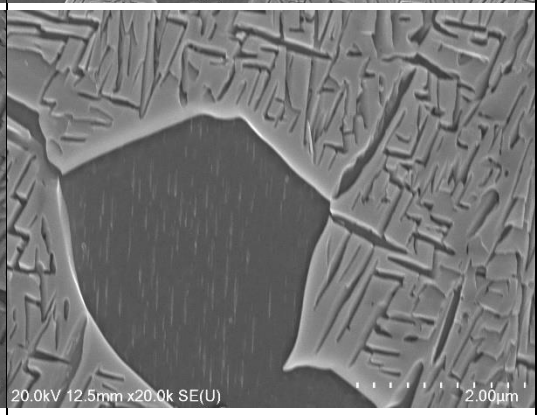

Ageing heating rate (10℃/min)	
Longitudinal Direction	Transverse Direction
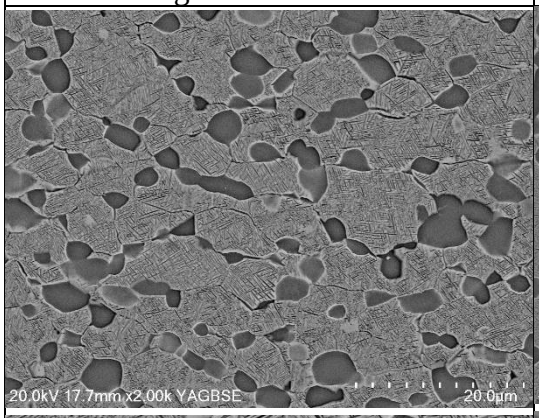	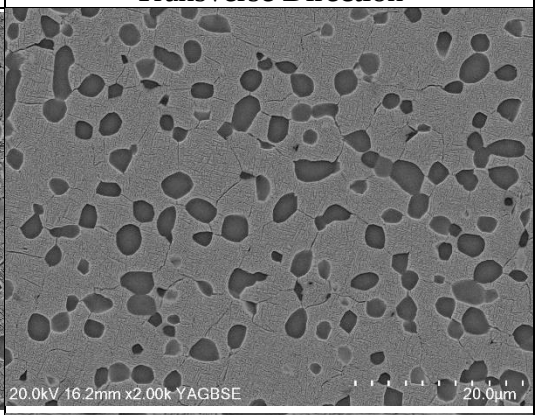
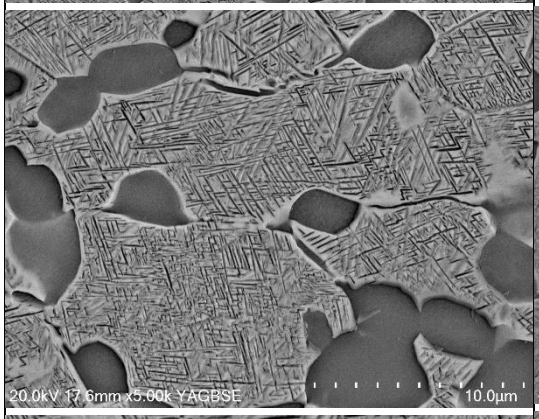	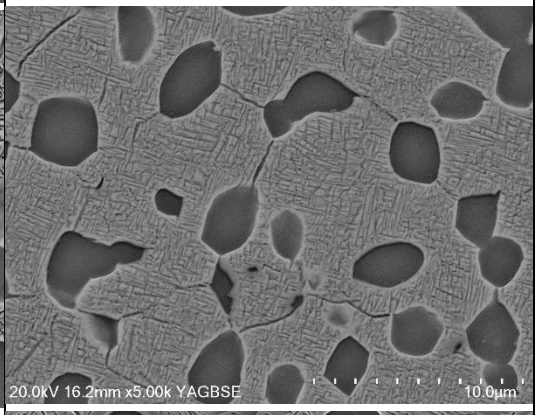
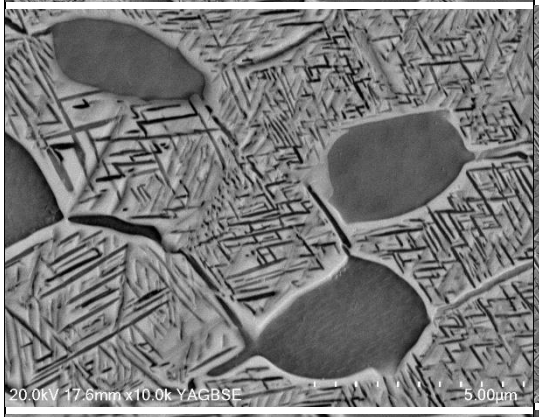	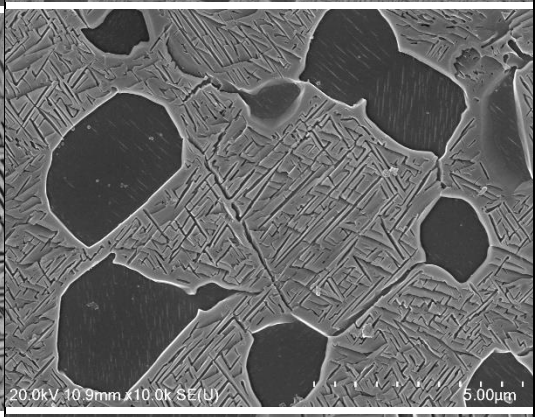
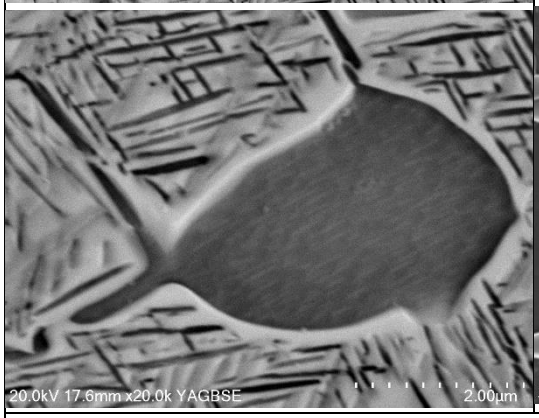	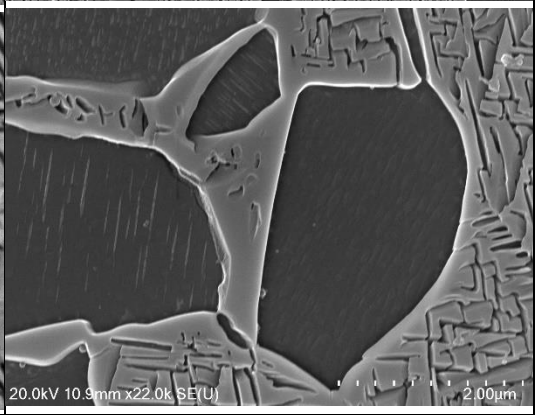

Ageing heating rate (15℃/min)	
Longitudinal Direction	Transverse Direction
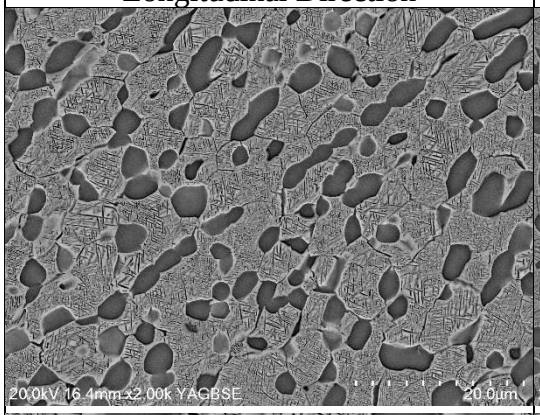	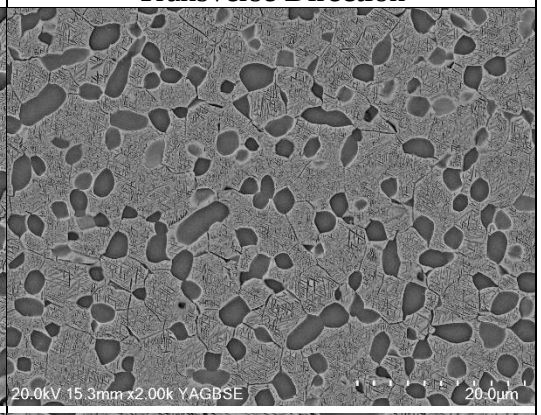
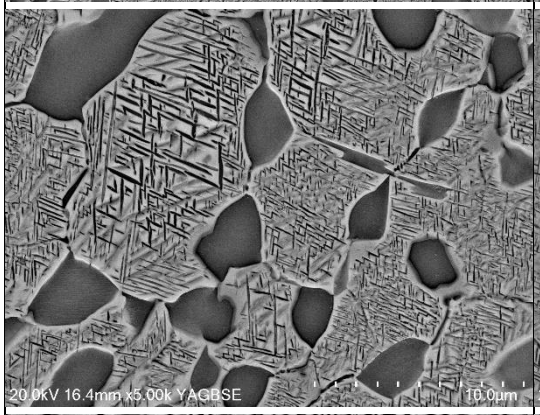	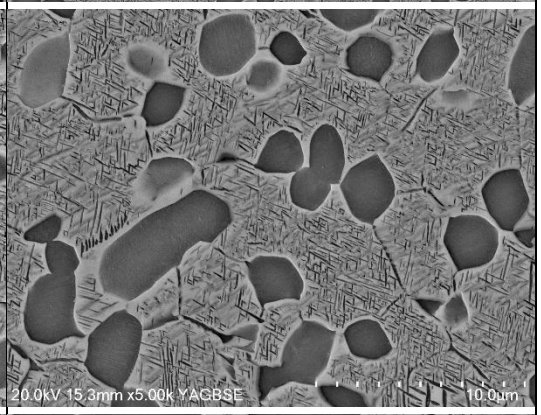
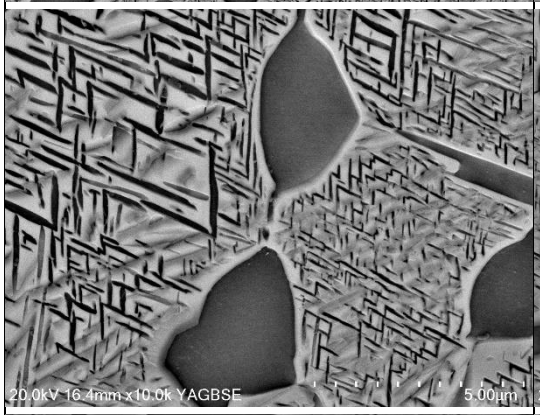	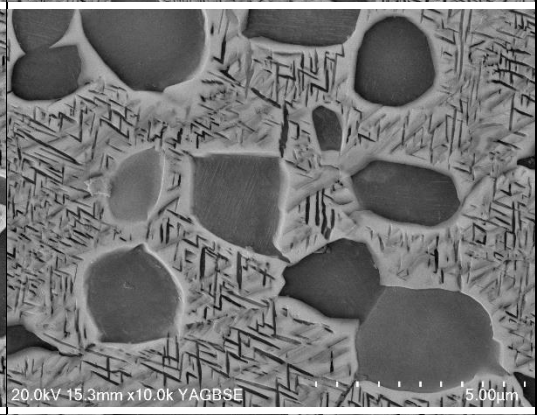
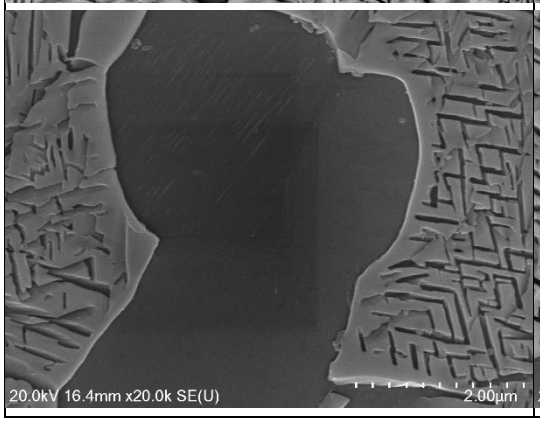	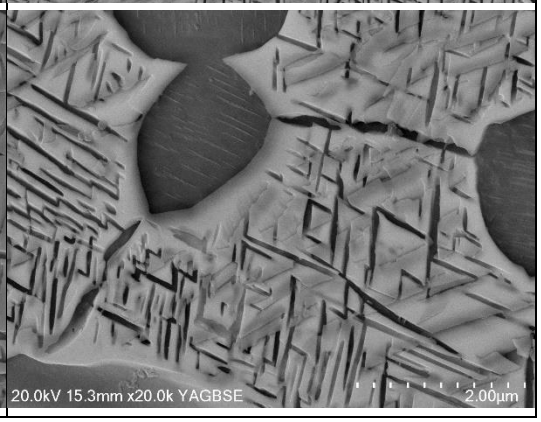

The following pages shows variations of microstructure across the entire sample in systematic order 1°C/min, 5°C/min, 10°C/min, and 15°C/min, respectively

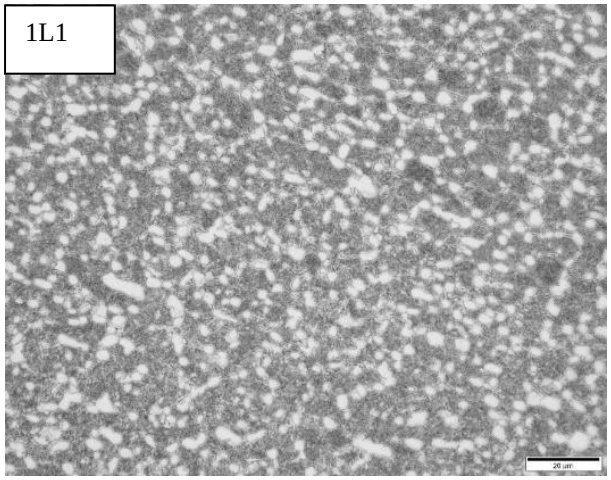
1L1

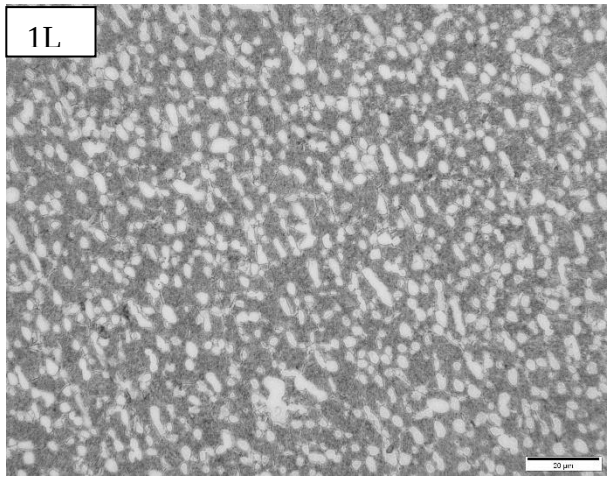
1L

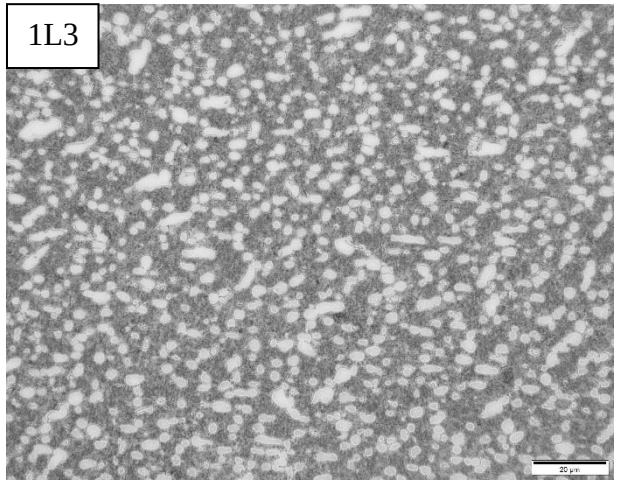
1L3

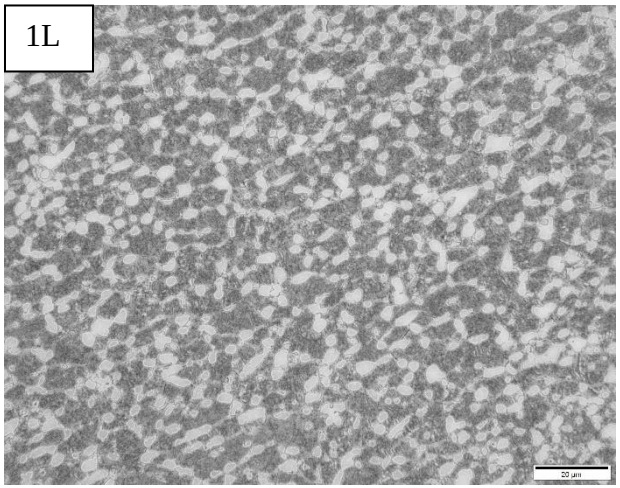
1L

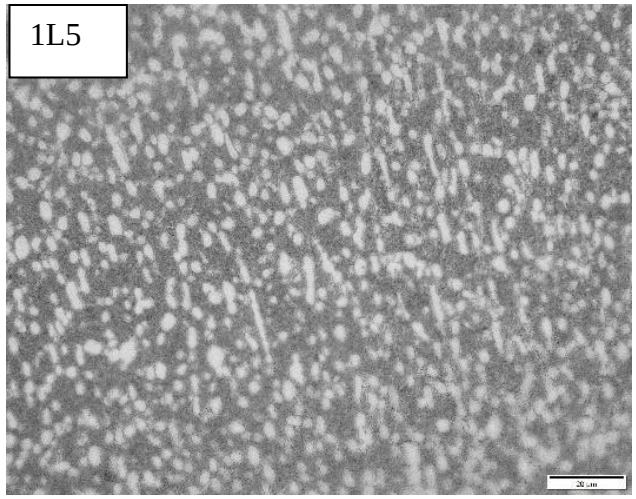
1L5

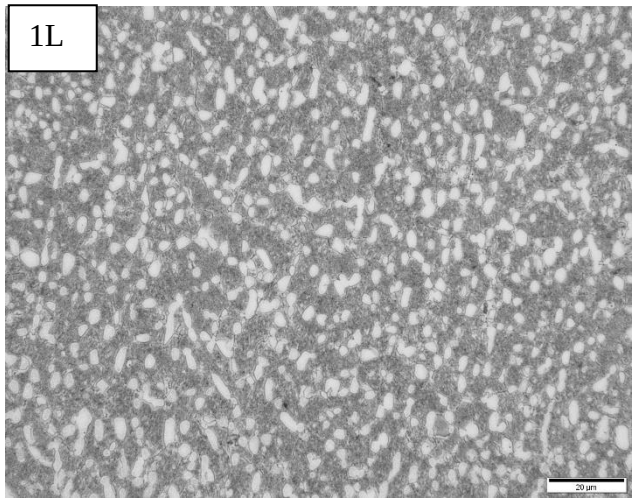
1L

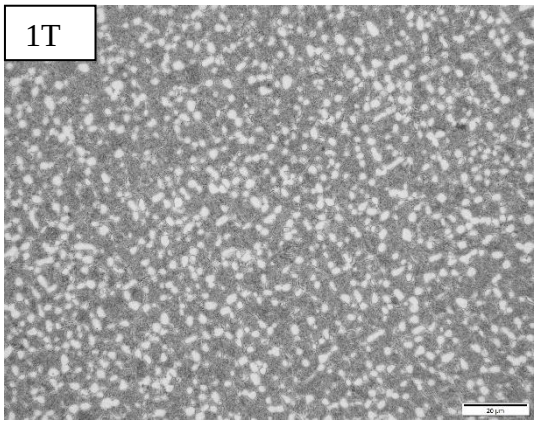
1T

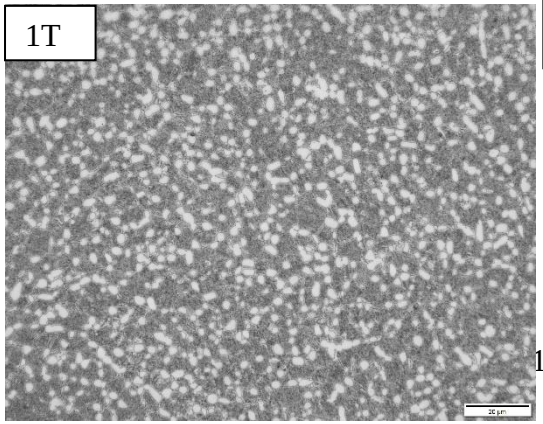
1T

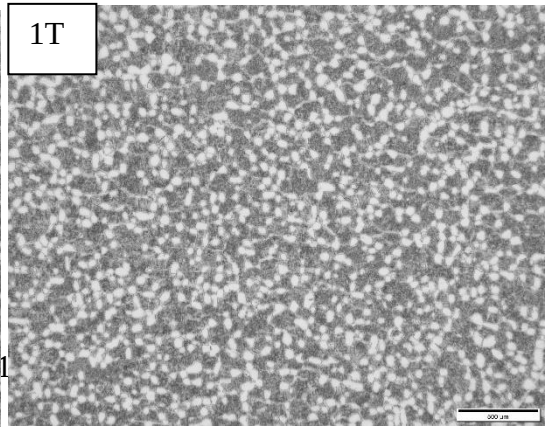
1T

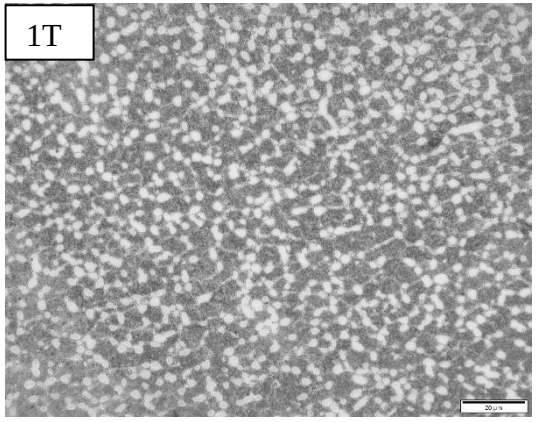
1T

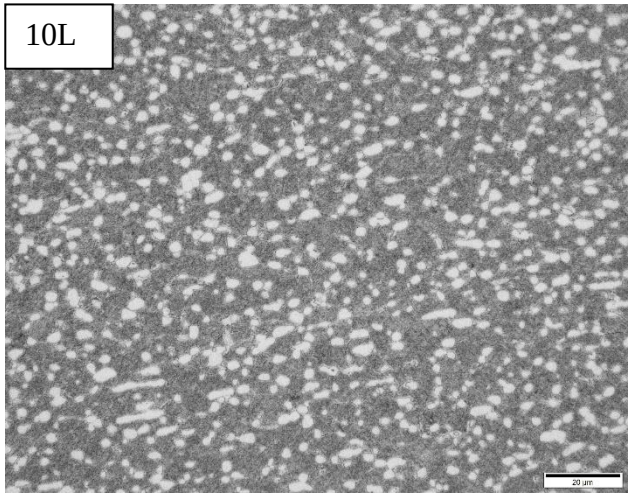
10L

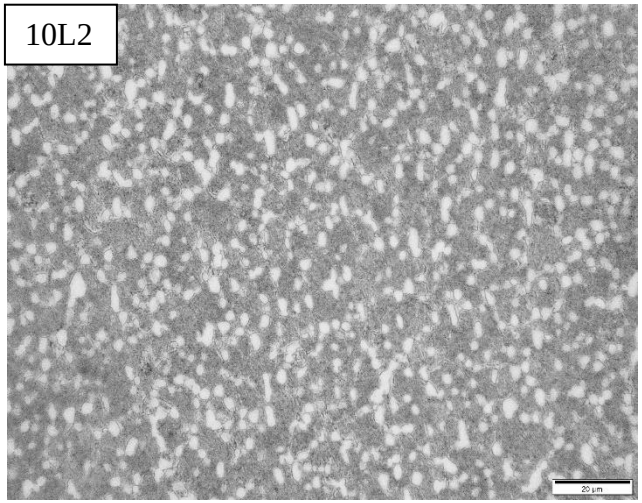
10L2

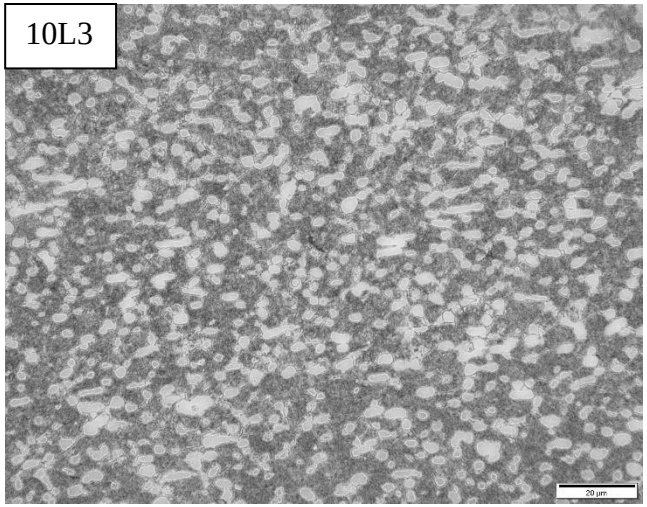
10L3

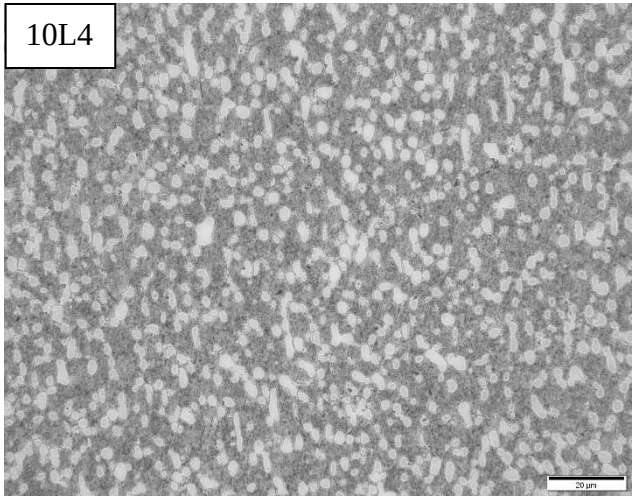
10L4

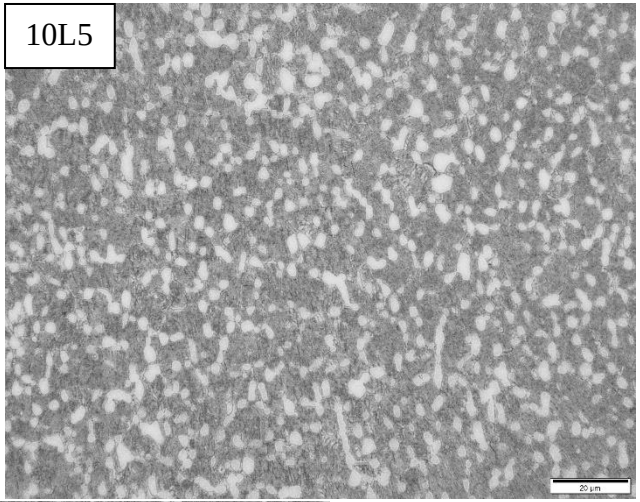
10L5

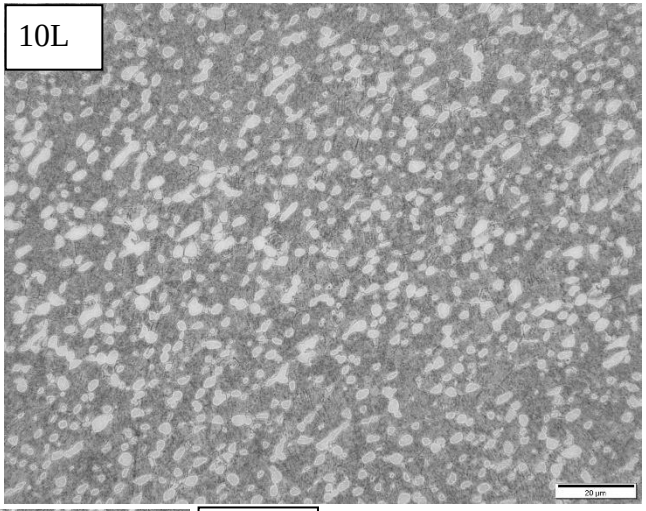
10L

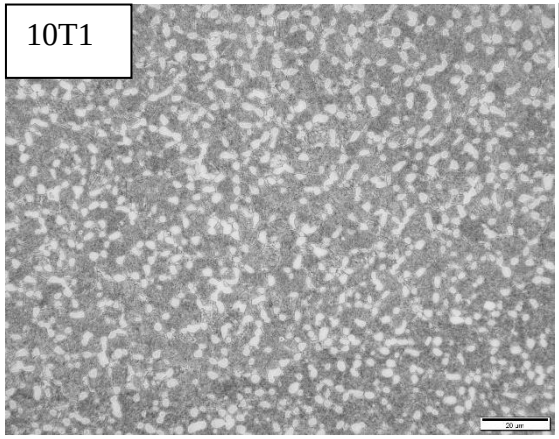
10T1

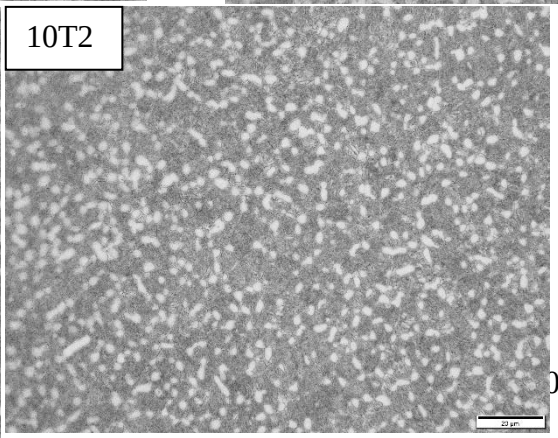
10T2

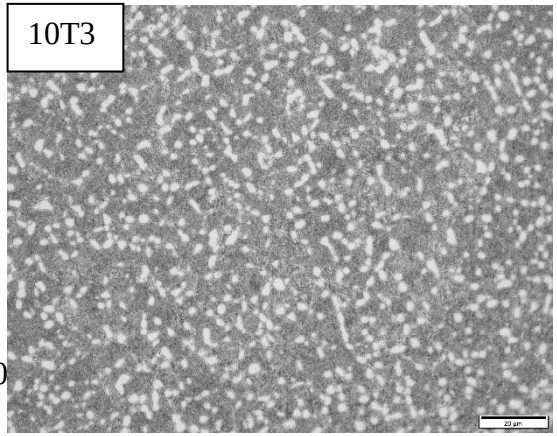
10T3

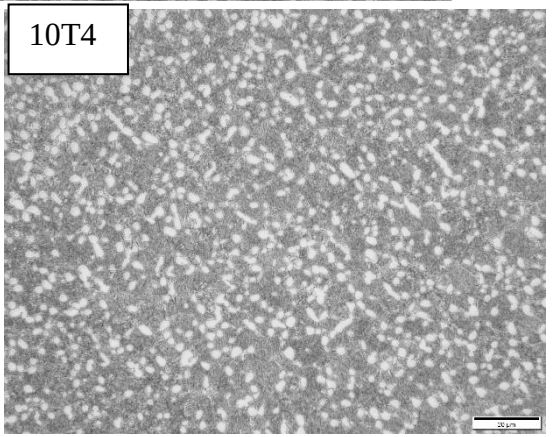
10T4

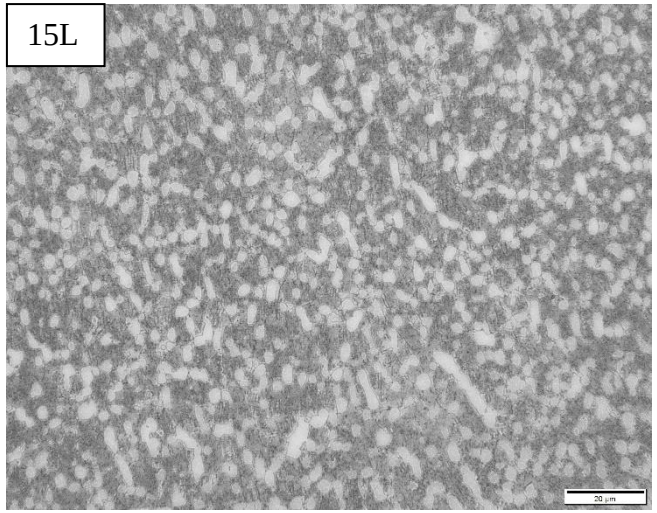
15L

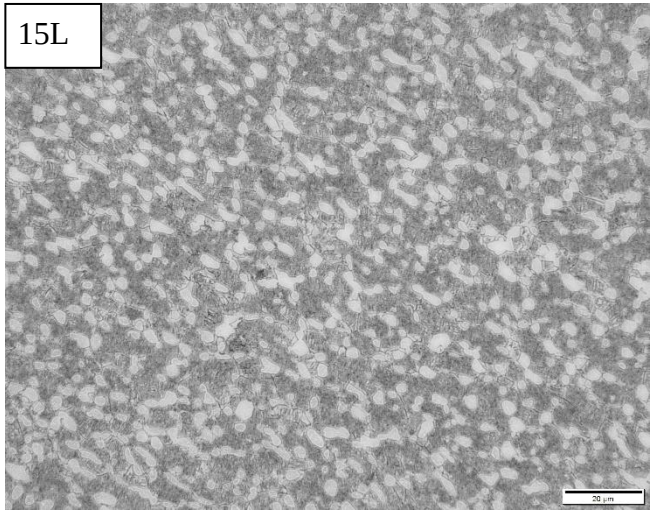
15L

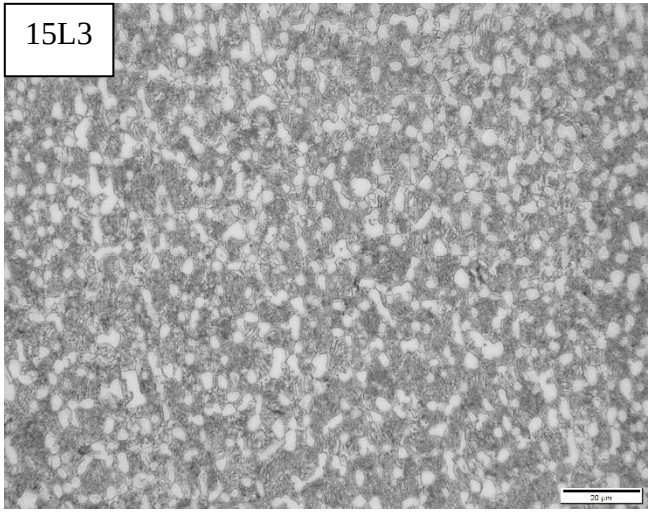
15L3

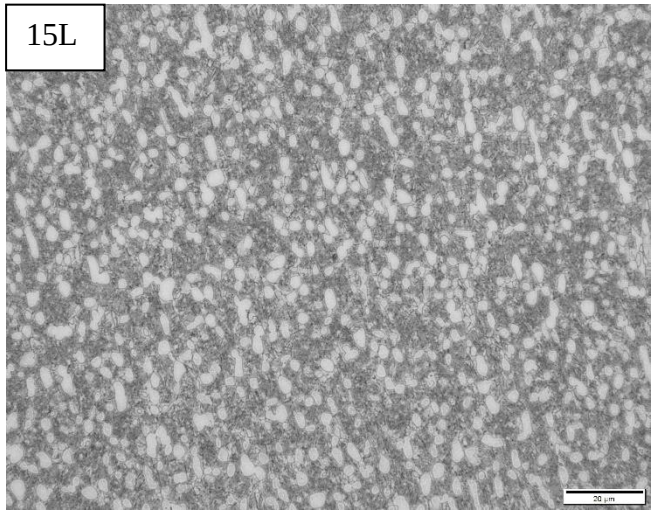
15L

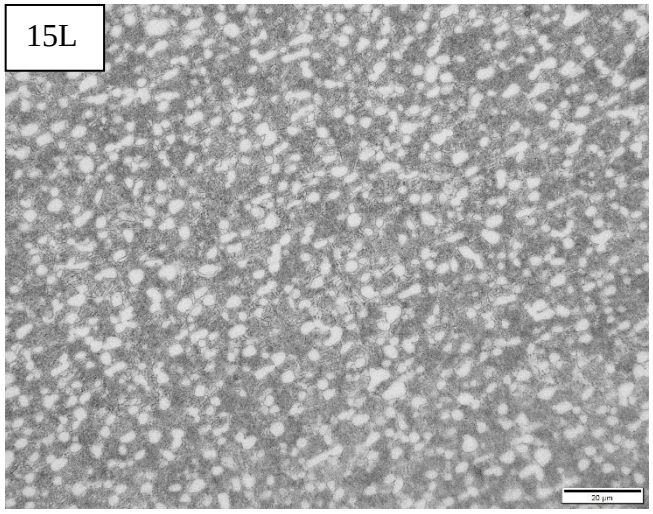
15L

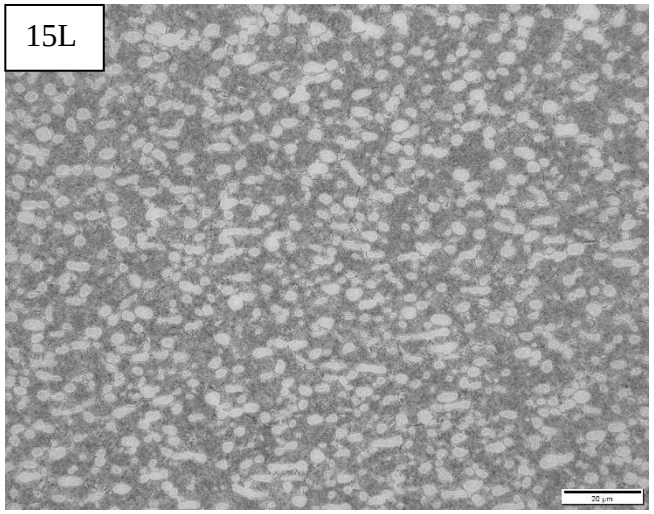
15L

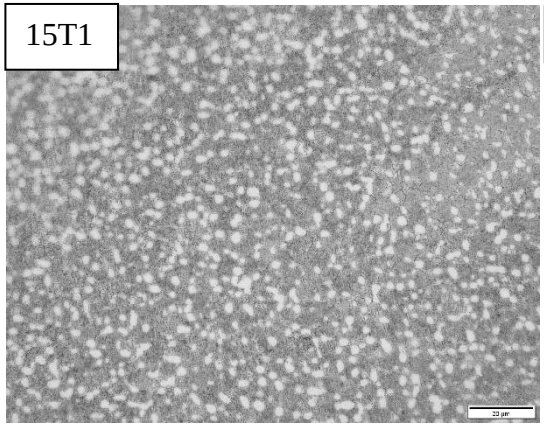
15T1

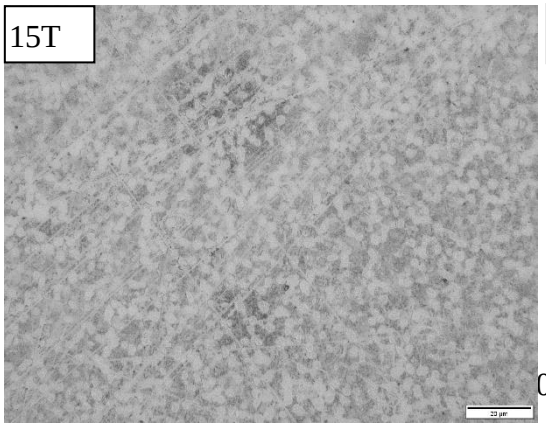
15T

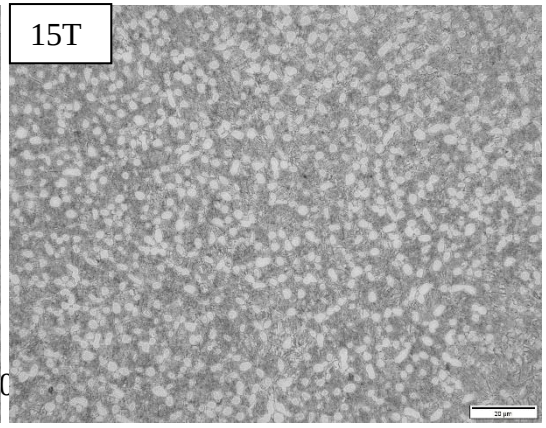
15T

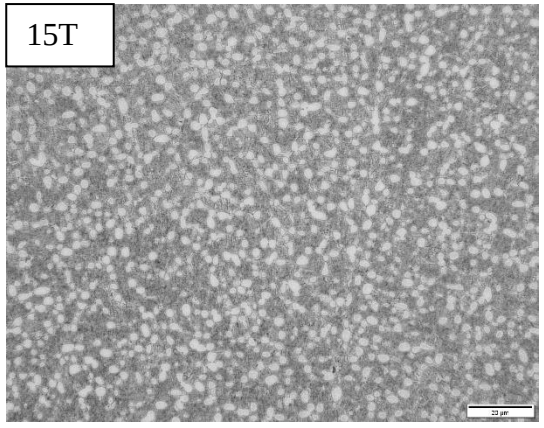
15T